

MICROCOPY RESOLUTION TEST CHART
NATIONAL BUREAU OF STANDARDS-1963-A

REPORT DOCUMENTATION PAGE		READ INSTRUCTIONS BEFORE COMPLETING FORM
1. REPORT NUMBER AFIT/GEP/PH82D-28	2. GOVT ACCESSION NO. AD A127810	3. RECIPIENT'S CATALOG NUMBER
TITLE (and Subtitle) ULTRA-STABLE LASER CLOCK		5. TYPE OF REPORT & PERIOD COVERED
AUTHOR(s) Roger L. Facklam 1st Lt USAF		6. PERFORMING ORG. REPORT NUMBER
PERFORMING ORGANIZATION NAME AND ADDRESS AF Institute of Technology (AFIT-ENP) Wright-Patterson AFB OH 45433		8. CONTRACT OR GRANT NUMBER(s)
10. PROGRAM ELEMENT, PROJECT, TASK AREA & WORK UNIT NUMBERS 60951535		12. REPORT DATE January 1983
1. CONTROLLING OFFICE NAME AND ADDRESS AFWAL/AAAN-1 WPAFB, OHIO 45433		13. NUMBER OF PAGES 134
4. MONITORING AGENCY NAME & ADDRESS (if different from Controlling Office)		15. SECURITY CLASS. (of this report) Unclassified
6. DISTRIBUTION STATEMENT (of this Report) Approved for release; distribution unlimited		15a. DECLASSIFICATION/DOWNGRADING SCHEDULE
17. DISTRIBUTION STATEMENT (of the abstract entered in Block 20, if different from Report)		DTIC ELECTE MAY 02 1983 S E
18. SUPPLEMENTARY NOTES Approved for public release; LAW AFR 190-17. LYNN E. WOLAVER Dean for Research and Professional Development Air Force Institute of Technology (AIC) Wright-Patterson AFB OH 45433		7 APR 1983
19. KEY WORDS (Continue on reverse side if necessary and identify by block number) Ring Laser He-Ne Laser Laser Clock Transfer Frequency Standard Laser Gyroscope		
20. ABSTRACT (Continue on reverse side if necessary and identify by block number) The Air Force has a requirement for a high accuracy Helium-Neon Ring Laser Gyro (RLG) and a high accuracy clock. The author has devised a method whereby a multi-oscillator RLG can be used simultaneously as a clock. The device uses a multi-frequency laser oscillator with an auxiliary detector to sense a 583 MHz clock signal. The experiment was conducted at the Sudbury, Massachusetts plant of the Raytheon Corporation. The square root of the Allan variance was measured for several different sample times. The best data obtained, for the given times		

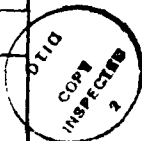
DTIC FILE COPY

83 04 28 115

BLOCK 20: Abstract (Cont'd):

was 4.6×10^{-10} for 1msec, 3.4×10^{-10} for 10msec, 8.7×10^{-11} for 0.1 sec, 1.6×10^{-10} for 1sec, 4.5×10^{-10} for 10sec, and 4.8×10^{-9} for 100 sec. The data was quantum limited from 1msec to 200 msec. The long-term degradation was caused by a drift in the Faraday rotator. A method for correcting the Faraday rotator drift is suggested.

Accession For	
NTIS GRA&I	<input checked="" type="checkbox"/>
DTIC TAB	<input type="checkbox"/>
Unannounced	<input type="checkbox"/>
Justification	
By _____	
Distribution/	
Availability Codes	
Dist	Avail and/or Special
A	



AFIT/GEP/PH/82D-28

ULTRA-STABLE LASER CLOCK

THESIS

Roger L. Facklam, B.S.

AFIT/GEP/PH/82D-28 1st Lt USAF

Approved for public release; distribution unlimited.

AFIT/GEP/PH/82D-28

ULTRA-STABLE LASER CLOCK

THESIS

Presented to the Faculty of the School of Engineering
of the Air Force Institute of Technology
Air University
in Partial Fulfillment of the
Requirements for the Degree of
Master of Science

by

Roger L. Facklam, B.S.

1st Lt USAF

Graduate Engineering Physics

March 1983

Approved for public release; distribution unlimited.

ACKNOWLEDGEMENTS

The experimental part of this effort required the help of certain people at the Sudbury, Massachusetts plant of the Raytheon Corporation. I wish to thank Jim Matthews for approving and supporting this effort; Al Zampello and his group for building the electronics package, as well as support in electronic debugging during the test; Bill Nelson for lab support during the experiment; Irl Smith and Terry Dorschner from Raytheon's Research Division in Waltham, Massachusetts, for discussions on laser theory; and Bob Gauthier, for help in setting up and coordinating the Raytheon part of the experiment. While Raytheon personnel and facilities were instrumental in completing this effort, the theory and interpretation of the results are those of the author except where noted. This effort used equipment which had evolved during early stages of the ring laser gyro program; and as a result, the information contained here-in is not representative of the current state of the art for laser gyroscopes.

At Wright-Patterson AFB, I wish to thank Ron Ringo, Branch Chief of the Reference Systems Branch at the Air Force Wright Aeronautical Laboratories, for supporting my effort; Bob Witters, Group Leader of the Reference Systems Technology Group, for his continuing technical and managerial support; Jerry Covert, for many discussions on clock application and listening to laser physics discussions; Nick Yannoni and Ferdinand Euler from Rome Air Development Center, Hanscom AFB, for background material on clocks and timing.

At the Air Force Institution of Technology, I wish to thank Dr Leno Pedrotti, Head and Professor of the Physics Department, for

his discussions on laser physics and academic support; Major M. R. Stamm and Dr W. B. Roh, for serving on the thesis committee. Finally, I wish to thank Colonel Hugo Weichel, adjunct professor, for chairing the thesis committee and providing technical support.

CONTENTS

ACKNOWLEDGEMENTS	ii
LIST OF FIGURES	vi
LIST OF SYMBOLS	viii
LIST OF TABLES	xii
ABSTRACT	xiii
I. STATEMENT OF PROBLEM	1
II. INTRODUCTION	2
III. REVIEW OF PRECISE CLOCKS AND STABILIZED LASERS	4
CLOCKS	4
QUARTZ CLOCK	5
ATOMIC CLOCKS	9
HYDROGEN MASER	13
CLOCK SUMMARY	15
LASERS	15
LINEAR LASERS	16
RING LASER GYROS	19
LASER SUMMARY	24
IV. THEORY	25
RATE EQUATIONS	26
LINEWIDTHS	26
EMPTY CAVITY LINEWIDTHS	28
QUANTUM LIMIT	30
MULTIMODE OPERATION	31
FARADAY ROTATOR	35
DISPERSION	37

	CLOCK OPERATION	38
	RECOMMENDED CLOCK/GYRO OPERATION	41
	RECOMMENDED METHOD OF TUNING/SETTING	44
V.	EXPERIMENT	47
	CLOCK ELECTRONICS	47
	EXPERIMENTAL SETUP	48
	SUMMARY OF EVENTS	50
VI.	RESULTS	56
	LASER #18	56
	LASER #68	56
	ERROR ANALYSIS	60
	POTENTIAL ERROR SOURCES	65
VII.	SUMMARY AND CONCLUSIONS	69
VIII.	RECOMMENDATIONS	72
	RECOMMENDATIONS FOR CURRENT RING LASER GYROS	72
	RECOMMENDATIONS FOR OTHER RING LASER GYROS	72
	RECOMMENDATIONS FOR OTHER TYPES OF LASER	72
	BIBLIOGRAPHY	75
	APPENDIX A: QUANTUM LIMIT	80
	APPENDIX B: NON-PLANAR CAVITY	96
	APPENDIX C: FARADAY ROTATOR	103
	APPENDIX D: DISPERSION	111
	VITA	121

LIST OF FIGURES

FIGURE		PAGE
1	TEMPERATURE COMPENSATION CIRCUIT	6
2	COMPARISON OF CLOCKS	8
3	RUBIDIUM ATOMIC CLOCK	10
4	CESIUM ATOMIC CLOCK	12
5	HYDROGEN MASER	14
6	STABILIZED LASER	17
7	SATURATED ABSORPTION STABILIZATION	18
8	OPTICAL BEAM	20
9	RING LASER GYRO	21
10	RLG LOCK-IN	23
11	GAIN CURVE	29
12	FOUR MODES ON GAIN CURVE	33
13	FOUR MODES ON GAIN CURVE	34
14	FOUR MODES ON GAIN CURVE (WITH FARADAY ROTATOR)	36
15	DISPERSION CURVE FOR TWO ISOTOPE MIXES	39
16	TOTAL FREQUENCY PULL-IN AS A FUNCTION OF DETUNING	40
17	CLOCK ELECTRONICS	42
18	RECOMMENDED ELECTRONICS	43
19	USER DEFINED FREQUENCY	45
20	EXPERIMENT SET-UP	49
21	STABILITY DATA GATHERED WITH LASER #18	57
22	STABILITY DATA GATHERED WITH LASER #68	58
23	STABILITY DATA GATHERED WITH LASER #68	59
24	STABILITY COMPARISON	61
25	ERROR ANALYSIS	63

FIGURE		PAGE
26	TEMPERATURE DRIFT	64
27	ESTIMATED PERFORMANCE WINDOW	73
28	TIME DEPENDENCE OF LASER LINEWIDTH	87
29	ELECTRIC FIELD PHASOR	89
30	PHOTON DISTRIBUTION	93
31	MODE STRUCTURE	97
32	NON-PLANAR CAVITY	98
33	NORMAL ZEEMAN EFFECT	104
34	FARADAY ROTATOR EFFECTS ON RING LASER GYRO	107
35	EFFECTS OF TEMPERATURE ON FREQUENCY PULL-IN	112
36	LARGE TEMPERATURE EFFECTS ON FREQUENCY PULL-IN	114
37	SMALL TEMPERATURE EFFECTS ON FREQUENCY PULL-IN	116
38	INTENSITY RATIOS	118
39	POSSIBLE INTENSITY RATIOS	119

LIST OF SYMBOLS

1. A circular enclosed area
2. α average distributed loss
3. α_e coefficient of expansion of the Faraday rotator
4. α_j temperature coefficient of the index of refraction
5. $|B|$ magnetic field magnitude
6. β ratio of spontaneous to stimulated photons
7. β_0 propagation constant
8. c speed of light
9. Δf frequency error of signal
10. Δf_{beat} frequency offset in clock
11. Δf_F change in Faraday frequency shift
12. Δf_p frequency limit on path length control
13. ΔE uncertainty in the energy
14. $\Delta \phi_k$ phase error of signal averaged over τ
15. $\Delta \phi$ uncertainty in phase
16. $\Delta \rho_F$ Faraday rotator phase shift
17. $\Delta \phi_{\text{rms}}$ root mean square phase noise
18. $\Delta \phi_\tau$ phase uncertainty for integration time
19. Δi drift current
20. Δn uncertainty in photon number
21. τ_R radiative lifetime
22. $\Delta \nu_C$ cavity linewidth
23. $\Delta \nu_D$ doppler broadened linewidth
24. Δf_G gyro beat frequency
25. $\Delta \nu_Q(\tau)$ quantum limited laser linewidth
26. $\Delta \omega$ uncertainty in angular frequency

27. $\Delta\omega_\tau$ uncertainty in angular frequency for an integration time τ
28. $\Delta\omega_T$ uncertainty in angular frequency for an integration time T
29. E_C energy of laser radiation field inside resonator
30. E_i i^{th} component of electric field ($i = x, y, z$)
31. E' electric field after one pass through resonator
32. $E_{r,l}$ electric field vector, $r =$ right hand circularly polarized;
 $l =$ left hand circularly polarized
33. $E'_{i,f}$ initial/final total electric field
34. E'_o electric field for a single photon with frequency
35. f_{ccw} counter-clockwise frequency
36. f_{cw} clockwise frequency
37. f frequency shift due to Faraday rotator
38. $!$ symbolizes one round trip of the cavity
39. $\gamma(\nu)$ gain as a function of frequency
40. i_d discharge current
41. K stimulated emission coupling coefficient
42. k Boltzman constant
43. L circumference of ring laser cavity
44. L_F pathlength through Faraday rotator
45. l distance between resonator mirrors of linear laser
46. M atomic mass
47. m_e mass of an electron
48. N_2 instantaneous population of upper laser level
49. N_1 instantaneous population of lower laser level
50. n number of cavity photons per mode
51. n_i index of refraction
52. λ wavelength of laser light

53. ν_c normal frequency of the clock
54. ν_{beat} empty cavity beat frequency
55. ν'_{beat} beat frequency with dispersion
56. ν_{clock} clock frequency
57. ν_d desired frequency
58. $\nu_{d,\text{tot}}$ total frequency pull-in
59. $\nu_{d,i}$ frequency pull-in of mode i
60. ν_{FSR} free spectral range
61. ν_i frequency of mode i
62. ν_o frequency of oscillation at line center
63. ν_{OBS} frequency observed by an atom moving at velocity V_x
64. ν_{oc} frequency seen by a rest atom
65. P power dissipated
66. Q quality factor
67. QLC quantum limited clock stability
68. q mode number
69. R_i reflectivity of mirror i
70. θ_F angle between magnetic field and direction of light propagation
71. T temperature
72. τ_c cavity photon
73. σ_x standard deviation of function
74. $\sigma_y(\tau)$ two sample deviation for time τ
75. τ integration time
76. ϕ phase
77. V Verdet constant
78. $\text{VAR}(X)$ variance of X

- 79. V_x velocity component in +x direction
- 80. ω_0 angular frequency of oscillation
- 81. Ω angular rotation rate

LIST OF TABLES

TABLE		PAGE
I	COMPARISON OF CLOCKS	7
II	EXPERIMENT SUMMARY	51

ABSTRACT

The Air Force has a requirement for a high accuracy Helium-Neon Ring Laser Gyro (RLG) and a high accuracy clock. The author has devised a method (patent applied for) whereby a multi-oscillator RLG can be used simultaneously as a gyro and as a clock. The device uses a multi-frequency laser oscillator with an auxiliary detector to sense a 583 MHz beat frequency and necessary electronics to produce a 5 MHz clock signal. The experiment was conducted at the Sudbury, Massachusetts plant of Raytheon Corporation. The square root of the Allan variance was measured for several different sample times. The best data obtained, for the given times, was 4.6×10^{-10} for 1 msec, 3.4×10^{-10} for 10 msec, 8.7×10^{-11} for 0.1 sec, 1.6×10^{-10} for 1 sec, 4.5×10^{-10} for 10 sec, and 4.8×10^{-9} for 10^2 sec. The data was quantum limited from 1 msec to 200 msec. The long-term degradation was caused by a drift in the Faraday rotator. A method for correcting the Faraday rotator drift is suggested.

10 to 100 msec 10^-10
10 to 100 sec 10^-9

I STATEMENT OF PROBLEM

A current Air Force problem is to provide high accuracy timing for fighter aircraft. The clock must operate between -50°C and $+75^{\circ}\text{C}$ with intermittent temperatures to $+95^{\circ}\text{C}$. The clock must also operate under a 6g load during an aircraft maneuver and up to a 10g maximum load for vibration. Current timing sources are heated to above $+75^{\circ}\text{C}$ so that the clock can use the environment as a heat sink. To achieve this temperature the clocks must first be warmed up and then allowed to stabilize. The process of thermal stabilization needs to be reduced or eliminated because aircraft cannot set on the runway while waiting for the clock to stabilize. Another consideration is the cost, which is \$40,000 for an aircraft grade Cesium atomic clock. The Air Force has requirements for high accuracy clocks that do not degrade under acceleration and have a lower unit system cost.

Ring laser gyros are now being developed for use in fighter aircraft. The ideal solution to the above stated problem is an adaptation of a ring laser gyro to provide both a clock frequency for timing and information for navigation.

The purpose of this thesis is to demonstrate the feasibility of using a multi-frequency ring laser to provide timing information while operating as a laser gyroscope.

II INTRODUCTION

Certain military applications (such as bi-static radar, secure/anti-jam communications, and aircraft identification avionics) require high accuracy timing sources. Current high accuracy timing sources need to be improved in the following areas: accuracy under acceleration, reductions in volume, weight, power consumption, acquisition cost, life cycle cost, and warm-up time.

One possible solution is the use of ring laser gyros, since these devices will be used in future military aircraft for rotation rate sensing. The advantages of the laser approach are smaller size, fast warm-up, low sensitivity to g loads, and reduced cost. The laser provides the timing frequency for the laser clock. The only additional requirement is the detection and output electronics. The electronics tested had a volume five (5) times smaller than a miniature rubidium oscillator. The additional volume can be reduced by replacing the clock present in the inertial measurement unit. Proper packaging and miniature electronic components will further reduce size. Power for the clock can be provided through the inertial measurement unit and will not require a separate source. The estimated additional cost of clock electronics is approximately \$2,000.00. This would reduce acquisition cost by a factor of twenty.

The scope of this effort is both theoretical and experimental with the key issue being the laser clock accuracy. Laser clock accuracy is determined by the stability of the optical path length and the theoretical section will cover the error sources that lead to

instability in the optical path length. The practical areas of clock operation will be included in this section. The experimental section will cover frequency stability measurements, the experiment performed, the result obtained, and a comparison of results. The effort was not to reach any predetermined performance level but to establish feasibility and determine the laser clock performance capability.

The background section covers quartz oscillators, atomic clocks, the hydrogen maser, linear lasers, and ring laser gyros. The theory section covers rate equations, linewidths, multi-mode operations, Faraday rotator, dispersion, clock operation, recommended clock/gyro operation, and a recommended method of tuning/setting. The experiment section covers the clock electronics, the experiment setup, and a summary of events. The results section includes test results, error analysis, and potential error sources. Finally, the conclusions and recommendations for further work are presented.

III REVIEW OF PRECISE CLOCKS AND STABILIZED LASERS

The background information will be covered in two sections. The clocks section covers the quartz oscillator, the rubidium atomic clock, the cesium atomic clock, and the hydrogen maser clock. The lasers section describes stabilized linear and ring laser gyro technology.

CLOCKS

Clocks interface with other devices by providing a constant frequency output. There are two classes of clocks. The first class includes atomic clocks and hydrogen masers, which are stabilized by electronic circuitry to a very narrow atomic transition. These are known as frequency standards because they have the same frequency every time they restart due to the stability of the atomic transition. The second class includes quartz oscillators and the laser clock, which are not stabilized to an atomic transition. These are known as transfer frequency standards because they must be set to an external standard after a cold start. The Q of the clock's resonator is given on each figure as the individual clock types are discussed. As Q increases the resonator's linewidth decreases and the resonator's ability to store energy increases. A more detailed discussion of Q is given in Chapter IV.

The standard method to characterize frequency stability in the time domain was established in 1971 by the Subcommittee on Frequency Stability of the Technical Committee on Frequency and Time of the IEEE Group on Instrumentation and Measurement (Ref 1: 105). The frequency

stability is expressed by the normalized root mean square of the difference between adjacent pairs of frequency measurements. An estimate of the two-sample standard deviation, $\sigma_y(\tau)$, the square root of the Allan variance, is given by

$$\sigma_y(\tau) = \frac{1}{\nu_c} \sqrt{\frac{m}{\sum_{k=1}^m (\Delta f_{k+1} - \Delta f_k)^2}} \quad (1a)$$

$$\Delta f_k = \frac{\Delta \phi_k}{2\pi\tau} \quad (1b)$$

where ν_c is the normal clock frequency, τ is the integration time,

$\Delta \phi_k$ is the integrated phase error, Δf_k is the k^{th} measurement of frequency, and m is the number of data pairs (Ref 1: 105).

QUARTZ CLOCK

A quartz clock uses the piezo-electric property of a quartz crystal oscillator. When a quartz crystal vibrates, a difference of electric potential is produced between two of its faces (Ref 2: 192). When a resonant circuit is used with a quartz crystal, the circuit and the oscillator operate at the same frequency. The resonant frequency of a quartz oscillator drifts with a change in temperature. This drift must be corrected if high accuracy is required. A typical temperature compensation circuit, which approximately corrects the temperature dependent frequency drift, is shown in Figure 1.

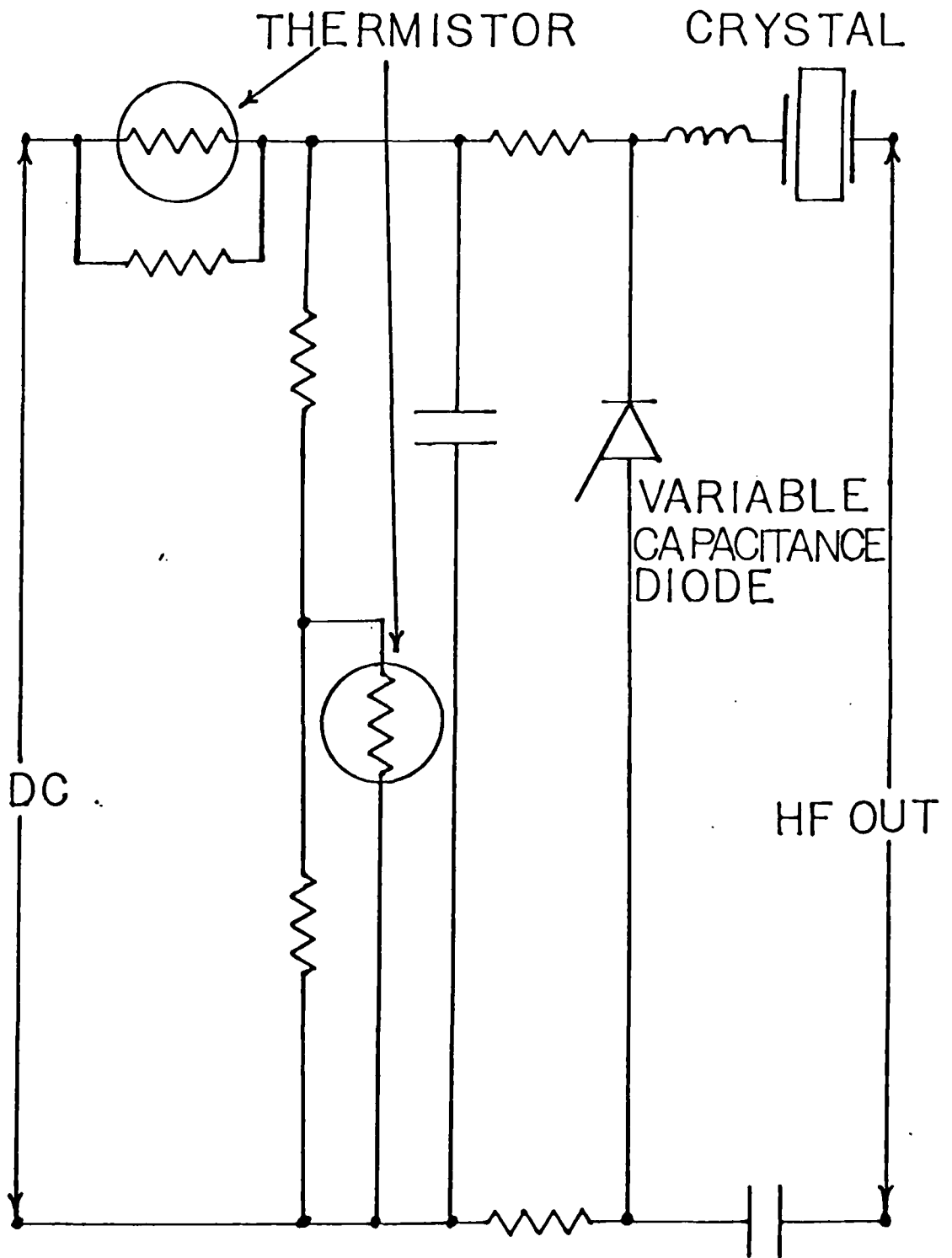


FIGURE 1 TEMPERATURE
COMPENSATION CIRCUIT (REF 3:113)

The advantages of quartz oscillators are their small size, light weight, and ruggedness. Quartz oscillators are also inexpensive when compared to atomic clocks. The disadvantage of quartz oscillators is their requirement for temperature compensation, which becomes an increasingly difficult task as the level of accuracy increases. Their output must also be corrected for acceleration effects when used on an accelerating platform (Ref 4). For a comparison of size and other data, see Table I; and for a comparison of accuracy, see Figure 2. Figure 2 is a plot of the square root of the Allan variance as a function of measurement time in seconds. A value of 1×10^{-10} for the square root of the Allan variance represents an accuracy of ± 1 sec in 318 years. The short term accuracy of a typical atomic clock improves as time increases, through the relationship $\tau^{-\frac{1}{2}}$. We see from Figure 2 that for 100 second measurement times, the most accurate clock is the hydrogen maser and the least accurate clock is the quartz clock.

Table I.
COMPARISON OF CLOCKS

	VOL $\times 10^3$ CM ³	WEIGHT Kg	POWER Watts	WARM-UP TIME(Min)	PRICE X\$1,000	REF
QUARTZ	.22	.31	2	10	1	6
RUBIDIUM	23.5	13.5	15.4	60	13.5 (Base)	6
CESIUM	34.2	22.7	48	20	26.0 (Base)	6
SMALL H MASER	100	45	20	NO DATA	NO DATA	5
LARGE H MASER	1000	200	30-100	NO DATA	100	5

- ① REF 5 LC OSCILLATOR
- ② REF 6 Cs CLOCK
- ③ REF 6 Rb CLOCK
- ④ REF 6 QUARTZ
- ⑤ REF 5 LARGE H MASER
- ⑥ REF 5 SMALL H MASER

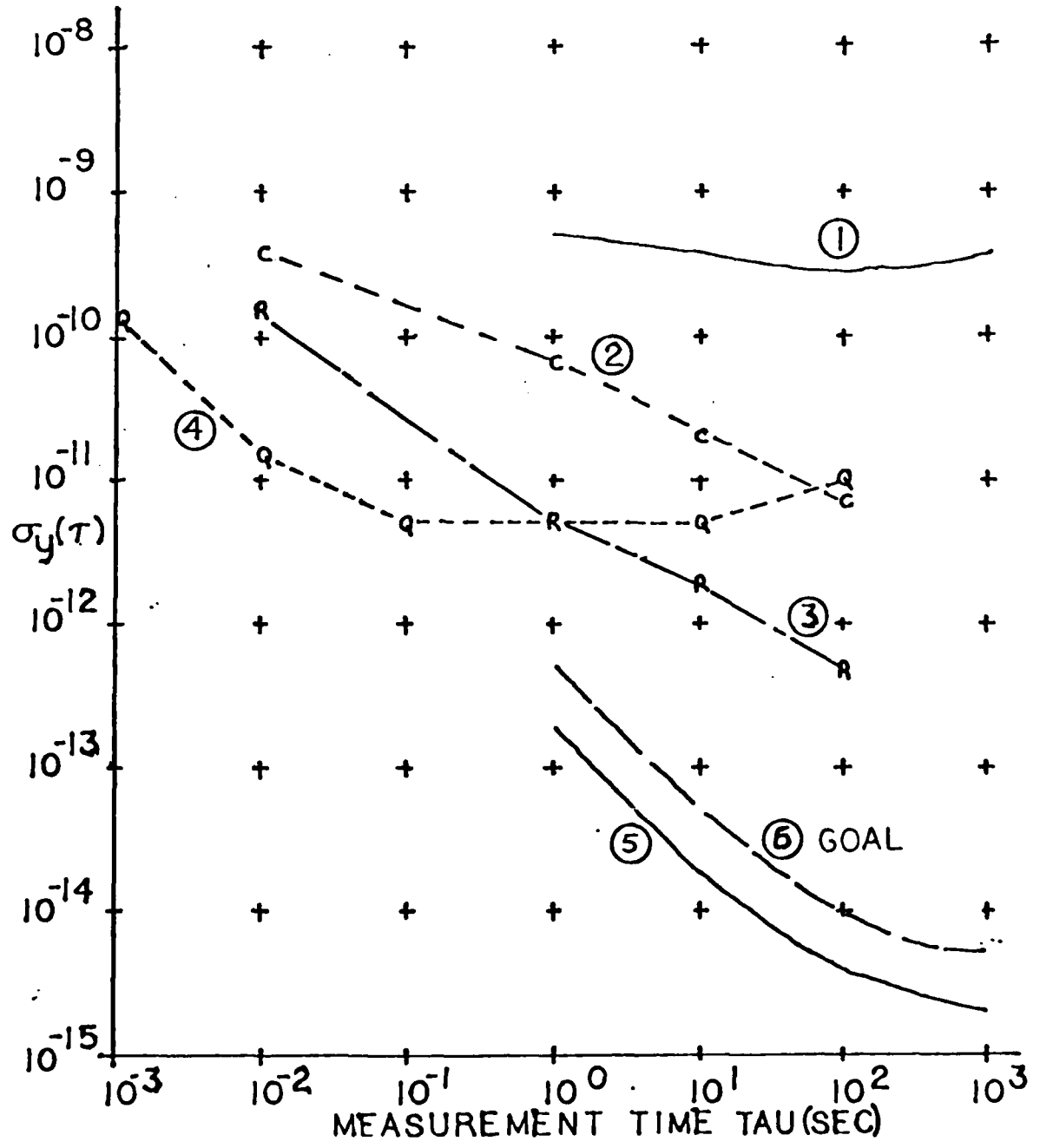


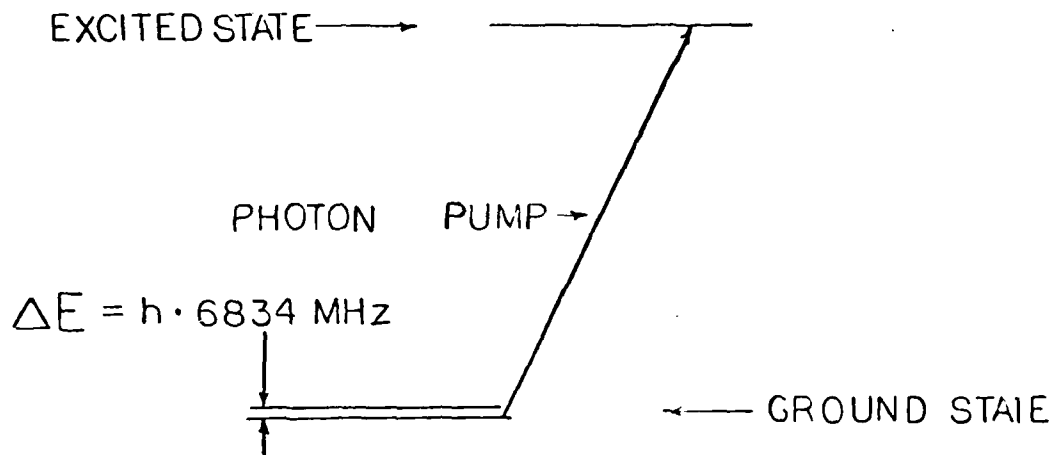
FIGURE 2 COMPARISON OF CLOCKS

ATOMIC CLOCKS

An atomic clock is a quartz oscillator whose frequency is stabilized with the aid of an atomic absorption line. The atomic frequency in the case of rubidium is the 6,834 Mhz ground-state hyperfine transition and in the case of cesium is the 9,192 Mhz ground-state transition. This transition is due to a spin flip of the electron. The atom is in the lowest state when the electron magnetic moment is aligned anti-parallel with the nuclear magnetic field. The frequency of the photon needed to change the alignment to parallel is 6834 MHz in the case of rubidium. Atomic clocks consist of a cesium or rubidium cell, a quartz oscillator, and supporting electronics. They combine the short term stability of the quartz oscillator and the long term stability of the atomic absorption line.

The rubidium atomic clock schematic is shown in Figure 3A. The output of the voltage controlled crystal oscillator (VCXO) is multiplied and combined with the signal from the frequency synthesizer to produce the nominal 6834 MHz resonant rubidium frequency. This signal is applied to the microwave cavity surrounding the Rb 87 resonance cell through which light from the rubidium lamp also passes. The light from the rubidium lamp is filtered so that it excites the Rb 87 in the resonant cell from the lower level of the ground-state hyperfine transition to an upper electronic level as shown in Figure 3B. The atom then decays to the ground-state with an equal probability of going into either the upper or lower state. After several pumping cycles all the ground-state atoms are pumped into the upper hyperfine level. At the Rb 87 resonance, the nominal 6834 MHz

(B) ENERGY LEVEL DIAGRAM



(A) SCHEMATIC OF RUBIDIUM ATOMIC CLOCK

$Q = 10^7 - 3 \times 10^7$

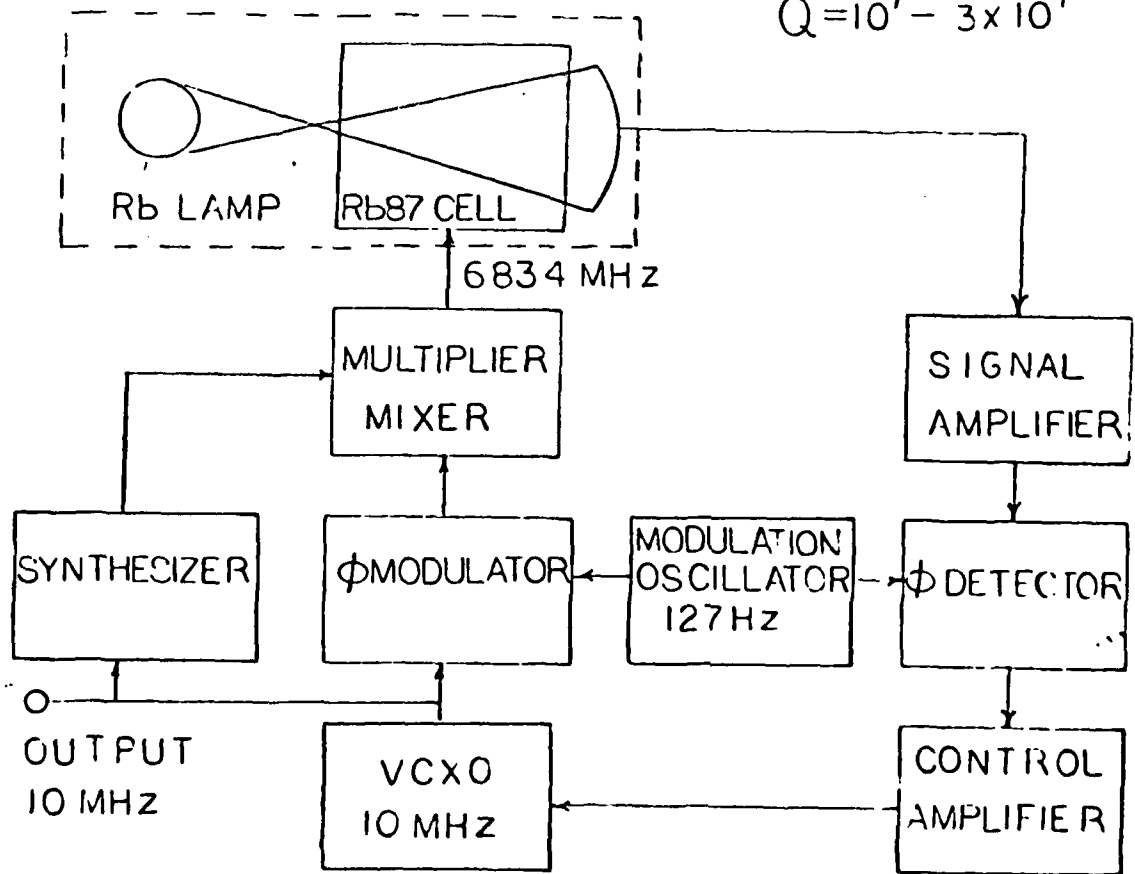


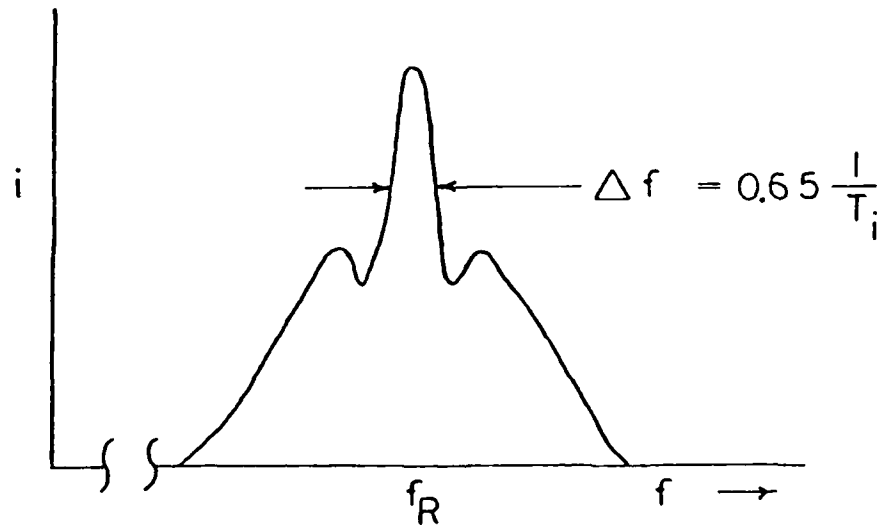
FIGURE 3 RUBIDIUM ATOMIC CLOCK (REF 7)

signal causes stimulated emission of Rb 87 atoms from the upper hyperfine state to the lower hyperfine state, thus increasing the number of Rb 87 atoms which can absorb the light (photons) from the rubidium lamp. When the nominal 6,834 MHz signal corresponds to the Rb 87 atomic resonance, the transmission of rubidium light through the resonant cell decreases and the output optical power decreases. The optical output signal from the Rb 87 resonant cell is sensed by the photo detector and a control signal is developed to steer the frequency of the voltage-controlled crystal oscillator (VCXO) to achieve Rb 87 absorption line center. Sensing of the Rb 87 absorption line center is done by varying the nominal 6834 MHz signal by ± 127 Hz and determining the change in the optical output signal.

The advantages of the rubidium clock are a high degree of short-term stability and better long-term stability than the quartz clock. The disadvantage is that the frequency has a weak dependence on buffer gas mixture and must be calibrated. Since rubidium clocks use a quartz oscillator, they must be temperature and acceleration corrected. (See Figure 2 and Table I for a comparison of other data).

The cesium atomic clock is constructed as shown in Figure 4. The components shown in Figure 4 are all enclosed within a vacuum. Magnetic shields to eliminate environmental fields and current conductors to introduce a controlled C field in the interaction region are not illustrated in Figure 4. The pressure in the cesium clock is typically 10^{-7} to 10^{-8} Torr. The beam of cesium atoms moves with a thermal velocity from the atomic source to the detector. The upper hyperfine state, spin up, is selected by the first state selector magnet. The atoms then move through a Ramsey type microwave cavity

$$Q = 10^7 - 3 \times 10^8$$



↑↑ UPPER HYPERFINE LEVEL
 ↑↓ LOWER HYPERFINE LEVEL

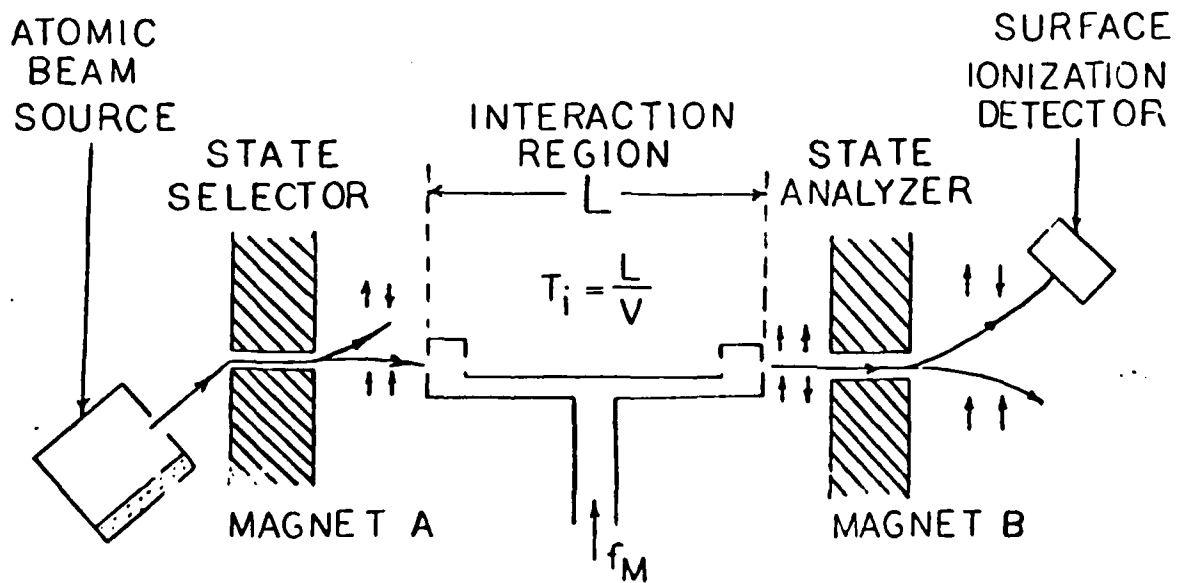


FIGURE 4 CESIUM ATOMIC CLOCK (REF 8:119)

where the atoms interact with the microwave radiation. When the input frequency, f_M , is on resonance the atoms decay to the lower hyperfine level. The states are again separated by another state separator magnet. The maximum number of stimulated emission transitions, from the hyperfine level, occurs when the signal frequency is at line center. This effect is used to control a quartz oscillator as in the case of the rubidium clock. The upper part of Figure 4 shows the actual profile which is a function of the length of the interaction region. This implies that for a fixed velocity the larger the interaction region the higher accuracy. The cesium clock uses an application of the Stern-Gerlach experiment (Ref 9: 254- 256).

The advantages of cesium atomic clocks are high frequency reproducibility and good long-term stability. The cesium frequency is used as the world standard. The disadvantages are problems with temperature and acceleration effects. Also, the cesium clock must be shielded from external magnetic fields. As a result, the cesium clock is one of the most sensitive magnetometers in existence. For a comparison of size and other data, see Table I. For a comparison of accuracy, see Figure 2.

HYDROGEN MASER

Another high accuracy frequency source is the hydrogen maser. The hydrogen atom has a hyperfine ground-state transition whose resonant frequency is 1,420 MHz. The first hydrogen maser was built at Harvard in 1960 (Ref 8: 117). A schematic of the hydrogen maser is shown in Figure 5. Helmut Hellwig describes the hydrogen maser as follows (Ref 10: 216).

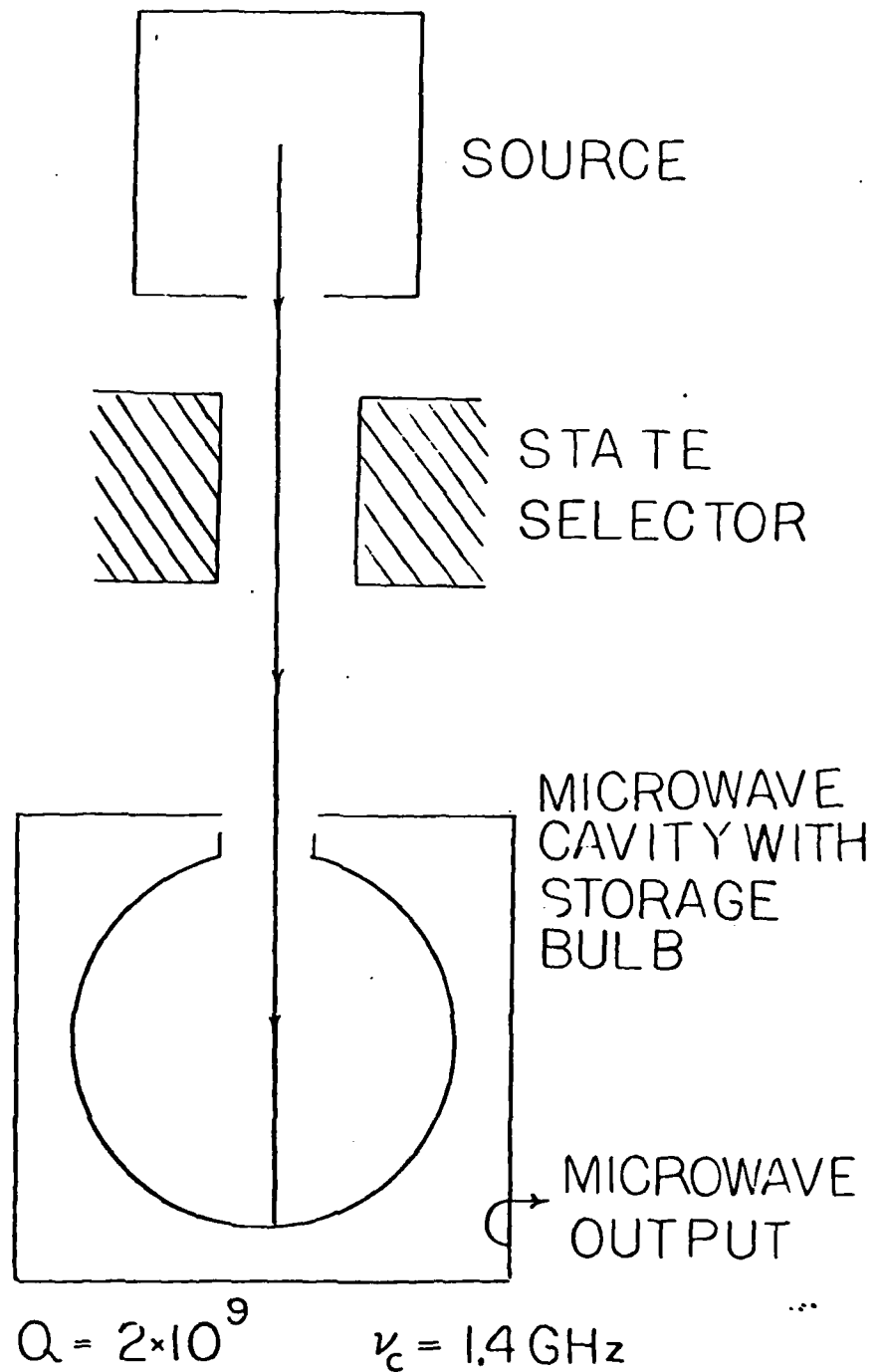


FIGURE 5 HYDROGEN MASER (REF 10:216)

"The hydrogen is produced usually by a radio frequency discharge from molecular hydrogen. The beam then emerges in a vacuum, passes a state hexapole magnet and enters a quartz vessel whose inside is lined with fluorocarbon coating. This storage bulb is located inside of a microwave cavity. If the cavity losses are low enough, self-sustained oscillations occur and a microwave output is generated." The output electronics is the same as shown in Figure 3A. The output frequency of a VCXO is multiplied up to the hydrogen resonant frequency. This signal is then scanned across the resonance to determine the center frequency. The information about the center frequency is used to generate a control signal, which is applied to the VCXO.

The advantages of the hydrogen maser are high frequency stability (See Figure 2), and very good repeatability. However, presently hydrogen masers are large and very expensive devices (See Table I).

CLOCK SUMMARY

The previous sections were intended to give the reader a general idea of current clock technology. Figure 2 shows that the quartz clock has good short-term stability but it degrades at longer times due to aging of the crystal. Rubidium is about an order of magnitude better than cesium with both clocks' short term performance increasing as $\tau^{-\frac{1}{2}}$. The hydrogen maser is two orders of magnitude better than the rubidium clock. Reference 10:221 gives a partial list of researchers working on clocks.

LASERS

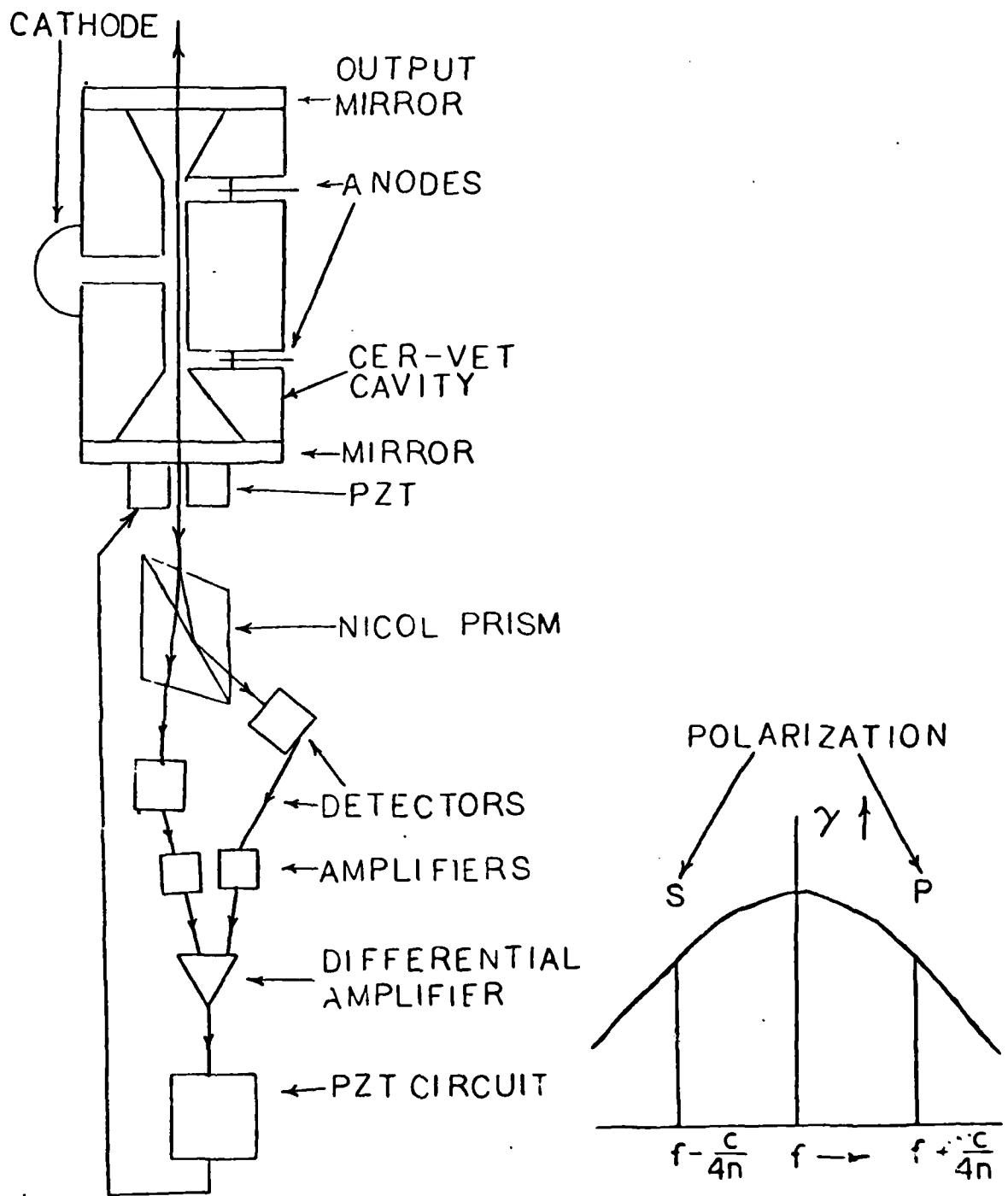
Lasers are currently being used for optical and infrared frequency standards. Both linear and ring lasers have been frequency stabilized. A frequency stabilized laser that has more than one output

frequency can beat two optical frequencies to generate a beat frequency in the 10^9 Hz range. This is the type of beat frequency used in the laser clock. This section will describe various stabilization methods.

LINEAR LASERS

Linear lasers can be frequency stabilized by several methods. Most methods do not have a frequency control that will allow ultra high stability. One possible method for high stability is to use a two-longitudinal mode linear inhomogeneously broadened laser. The frequency stability can be obtained by balancing the intensity of the s and p modes (Ref 29). Figure 6A shows a he-Ne laser built with a CER-VET cavity. This design uses a balanced discharge to minimize flow effects. The output is two beams, one with s polarization and one with p polarization, which is separated by the Nicol prism. The s and p intensities are measured and the difference is set to zero by means of a piezo-electric transducer (PZT), which adjusts cavity length. Figure 6B shows a gain curve with balanced intensities between s and p polarizations.

A second technique for laser stabilization is based on the method of saturated absorption shown in Figure 7. The light from the laser passes through a beam splitter and through a gas cell containing low pressure methane. The light reflects off a mirror and passes back through the cell. Then the light reflects from the beam splitter into a detector. The signal seen by the detector is at a minimum when the absorption in the cell is at a maximum. The detector signal is used to control a piezoelectric transducer (PZT) mounted on the rear mirror of the laser. This method has given good results but the 88 THz



(A) LINEAR LASER

(B) GAIN CURVE

FIGURE 6 STABILIZED LASER

$\nu = 88$ THZ REGION

$$Q = 10^9 - 10^{11}$$

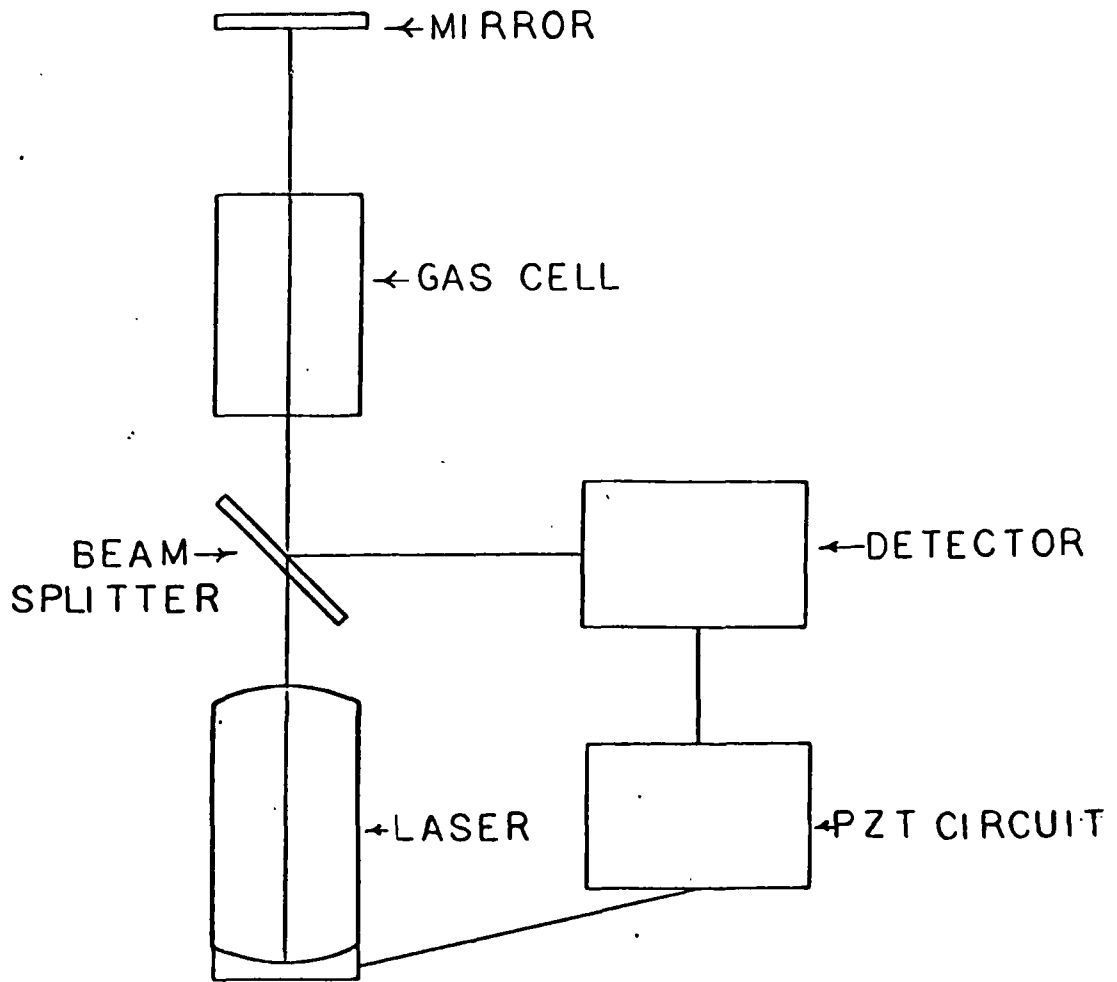


FIGURE 7 SATURATED ASORPTION STABILIZATION (REF 10:219)

methane resonant frequency ($\lambda = 3.39\mu\text{m}$) is too high to be used with current technology.

Another similiar method is shown in Figure 8. This method uses an iodine beam source and detects the fluorecence (detector displaced) or the absorption (detector in line) of the laser light. The laser uses argon ions whose output frequency contains the iodine resonance. The information from the detector pertaining to the position of the laser linecenter relative to the iodine resonance is then used to control the path length of the laser. This control is given by means of the PZT. This device has the problem of running at 583 THz ($\lambda = 515\text{nm}$) which is currently beyond easy electronic access, but does provide an optical frequency standard.

RING LASER GYROS

The simplest ring laser gyro (RLG) is shown in Figure 9 (Ref 11: 1- 6). The RLG is based on the fact that there is a difference in path lengths of the clockwise and counter-clockwise beams when the device rotates. If the gyro rotates clockwise then the clockwise beam has a longer round trip path length than the counter-clockwise beam. This shifts the frequency of the beams due to the boundary condition of the cavity. The beams are optically mixed with the output beat frequency being linearly proportional to the rotation rate. The beat frequency between two oppositely traveling beams is given by

$$\Delta f_G = f_{\text{CW}} - f_{\text{CCW}} = \frac{4A}{L\lambda} \Omega \quad (2)$$

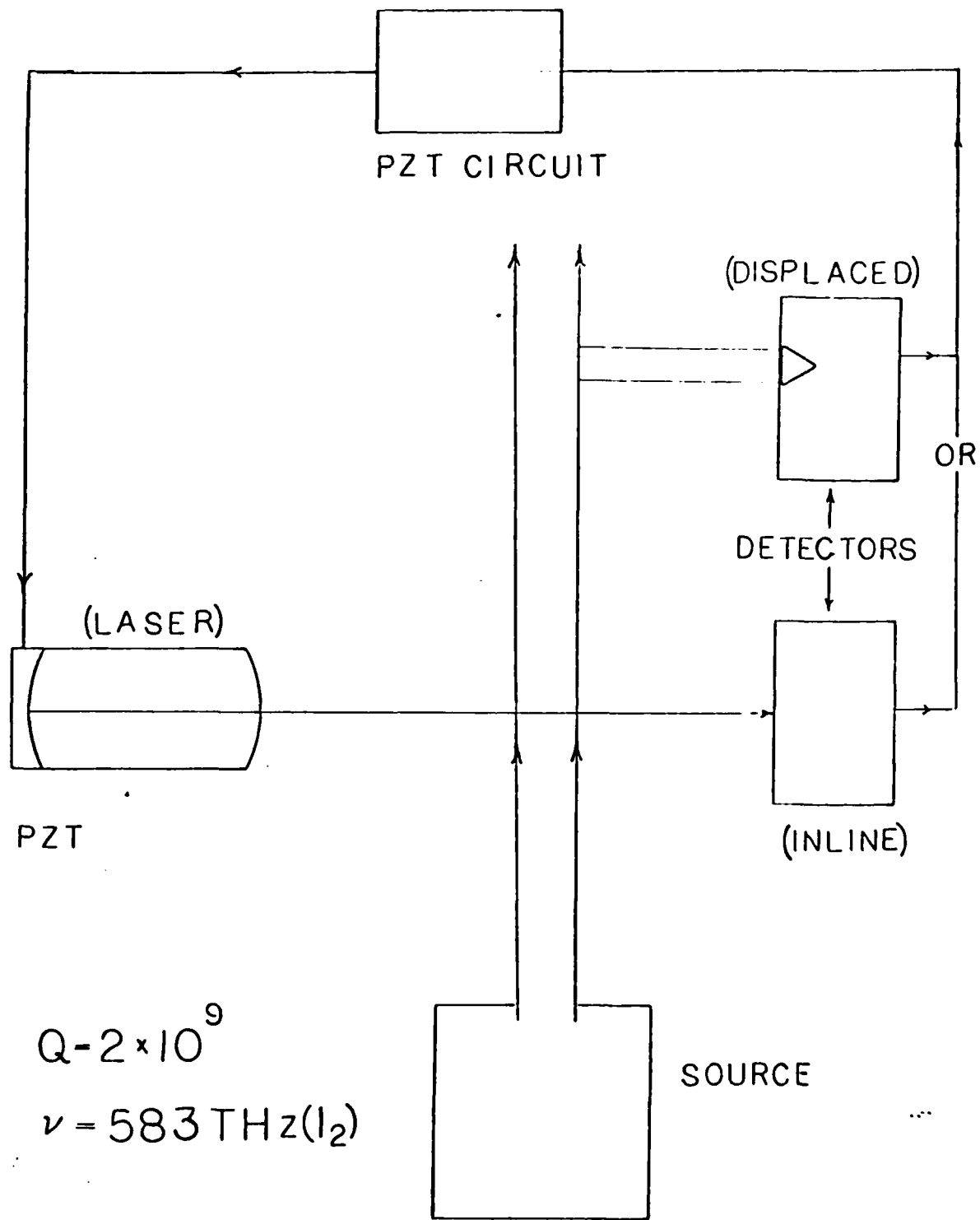


FIGURE 8 OPTICAL BEAM (REF 10:216)

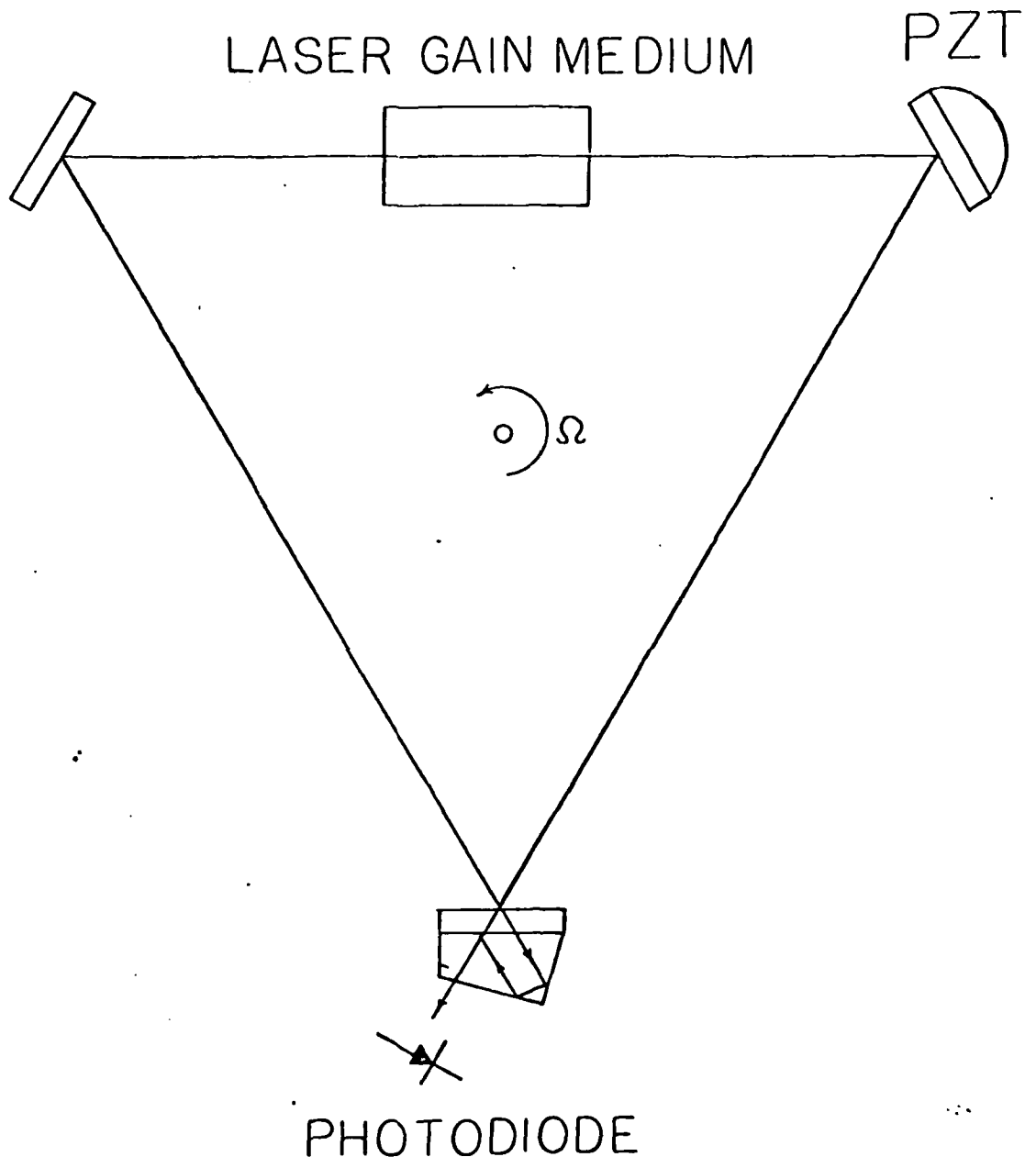


FIGURE 9 RING LASER GYRO(REF 111-6)

where Δf_G is the gyro beat frequency, f_{CW} is the clockwise (CW) frequency, f_{CCW} is the counter clockwise (CCW) frequency, A is the enclosed area, L is the circumference, λ is the wavelength and Ω is the angular rotation rate (rad/sec) (Ref 11: 1-6). The major problem with RLGs is lock-in. Lock-in is caused by an energy exchange between modes due to backscattering. Figure 10 is a plot of the ideal output frequency as a function of rotation rate. The solid line shows the ideal condition and the dotted line shows the lock-in band.

There are two types of lock-in compensation techniques: dithered and non-dithered. This section describes two dithered and four non-dithered techniques.

Mechanical dither is when the laser block is rotated back and forth at a mechanical resonance of typically 250 Hz. This is a first order compensation, because the gyro still spends an appreciable amount of time in the lock-in band and the non-linear region. The second dither technique is based on the use of a magnetic mirror. The magnetic mirror has a ferromagnetic material below the multilayer dielectric (MLD) coating which is above the substrate. The magnetic mirror uses the polar Kerr effect to rotate the plane of polarization. The magnetic mirror along with the cavity applies an optical bias which is alternated at about 5 Hz by means of an external electromagnet. This looks like a square wave correction because the current to the electromagnet is in the form of a square wave. The mechanical oscillation is by nature a sine wave a correction. The magnetic mirror system allows much less time in lock-in band because the correction given by the magnetic mirror changes sign in a very short time, whereas in the mechanical system the correction gradually changes

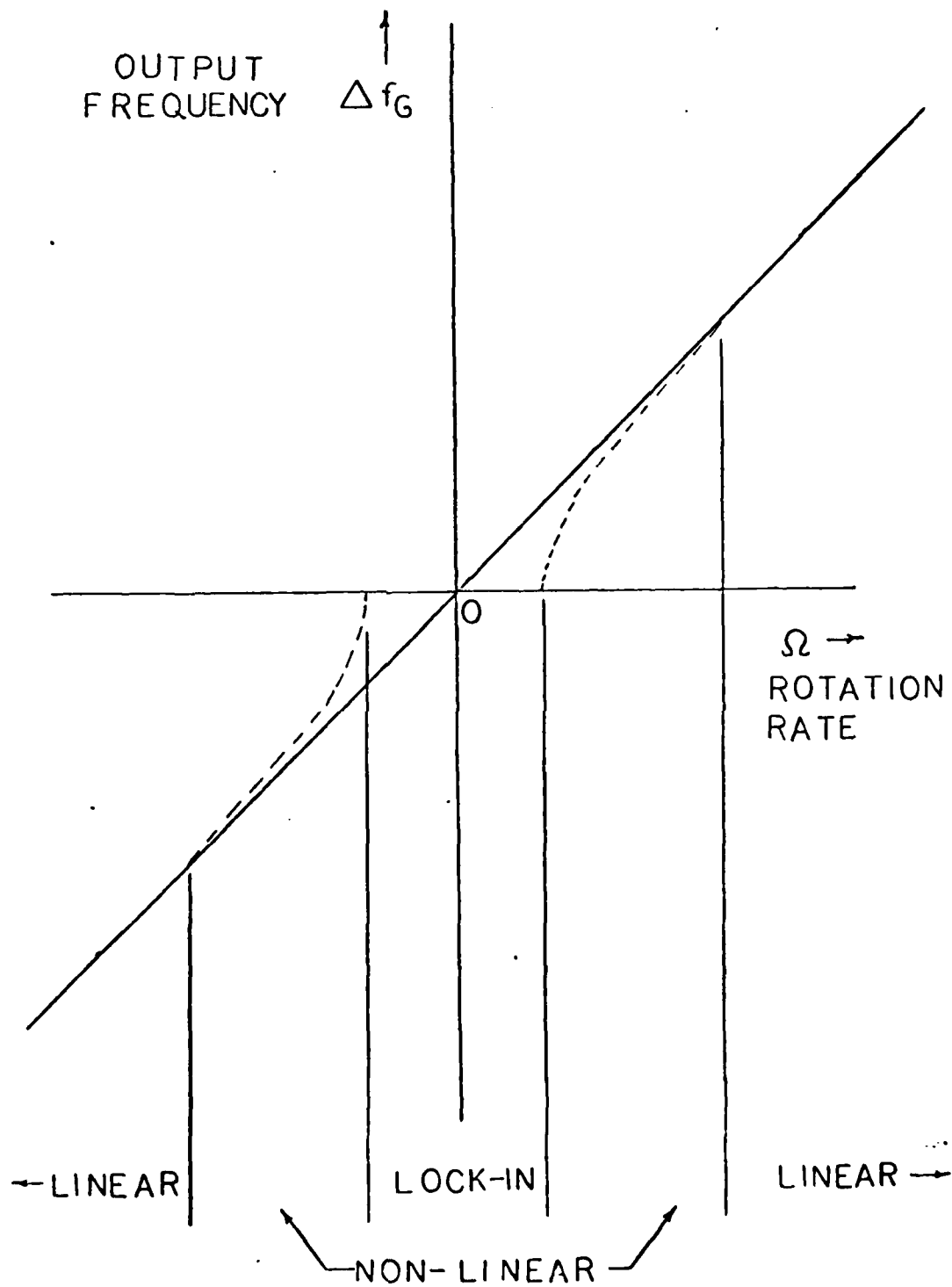


FIGURE 10 RLG LOCK-IN (REF 13:3)

sign. The longer the gyro stays in or near the lock-in region the greater will be the distortion in the data. Dithered gyros cannot be used as clocks because there are no stable frequencies.

The second type is referred to as a multi-frequency RLG. The first multi-frequency RLG used a quartz rotator as quarter wave plate to give left and right hand circularly polarized light. The left and right hand polarizations are further split by a Faraday rotator. See Appendix C (Figure 33) for more detail. The frequency splitting between the left and right hand modes is typically 500 MHz. The frequency splitting between clockwise and counter-clockwise traveling modes, given by the Faraday rotator, is typically 500 kHz. Another method is very similar, but uses a magnetic mirror instead of a Faraday rotator. The magnetic mirrors need not be dithered in this case. Any errors due to the magnetic mirror are biased out by taking the difference between the left hand polarization pair and the right hand polarization pair. A method using a $TEM_{q,0,0}$ mode and a $TEM_{q,0,1}$ mode instead of left and right hand polarizations is described in detail in Ref 12. The non-planar cavity method replaces the quartz rotator with an image rotating cavity. See Appendix B for more detail. The Faraday rotator is still required in this method. This is the configuration used in this paper.

LASER SUMMARY

There are several types of linear lasers that could be used for clock applications. The dithered type of RLG cannot be used as a clock but the multi-frequency gyro can be. The multi-frequency RLG can be used as a gyro and a clock simultaneously.

IV THEORY

The two desirable characteristics of a frequency standard are the narrowness of the signal in frequency space and the stability of the center frequency as a function of time. The ultimate narrowness of the laser clock frequency is determined by the quantum limited linewidth. Laser rate equations must be considered to determine the quantum limit. The following section covers linewidths in order of increasing narrowness. The atomic linewidth which determines gain curve of the laser is discussed first, then the empty cavity linewidth and finally the active cavity linewidth or the quantum limited linewidth. The first two will also be important in determining the effects of dispersion. The section on multimode operation describes the three ways to obtain 4 mode operation. The Faraday rotator section describes the physics of the Faraday rotator and the effects which cause instability in the linecenter frequency. The section on dispersion covers other effects which affect the stability of the optical path length. The clock operation section describes frequencies that were actually used in the clock. The next section describes the recommended clock/gyro operation. The final section describes the recommended method of timing/setting of the laser clock. This method allows the user to define the output frequency. In summary, this chapter covers laser rate equations, quantum limited linewidth, multimode operation, Faraday rotator, dispersion, clock operation, recommended clock/gyro operation and the recommended method of timing/setting.

RATE EQUATIONS

The rate equation of interest is the photon rate equation. This equation is given by

$$\frac{dn}{dt} = K(N_2 - N_1)n + KN_2 - n/\tau_c \quad (3)$$

where n is the instantaneous number of photons per cavity mode, N_2 is the instantaneous number of atoms in the upper laser level, N_1 is the instantaneous number of atoms in the lower laser level, τ_c is the cavity photon lifetime, and K is the stimulated emission coupling coefficient (Ref 31: 421). The ratio β of the spontaneous photons to stimulated photons is given by

$$\beta = \frac{1}{n} \frac{N_2}{N_2 - N_1} \quad (4a)$$

$$\beta = \frac{1}{n} \quad \text{for } N_2 \gg N_1 \quad (4b)$$

These equations will be applied in the next section.

LINEWIDTHS

The laser to be considered is a He-Ne laser with a transition in the visible with a wavelength of 6328Å. He-Ne lasers usually are Doppler broadened. Doppler broadening may result in inhomogeneous

broadening of the gain coefficient. The atoms see a doppler shift according to

$$\nu_{OBS} = \nu_{OC} (1 + V_x/c) \quad (5)$$

where ν_{OC} is the frequency seen by a rest atom, V_x is the velocity component in the direction of photon translation, and c is the velocity of light in the medium (Ref 4: 92). The atoms of the gas have a Maxwellian velocity distribution. The resulting gain curve has a Gaussian profile. The gain as a function of frequency $\gamma(\nu)$ is given by

$$\gamma(\nu) = \frac{c}{\nu_{OC}} \left(\frac{M}{2\pi kT} \right)^{\frac{1}{2}} e^{-\frac{M}{2kT} (c/\nu_{OC})^2 (\nu - \nu_{OC})^2} \quad (6)$$

where M is the atomic mass, k is the Boltzman constant, and T is the absolute temperature (Ref 14: 93). This can be rewritten as

$$\gamma(\nu) = \frac{2(1n2)^{\frac{1}{2}}}{\pi^{\frac{1}{2}} \Delta\nu_D} e^{-4(1n2)(\nu - \nu_{OC})^2 / \Delta\nu_D^2} \quad (7a)$$

where

$$\Delta\nu_D = 2 \nu_{OC} \sqrt{\frac{2(1n2)kT}{Mc^2}} \quad (7b)$$

and $\Delta\nu_D$ is the Doppler linewidth (Ref 14: 93,94). Taking $M = 20$ AMU for Ne^{20} and $T = 300$ °K, $\Delta\nu_D$ is about 1500MHz. Figure 11 shows a doppler broadened gain curve.

The free spectral range between two longitudinal mode of a linear optical resonator is given by

$$\nu_{\text{FSR}} = \frac{c}{2n_i l} \quad (8a)$$

For a ring laser, the free spectral range is given by

$$\nu_{\text{FSR}} = \frac{c}{n_i L} \quad (8b)$$

where l is the length of a linear laser (Ref 14:128), n_i is the index of refraction and L is the circumferencce of a ring laser (Ref 32: 19). The frequency of the q^{th} mode is given by

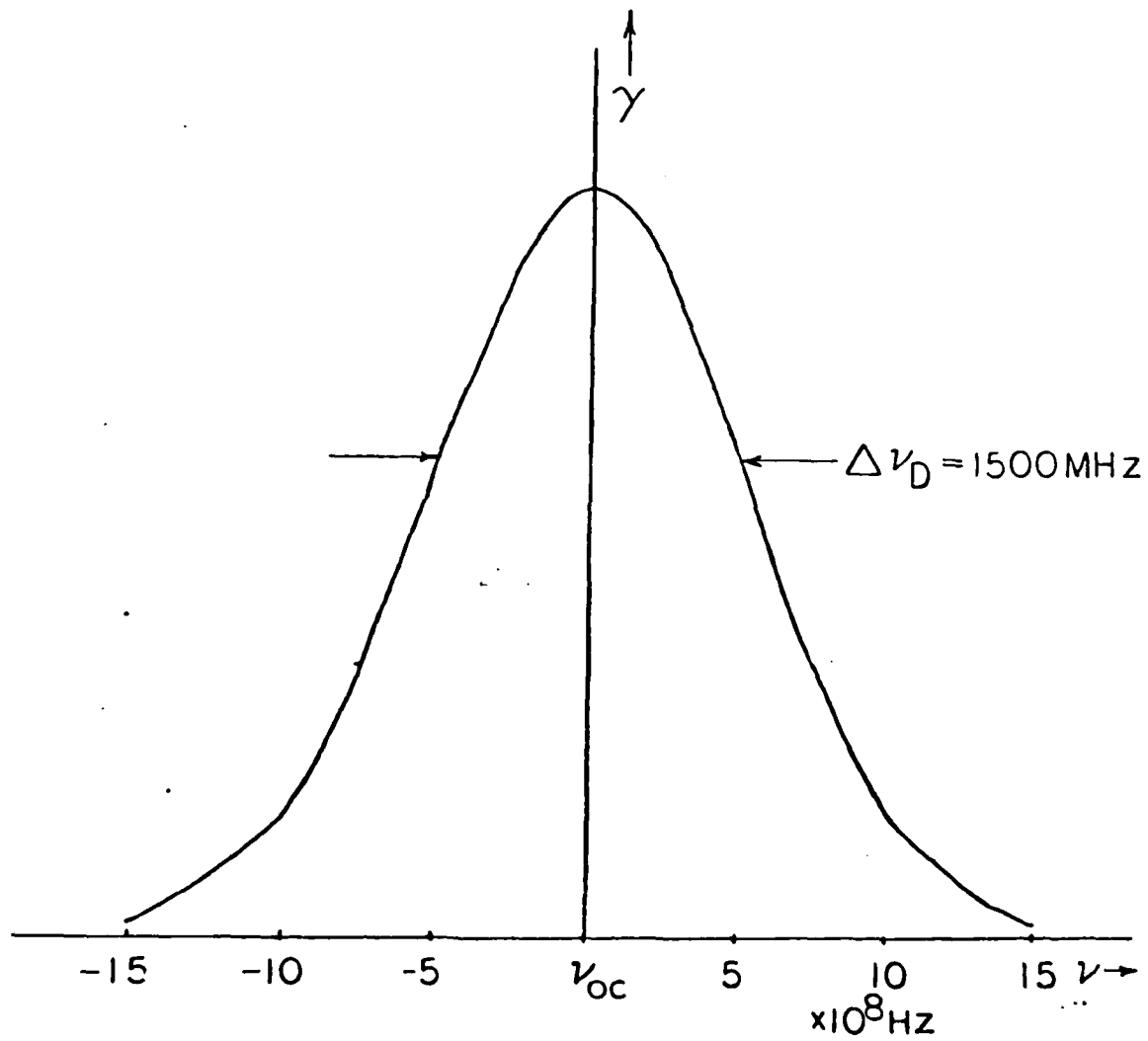
$$\nu_0 = q \nu_{\text{FSR}} \quad (9)$$

where q is the mode number.

EMPTY CAVITY LINEWIDTHS

The width of the cavity modes in frequency space is given by

$$\Delta\nu_c = \nu_0/Q \quad (10)$$



$$\nu_{oc} = 4.74 \times 10^{14} \text{ Hz}$$

FIGURE II GAIN CURVE

The Q of a resonator is a measure of the resonator's ability to store energy. As the Q of the resonator increases the resonator modes narrow in frequency space and the resonator stores more energy. The Q is given by

$$Q = \frac{2\pi\nu_0 E}{P} = 2\pi\nu_0 \tau_c = \frac{2\pi\nu_0 n_i}{c[\alpha - (1/l)\ln R_1 R_2]} \quad (11)$$

where ν_0 is the frequency of oscillation, E is the stored energy, P is the circulating power per mode, τ_c is photon lifetime, α is the average distributed loss constant, l is the path length, R_1 and R_2 are the mirror reflectivities, and $\Delta\nu_{\frac{1}{2}}$ is by Eq. 10. A typical $\Delta\nu_{\frac{1}{2}}$ is given by

$$\Delta\nu_{\frac{1}{2}} = \frac{4.74 \times 10^{14}}{4.6 \times 10^8} \text{ Hz} = 1.03 \times 10^6 \text{ Hz} \quad (12)$$

with $Q = 4.6 \times 10^8$ (Ref 15: 1378).

QUANTUM LIMIT

The quantity that determines the fundamental limit in the narrowness of the clock frequency is the quantum limited laser linewidth. The quantum limited frequency uncertainty is given by

$$\Delta\nu_Q(\tau) = \nu_0/Q \sqrt{h\nu_0/2P\tau} \quad (13)$$

where, h is Planck's constant, P is the circulating power per mode, and τ is the measuring time (Ref 15: 1377). The quantum limit for the clock (QLC) is the ratio of the quantum limited linewidth to the clock frequency. Thus,

$$\text{QLC} = \text{QUANTUM } (\tau) = \frac{\sqrt{2}v_0}{Qv_{\text{clock}}} \sqrt{\frac{hv_0}{2P}} \sqrt{\frac{1}{\tau}} \quad (14)$$

where v_{clock} is the clock frequency (Ref 30). The beat frequency used in the laser clock is a beat between two modes (balanced intensities implied) each having a width Δv_Q , the resulting root mean squared (RMS) width is $\sqrt{2}\Delta v_Q$. Appendix A gives two derivations of the quantum limit.

MULTI-MODE OPERATION

Multi-mode operation is required in the case of the ring laser to avoid the lock-in region. There are three ways to obtain 4-mode operation. The first is by the insertion of a quartz quarter wave plate. If the laser originally had one longitudinal mode, this mode would split into 2 modes. One mode would be right hand circularly polarized and one would be left hand circularly polarized. Each mode contains a clockwise traveling and counter-clockwise traveling component. The frequency shift is given by

$$\nu_{\text{SHIFT}} = \frac{c}{n_i L} \frac{\phi}{2\pi} = \frac{c}{4n_i L} \quad (15)$$

where ϕ is $\pi/2$ for a quarter wave plate and $c/n_i L$ is the free spectral range. One polarization is shifted up and one is shifted down in frequency (Ref 16). The beat frequency is given by

$$\nu_{\text{BEAT}} = 2\nu_{\text{SHIFT}} = \frac{c}{4n_i L} \quad (16)$$

where ν_{BEAT} is the beat frequency between the modes.

The second method is through the use of the non-planar ring laser cavity as described in Ref 16. The phase shift ϕ_{cav} is now provided by the cavity. Further information is given in Appendix B on the physics of the non-planar cavity.

Figure 12 shows the mode structure for both methods of splitting. The third method is shown in Figure 13. This method uses a longitudinal mode and a transverse mode, each having a CW and CCW component (Ref 12). The two low intensity modes provide an internally generated dither effect. This is provided by a non-linear coupling between the gain medium and the four laser modes. This coupling effect can reduce or completely eliminate the lock-in region.

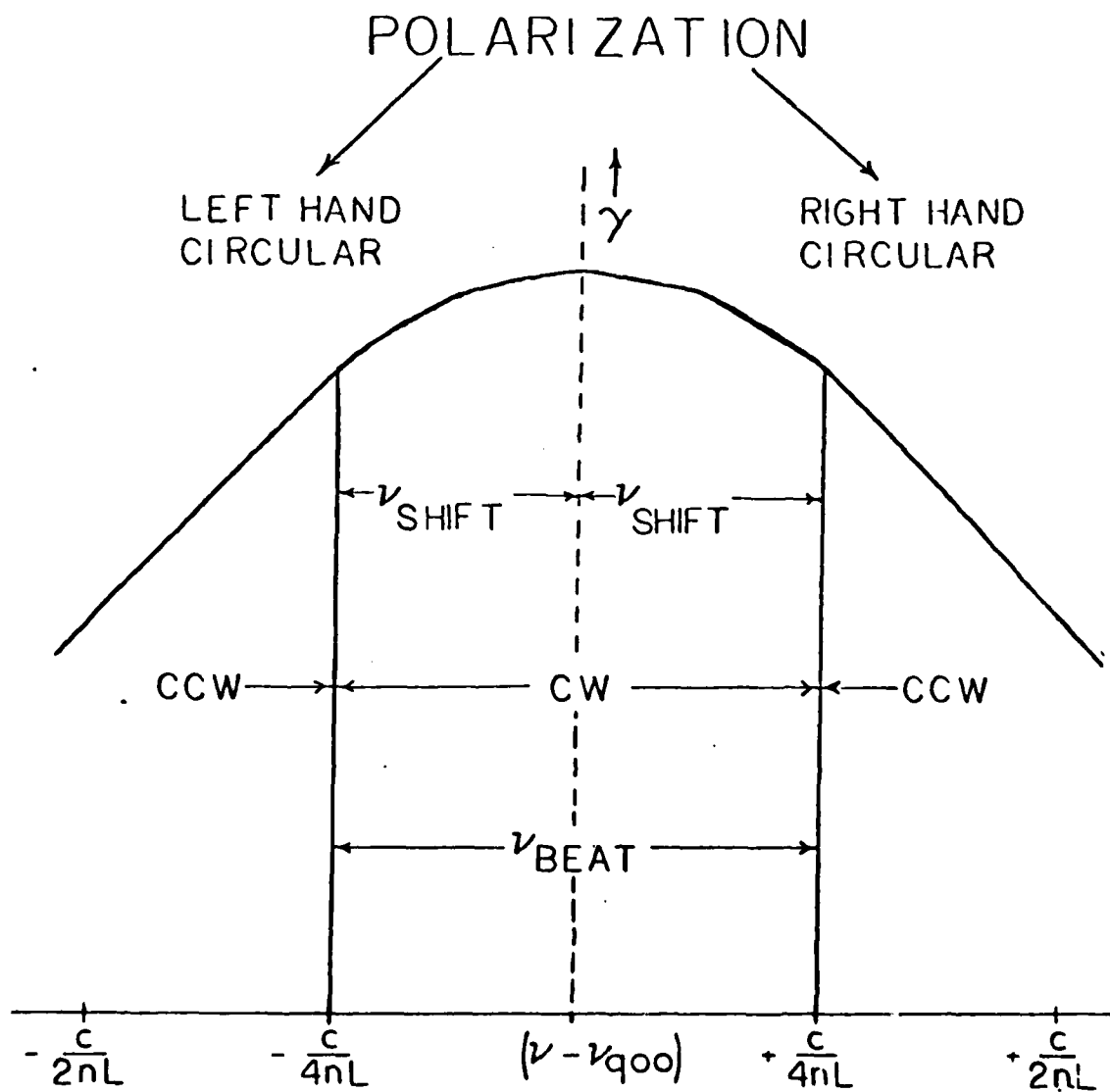


FIGURE 12 4 MODES ON GAIN CURVE

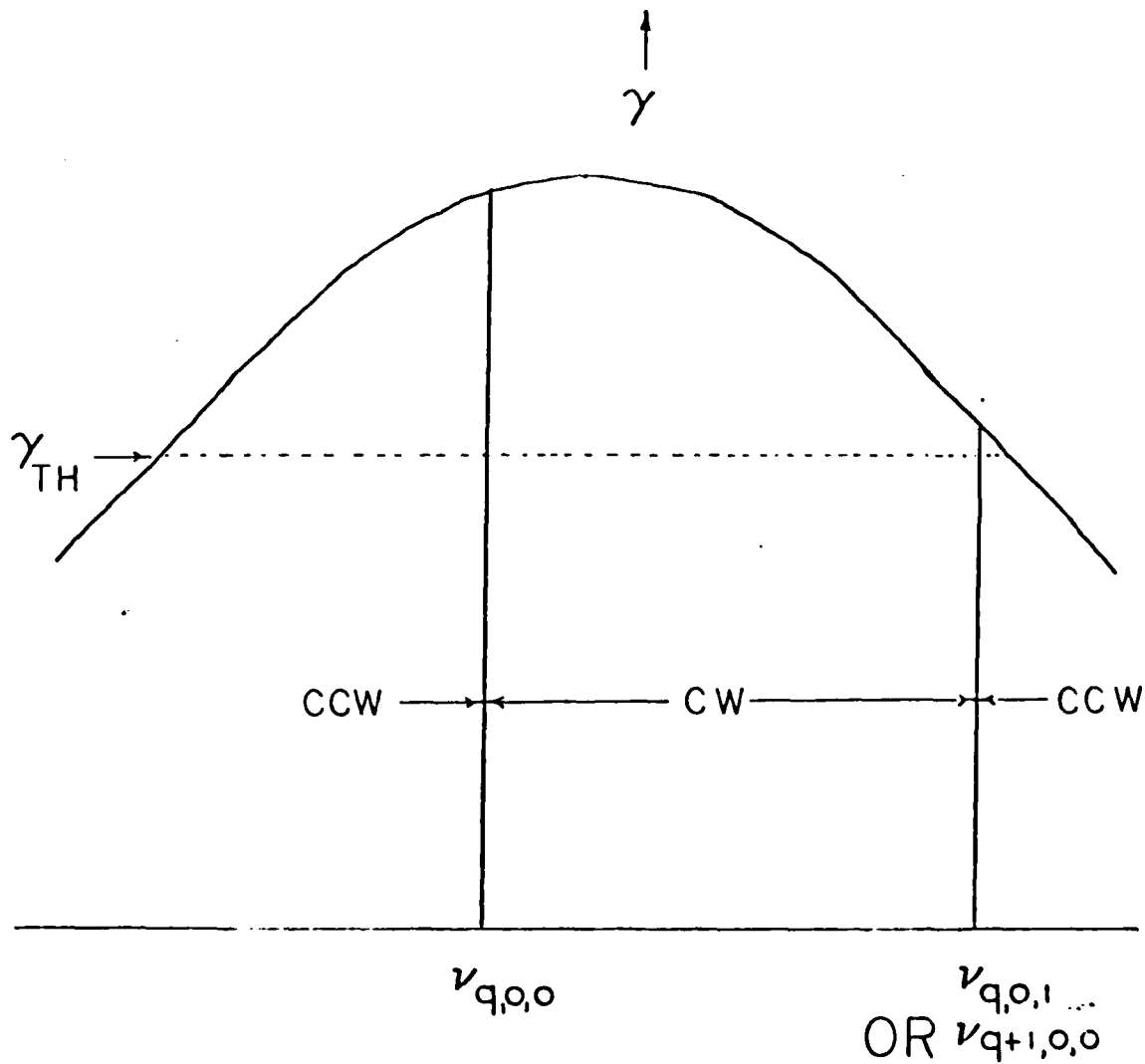


FIGURE 13 4 MODES ON GAIN CURVE

FARADAY ROTATOR

A Faraday rotator is an optical device which rotates the plane of polarization of an incident electromagnetic wave (Ref 17: 71). This device consists of an optically transparent medium under the influence of an external magnetic field. The amount of rotation $\Delta\rho_F$ is given by

$$\Delta\rho_F = VL_F |\underline{B}| \cos \theta_F \quad (17)$$

where V is the Verdet constant, L is the distance through the material, $|\underline{B}|$ is the magnitude of the magnetic field, and θ_F is the angle between the external magnetic field and the direction of light propagation (Ref 18: 299). This phase shift is converted into a frequency shift by the laser cavity. Each of the four modes has a different optical path length because the Faraday rotator is a non-reciprocal. The amount of shift is given by

$$f_F = \frac{c}{L} \frac{\Delta\rho_F}{2\pi} \quad (18)$$

where f_F is the Faraday frequency shift (Ref 16), see Figure 14 and Appendix B for a derivation of (18). The stability of the Faraday frequency shift is given by

$$\frac{\Delta f_F}{f_F} \propto \frac{\Delta T}{T} = (\alpha_i + \alpha_e (n_i - 1)) \frac{\Delta T}{T} \quad (19)$$

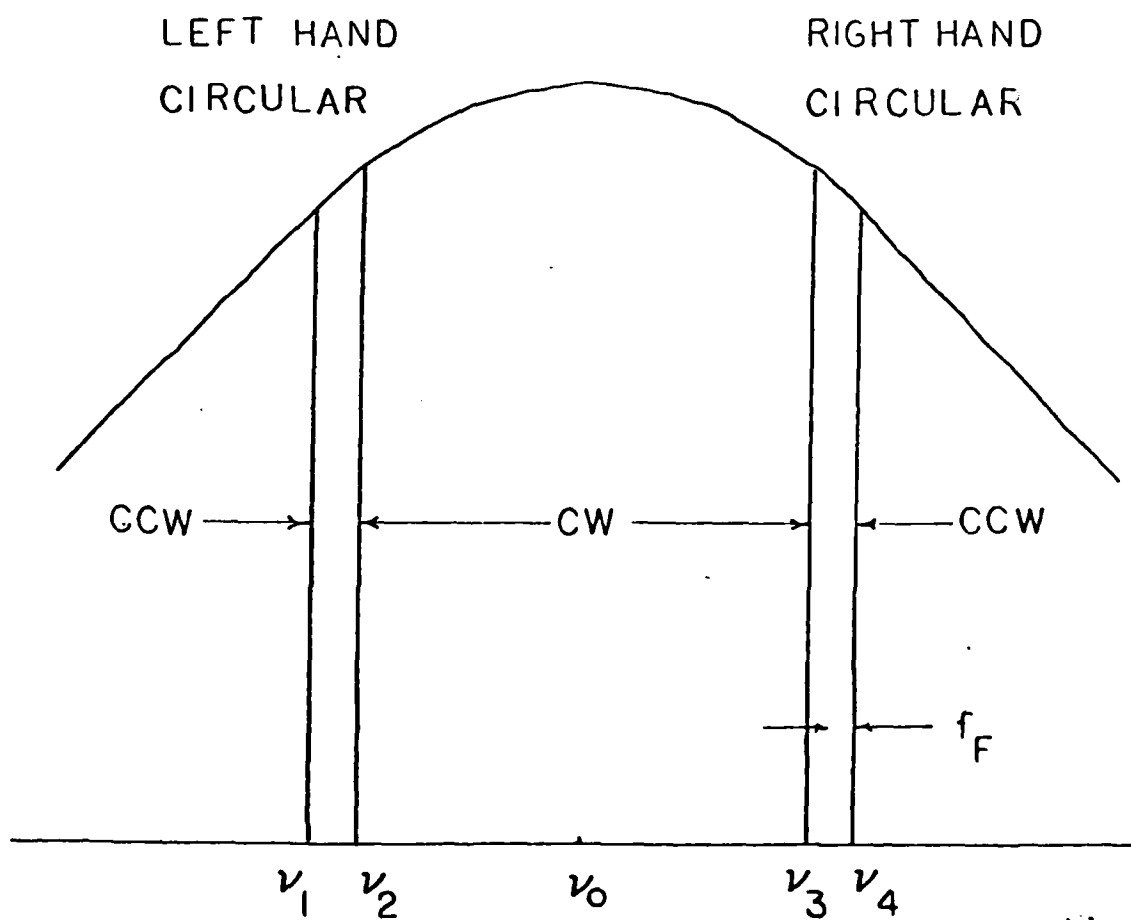


FIGURE 14 4 MODES ON GAIN CURVE
(WITH FARADAY ROTATOR)

where f_F is the Faraday frequency, ΔT is the change in temperature, T is the temperature, α_i is the temperature coefficient of the index of refraction and α_e is the coefficient of expansion of the Faraday rotator (Ref 19). Further information is given in Appendix C on the physics of Faraday rotator and the rotator's effect on the cavity frequency.

DISPERSION

The effect of optical dispersion is to modify the index of refraction, which changes the beat frequency of a laser by

$$\nu'_{\text{beat}} = \nu_{\text{beat}} - \nu_{d,\text{tot}} \quad (20)$$

where ν_{beat} is the empty cavity beat frequency, ν'_{beat} is the beat frequency with dispersion, and $\nu_{d,\text{tot}}$ is given by

$$\nu_{d,\text{tot}} = \nu_{d,1} + \nu_{d,2} \quad (21a)$$

and

$$\nu_{d,i} = \frac{|\nu_0 - \nu_i|}{\Delta\nu_D/2} \frac{\Delta\nu_i}{2} \frac{1}{1 + \left(\frac{|\nu_0 - \nu_i|}{\Delta\nu_D/2}\right)^2} \quad (21b)$$

where $\nu_{d,i}$ is the frequency pull-in of mode i , ν_0 is the center frequency, $\Delta\nu_D/2$ is the atomic half width at half maximum, and

$\Delta\nu_{\frac{1}{2}}$ is the cavity linewidth at half maximum. Equation (21b) is an approximate equation for a Lorentzian lineshape. The He-Ne laser has primarily a Doppler broadened lineshape which is complicated by having two isotopes Ne^{20} and Ne^{22} whose linecenters are 875 MHz apart. This is shown in Figure 15. Note that at frequencies higher than linecenter the mode is shifted down and at frequencies lower than linecenter the mode is shifted up in frequency. The effect is to pull the modes closer to linecenter, hence the term frequency pull-in. There are two curves shown in Figure 15 for two different isotope mixes. The dispersion of a single mode is not the important quantity for the clock application. The important quantity is the total frequency pull-in (21a), which is shown in Figure 16. The stability of this quantity along with the stability of path length control will determine the clock stability. The details of the dispersion effect are in Appendix D.

CLOCK OPERATIONS

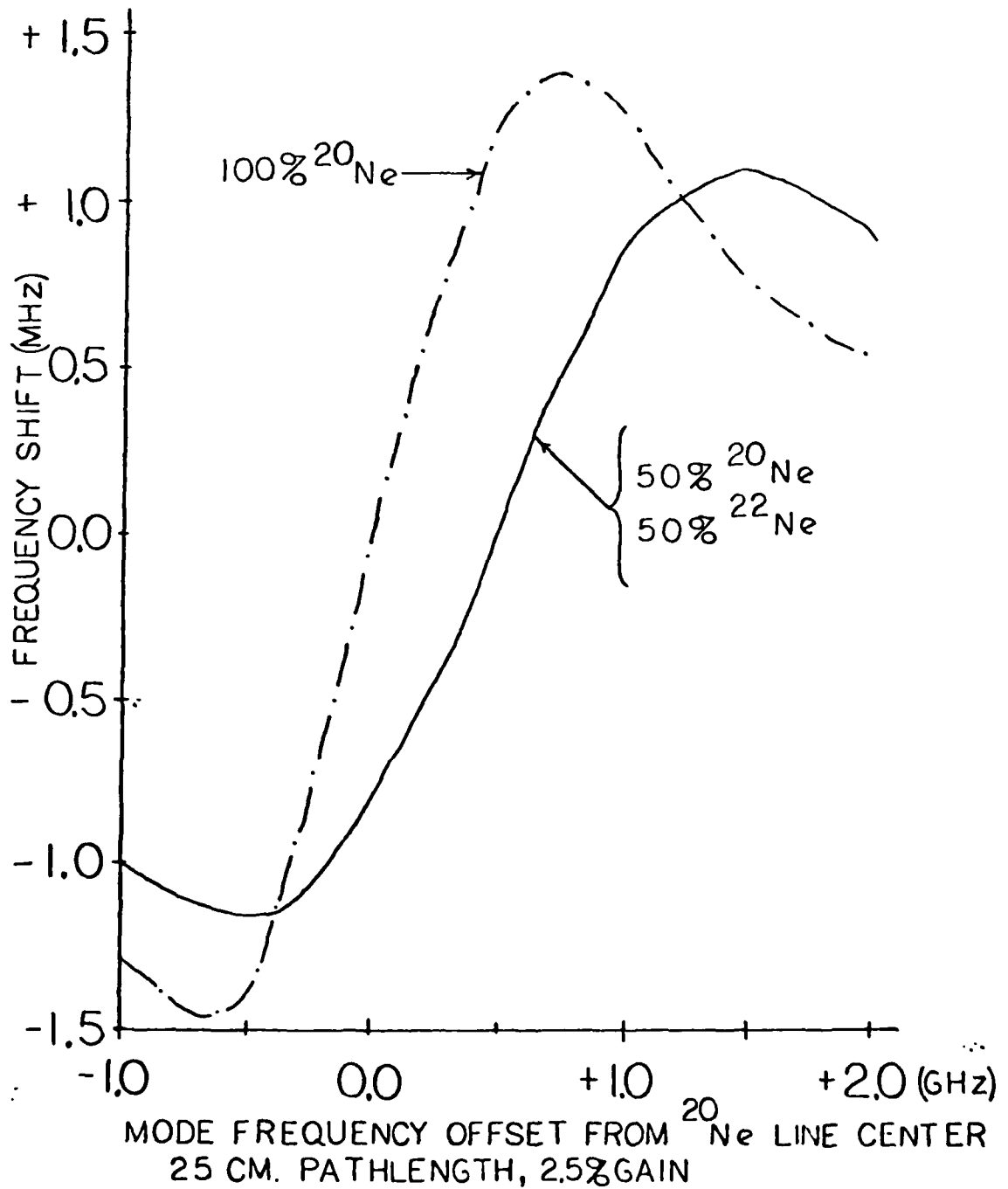
A ring laser without a Faraday rotator produces a clock frequency clock given by

$$\nu_{\text{clock}}(\text{CW}) = \nu_4 - \nu_1 \quad (22a)$$

$$\nu_{\text{clock}}(\text{CCW}) = \nu_3 - \nu_2 \quad (22b)$$

where the two beat frequencies are equal (See Figure 12). A ring laser with a Faraday rotator produces a clock frequency given by

$$\nu_{\text{clock}}(\text{CW}) = \nu_4 - \nu_1 \quad (23a)$$



(REF 34)

FIGURE 15 DISPERSION CURVE FOR
TWO ISOTOPE MIXES

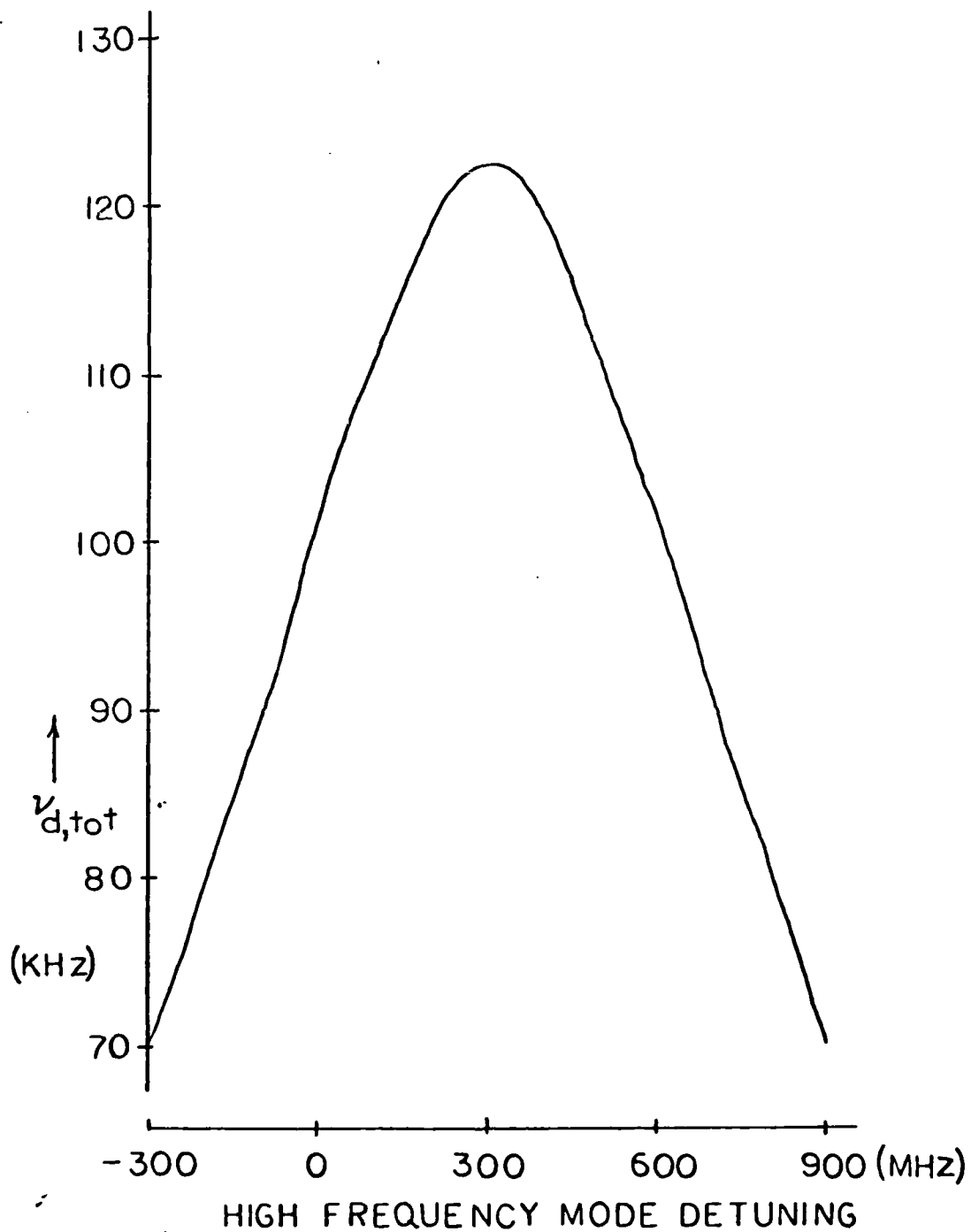


FIGURE 16 TOTAL FREQUENCY PULL-IN AS A FUNCTION OF DETUNING

$$\nu_{\text{clock}}^{(\text{CCW})} = \nu_3 - \nu_2 \quad (23b)$$

where the CW beat is about 800 KHz higher than the CCW beat due to the Faraday rotator (See Figure 14). The two optical frequencies are focused on an avalanche photodiode which detects the 583MHz beat frequency. The signal is amplified and filtered. The output can be taken directly or divided by a factor of 120. The clock processing electronics is shown in Figure 17. The clock frequency generated by 23a or 23b is subject to drift in the Faraday rotator that was given in equation 19.

RECOMMENDED CLOCK/GYRO OPERATION

The clock frequency drift is due to temperature effects in the Faraday rotator. This drift was given in (19). The Faraday rotator temperature sensitivity can be corrected. This is accomplished by the use of dual detectors as shown in Figure 18. The Faraday stabilized clock frequency is given by

$$\nu_{\text{clock}} = \nu_{\text{clock}}^{(\text{CW})} + \nu_{\text{clock}}^{(\text{CCW})} \quad (24a)$$

$$\nu_{\text{clock}} = (\nu_4 - \nu_1) + (\nu_3 - \nu_1) \quad (24b)$$

When the Faraday effect increases, $(\nu_4 - \nu_1)$ is increased by the same amount that $(\nu_3 - \nu_2)$ decreases, thus holding a constant sum. This should allow the clock to reach the quantum limit at longer times.

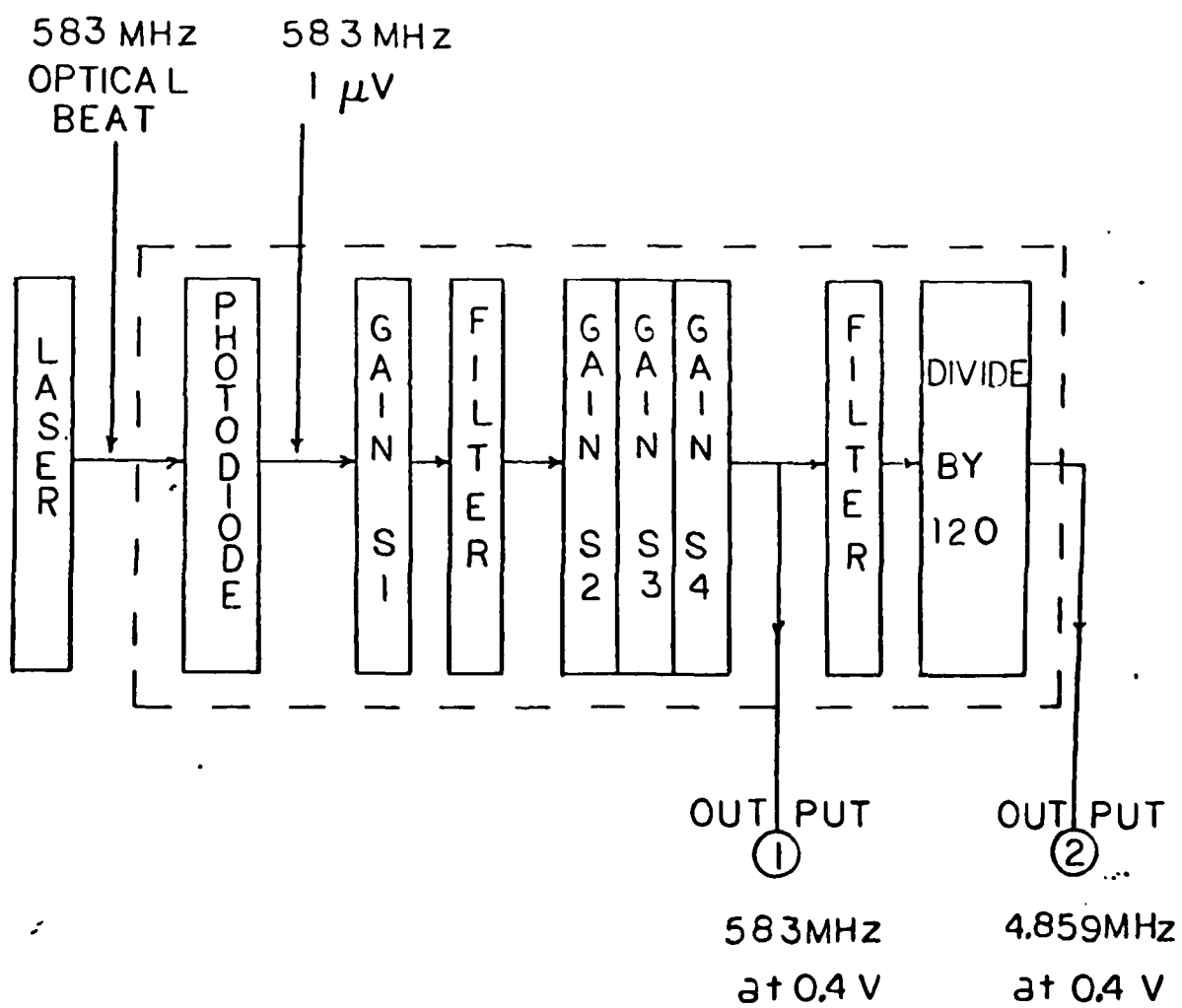


FIGURE .17 CLOCK ELECTRONICS

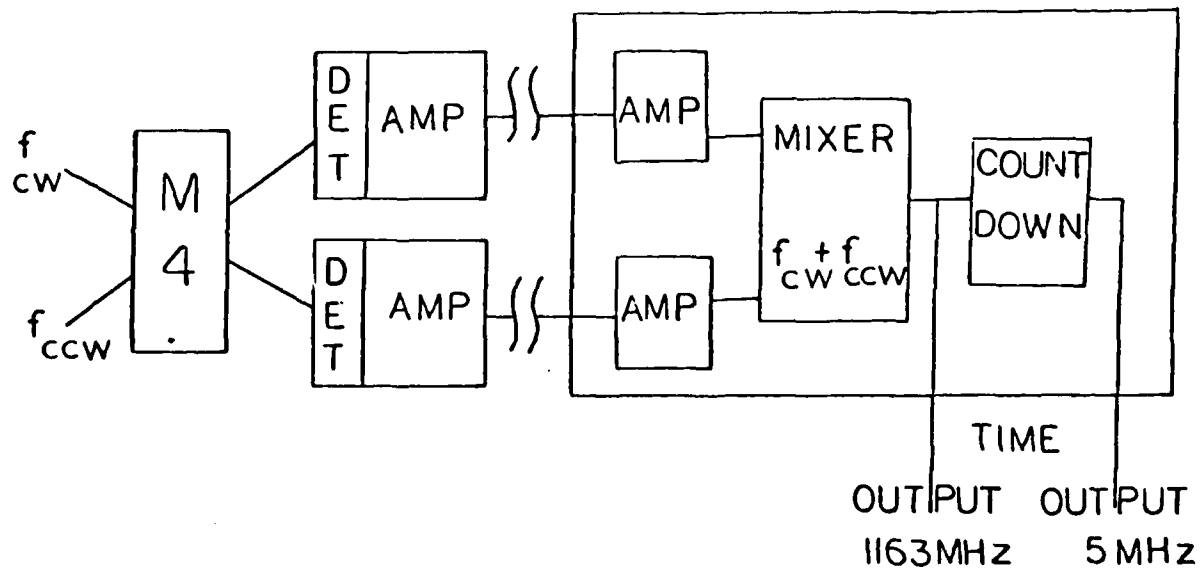
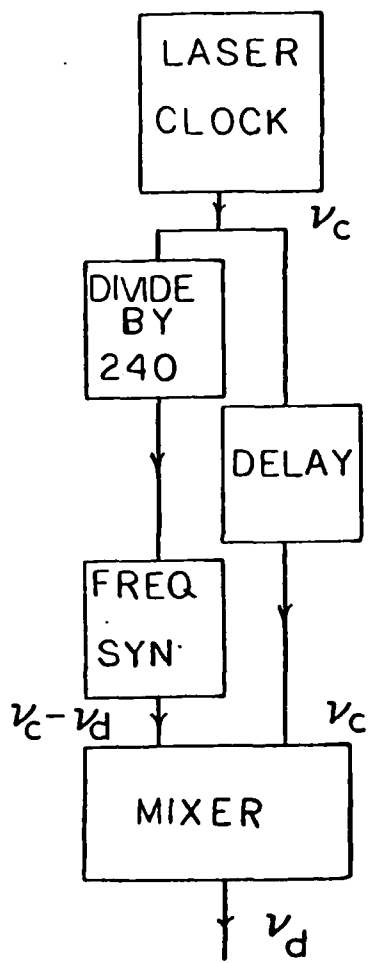


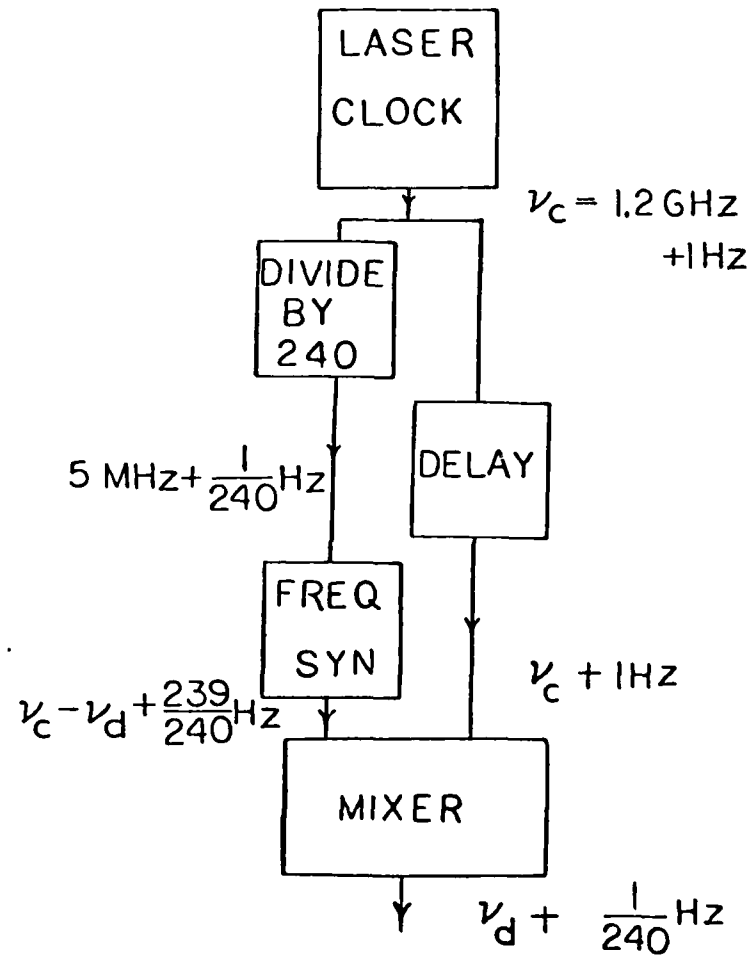
FIGURE 18 RECOMMENDED ELECTRONICS

RECOMMENDED METHOD OF TIMING/SETTING

The synchronization of an atomic clock is done by setting it to an external time reference. Atomic clocks which are frequency standards only drift by a small amount, typically $\nu_c \times 10^{-10}$. To set the clock, the clock frequency is mixed with the reference and the beat frequency is the offset. The offset is the amount that the users clock is off the reference. The user can then use this information to determine the correct time. The clock usually is not actually adjusted. The known offset is used as a correction term. A transfer frequency standard can be so far off as to be undesirable because the correction term should be $\nu_c \times 10^{-8}$ or better. The laser path length controller (PLC) provides a degree of tuning but this might either affect the gyro function or still not be enough tuning to reach the desired frequency. The optimum method of tuning would be a frequency synthesizer. A frequency synthesizer takes in a standard frequency and outputs a user defined frequency. The signal would be divided into two components. The first would be divided down to near 5 MHz. Then this frequency could be used as the time base for the synthesizer. This output would then go to the mixer. The synthesizer would produce a frequency $\nu_{\text{clock}} - \nu_{\text{desired}}$. The second signal would go through a delay line into the mixer. The mixer output would be the desired frequency ν_d , which could be user defined. There are at least three standard frequencies. This recommended method of setting will provide a greater flexibility. Figure 19 shows a block diagram of the required electronics and Figure 19b shows the effects of a 1Hz frequency drift on the output. If the clock frequency drifts the net



A) NO DRIFT



B) DRIFT 1Hz
($\nu_d = 5 \text{ MHz}$)

FIGURE 19 USER DEFINED FREQUENCY

effect is reduced by the count down ratio. Also laser frequency stability is

$$\frac{\Delta\nu_c}{\nu_c} = \frac{\Delta\nu_d}{\nu_d} = \frac{\Delta\nu_c/240}{\nu_c/240} \quad (25)$$

Both the laser frequency and the uncertainty in the frequency are reduced by the count down ratio and thus accuracy is preserved.

IV EXPERIMENT

The purpose of the experiment was two fold. The first objective was to measure the frequency stability of the laser clock. In order to get the highest accuracy results possible all the error sources must be minimized. Once all controllable error sources have been minimized, then the frequency stability data will be collected and analyzed. The second objective was then to determine what error sources were still present in the best data and what error sources would be of concern in the future. The experiment was conducted in ten days starting 1 March 82 at the Sudbury, Massachusetts plant of the Raytheon Corporation. The original plans were to test a dual detector system on an operating gyro as shown in Figure 18. This approach would avoid errors due to the sensitivity of the Faraday rotator. However, this proved to be too costly, so the use of a gyro without a Faraday rotator was considered. Laser #18 was available without a Faraday rotator. Laser #18 would not work as a gyro for low rotation rates because of the lock-in phenomenon. A design was developed to provide a clock output as shown in Figure 17. This approach minimized the electronics to be developed and the associated cost.

CLOCK ELECTRONICS

The purpose of the clock electronics is to detect the optical beat frequency between the laser modes and output a very low noise electrical signal whose frequency matches the beat frequency. The processing electronics used in the experiment are shown in Figure 17.

The laser beam is directed on the avalanche photodiode. The diode output is a 583 MHz signal with 1 μ V peak-to-peak amplitude. The 583MHz signal is then amplified and passed through a 13 MHz bandpass comb filter. The comb filter, filter #1 in figure 17, had 13 MHz bandpass windows spaced such that over a large range of frequencies the transmission as a function of frequency looks like a comb. In this experiment only one window was centered at the laser beat frequency. Then the signal is amplified to 0.4V peak-to-peak at 583 MHz , which is output number one. The second output is filtered with a wide bandpass filter and then divided by 120 to give 4.859 MHz at .4V peak-to-peak.

EXPERIMENTAL SETUP

The experimental setup shown in Figure 20 was used to measure the stability of the laser clock frequency. The laser clock frequency was compared to an external frequency standard by using a mixer and measuring the difference frequency using a counter. The counter measures the frequency for an integration time τ and the calculator uses this data to compute the Allan variance. The laser clock output was fed to the mixer (HP 10830A), as was the frequency synthesizer (HP 8660C) output. The frequency reference for the frequency synthesizer and the counter was the Loran C cesium based system. The Loran C is an aircraft navigation system that uses a central cesium clock. An experimenter can use a Loran receiver to control a local crystal oscillator to produce a synchronized local clock frequency. The filtered output of the mixer is a difference frequency between the

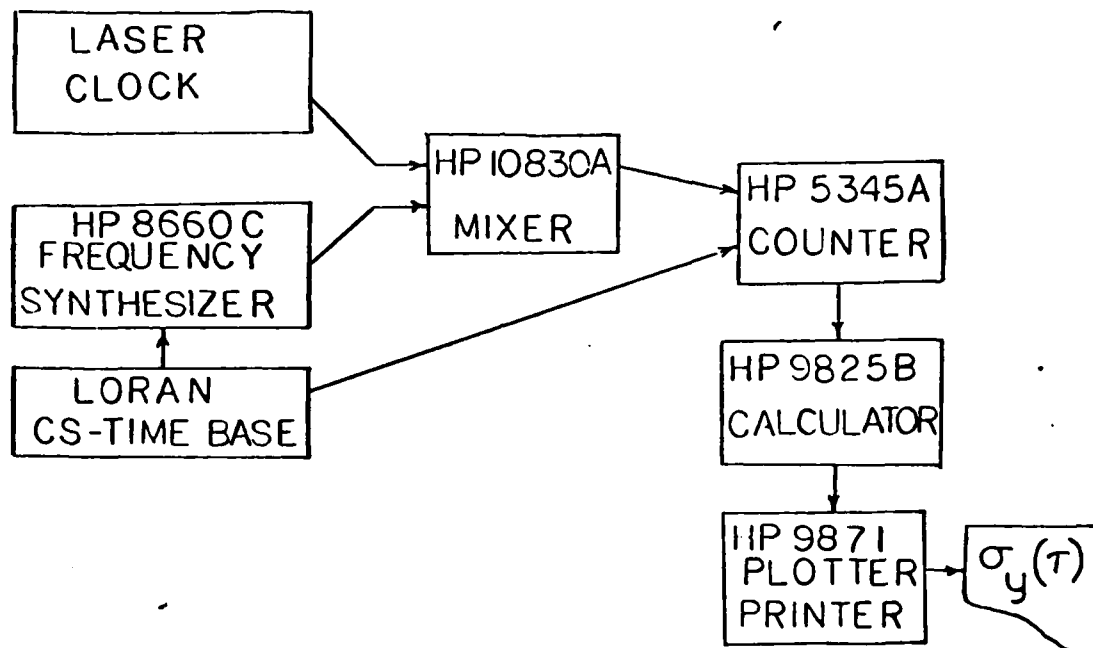


FIGURE 20 EXPERIMENTAL SETUP

laser clock and the reference. This provides a low frequency (>100 kHz) output which is easy to count and allows greater accuracy. The mixer output was fed into the counter (HP 5345A) which was controlled by the calculator (HP 9825B). The calculator controls the counter and calculates the Allan variance as given in (1). The calculator outputs were produced using the printer/plotter(HP 9871). This configuration provided the highest accuracy system available.

SUMMARY OF EVENTS

The first four days were spent debugging the electronics and taking supporting data. The days four through eight were spent taking data on laser serial number #18 with the first day spent in preparation and days 6 through 8 collecting performance data. The last two days were used working on laser #68. Table II shows a summary of the experiment.

TABLE II
EXPERIMENT SUMMARY

SECTION	DATE	ACTIVITY	APPROX. AMOUNT OF DATA
1	1-4MAR82	OVER NIGHT RUNS WORK ON ELECTRONICS	48 HOURS
2	5-8MAR82	OVER NIGHT RUNS SHORT TIME RUNS	60 HOURS
3	9MAR82	WAITED ON LASER # 68 PREPARATION	NO DATA
4	10MAR82	STEP-UP EXPERIMENT TOOK SHORT TIME RUNS	12 HOURS

SECTION ONE

To attain the first objective, stated at the beginning of this chapter, required an initial analysis of the clock output and debugging phase. The frequency was measured for 100 second integration times contiguously over the weekend of 27-28 Feb 82. This allowed detection of short term deviations in the frequency as well as long term trending. The first activity was to examine the data. Most of the frequency measurements were within 13 Hz of the mean carrier frequency, but there were spikes in the data. These spikes were always between 200 and 100 seconds long in time. Several tests were applied to determine the cause of the spikes.

The first test was to determine the effect of light on the photo detector. When the room lights were off, the frequency increased by 20 Hz. The effect of a small amount of light was to reduce the detectors signal to noise ratio which caused false counting. A flashlight at a distance of 10 cm. totally saturated the diode or the noise became greater than the signal. The room lights could not have caused the large frequency seen in the spikes. The Tesla coil, used to start the laser, produced KHz changes in frequency. A nearby Tesla coil could have caused the spikes since the laser was not shielded from electromagnetic interference (EMI). The laser and detector were covered by a box which was covered with aluminum foil and grounded. This provided shielding from both EMI and light. The frequency was again measured overnight and the measured frequency had a standard deviation of 2.5 Hz for the last 12 hours of the run. There were no spikes during the last 12 hours of the run.

The second test involved replacement of filter #2 in Figure 17 to check for proper filter performance. The frequency was again measured overnight and the measured frequency had a standard deviation of 750 mHz for the last 11 hours of the run. The laser control electronics were set up to allow remote control of the laser pathlength for a later dispersion test. The amount of detuning was calibrated using a Fabry-Perot interferometer. The key remaining error source seemed to be due to temperature effects. The room air conditioning cycled about every nine minutes. The output of the laser clock was also cycling with a period of nine minutes but with a time delay due to the thermal inertia of the laser block. The equipment was moved to a lab with a high accuracy temperature controlled oven. Later in the day the

frequency started changing rapidly. This rapid change was not due to the laser but indicated an electronics failure.

The overnight test on 4 March was a total failure. The problem was isolated and found to be in the count down chip that reduces the frequency to near 5MHz(see Figure 17). When the replacement chip was inserted and bench tested the clock electronics functioned properly; however, after being reassembled on the laser test stand it did not function. It was concluded that the Tesla coil had damaged the count down chips during the laser start up. Due to the problems encountered with the count down chip, efforts were undertaken to instrument the 583 MHz output #1 of figure 17. The counter being used could not count the full 583 MHz frequency, directly, so an alternate approach was selected to mix the clock output with the reference frequency from a frequency synthesizer to produce a low frequency output (see Figure 20).

SECTION TWO

The second part of the first objective, stated at the beginning of this chapter was obtained in the next four days. Once the hardware problems had been solved the next set of problems were environmental. On day 5 a HP 8660C frequency synthesizer was selected(see Figure 20). The first Allan variance measurements taken on laser #18 were made on 5 March 82. The laser clock was temperature sensitive as stated in section one and the frequency stability depended on both temperature and the stability of the temperature. The best operating temperature seemed to be +15°C. At temperatures above 31.5°C the laser beat frequency began self oscillation due to the gyro going in and out of lock-in. When the gyro is setting still in the lab it measures a

component of earth rate, however the clockwise and counter-clockwise modes of like polarizations have the same frequency due to lock-in. When vibration of sufficient amplitude is coupled to the instrument the gyro breaks out of the lock-in region into the non-linear region shown in Figure 10. In the non-linear region there is strong mode competition and the beat frequency ceases to be stable.

As a result the long term frequency measurements were far from being quantum limited, but the best short term data was not effected as much because in a short time the frequency did not drift far. The problem with the data stems from the fact that the table supporting the oven was not very solid so vibration was being transmitted through the table to the laser. To solve the vibration problem the equipment was moved back to the first lab, which had a granite table but no oven. If the gyro was rotated by hand the path length control respondent, because the gyro broke lock-in. This test confirmed that the problem was due to the laser acting as a gyro and sensing rotation.

SECTION THREE

This section deals with another hardware problem that had to be solved. The vibration effects should have caused only an increase in the noise, but there was also a drift of the frequency. This pointed to a drift in the pathlength control. By using the Fabry-Perot interferometer it was discovered that the pathlength control was drifting even though the test voltage was held constant. The pathlength control problem could not be solved in the time remaining so it was decided that measurements should be taken on laser #68. Laser #68 is an operational 4 frequency RLG. Several components had

to be changed before laser #68 could be used to provide optimum output. This was completed early on day 9 and frequency stability data was taken till the next day.

SECTION FOUR

The frequency stability data taken in this section reached the objective of the experiment, stated at the beginning of this chapter, in that it was the best data obtainable without modification of the equipment. Final data was taken on day 10. The number of samples in each data point was reduced from 11 to 5 measurements, which lowered the effect of the temperature induced Faraday rotator frequency drift (about 200 Hz per hour). The last data was taken with an insulated covering over the laser test stand to increase the thermal inertia. The idea was to allow the laser to come to equilibrium, but in still followed the room temperature never reaching an equilibrium. This was the final data taken. The results section outlines the error sources. In general the short term performance (1-100mS) was quantum limited and the long term performance (.1-1000 S) was limited by the drifting of the induced Faraday rotator frequency.

V RESULTS

LASER #18

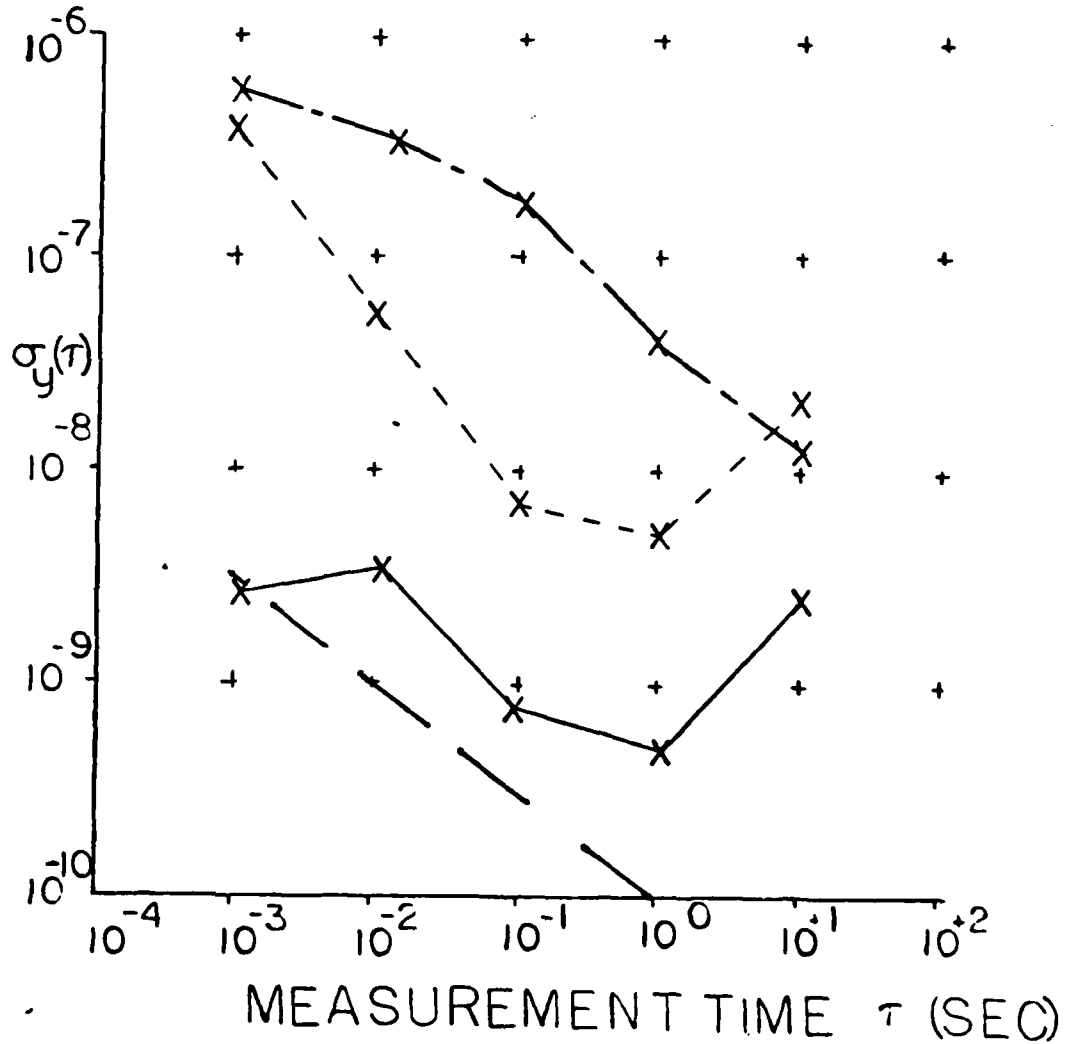
Data from the test of laser #18 is shown in Figure 21. The data shows improved performance as the experiment proceeded. This was due to efforts that reduced noise affecting the ring laser as described in the experiment section. The best short term data was quantum limited for integration times of 1 msec, 10 msec and 100 msec. However, the longer term data showed increased instability. After using a Fabry-Perot analyzer to observe all 4 of the modes, it was discovered that the path length controller(PLC) was drifting, thus causing the problem in the long-term stability data. Laser #18 had a PLC, that was an older experimental design with too small a bandwidth in the controller causing it to lose control. The PLC drift was the reason that additional testing was done using a state-of-the-art RLG #68. Laser #68 had a Faraday rotator which could not be temperature compensated since another set of electronics was not available to implement the approach shown in Figure 18. It was believed that even though Laser #68 was temperature sensitive, laser temperature drift could be minimized using a temperature controlled oven and thus obtain better clock data.

LASER #68

The clock test data for laser #68 is shown in Figures 22 and 23. Figure 22 shows the data sets containing the best data points for integration times of 1 msec, 10 msec, and 100 msec. Figure 23 shows

- - - MARCH 5
 - - - MARCH 6
 ——— MARCH 7
 ——— QUANTUM LIMIT

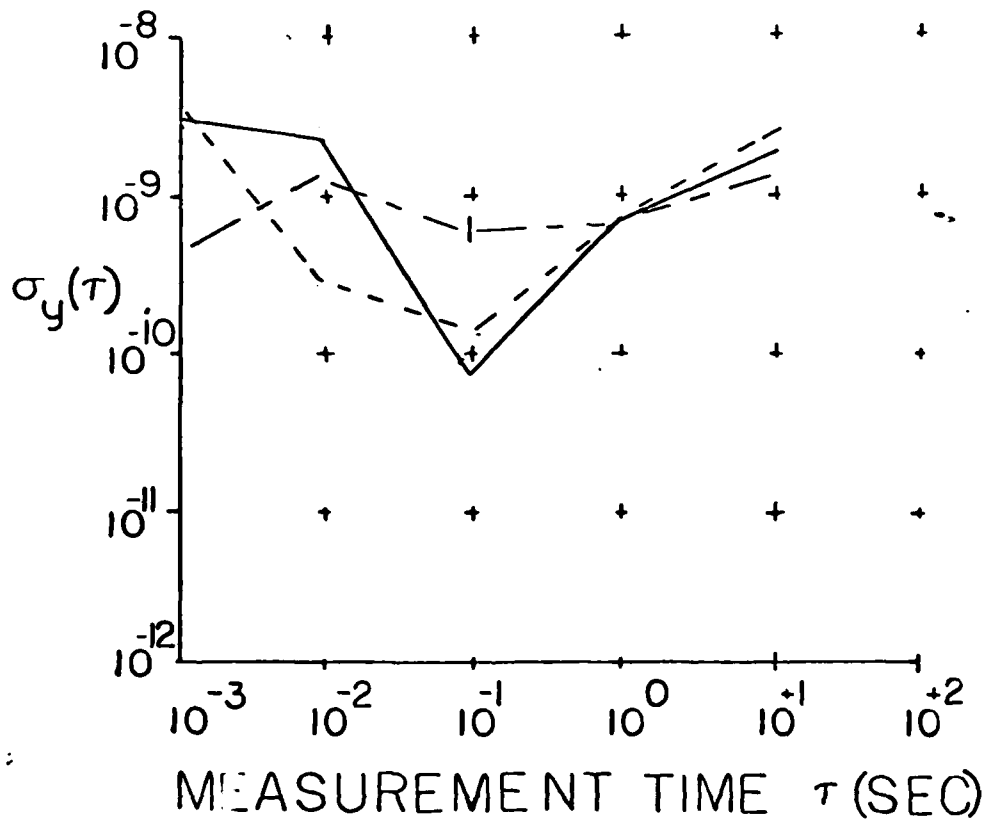
LASER # 18



STABILITY DATA
 FIGURE 21 GATHERED WITH LASER #18

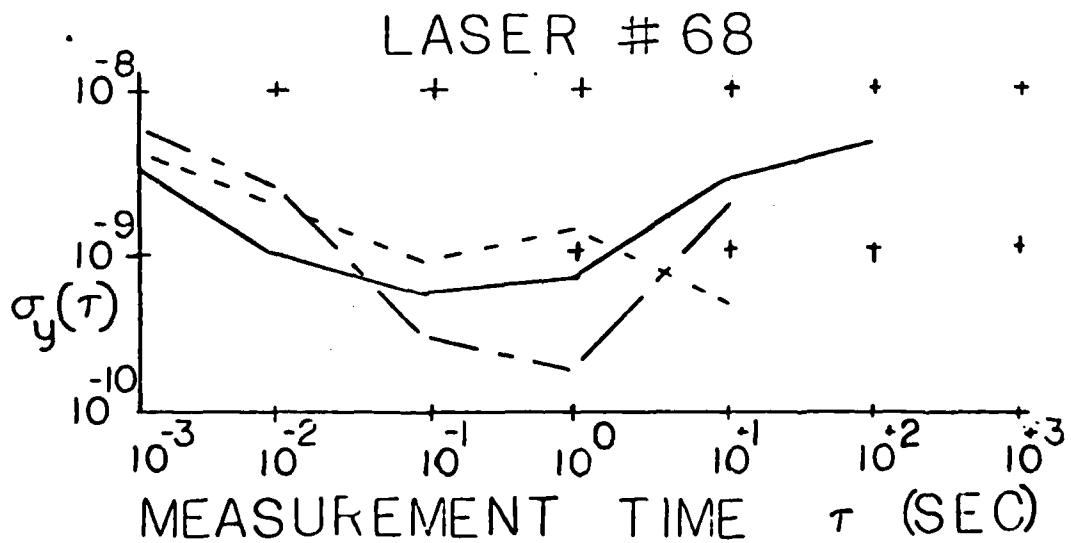
	MARCH 82	BEST DATA FOR
---	10	1 mSEC
- - -	9	10 mSEC
—	10	100 mSEC

LASER #68



STABILITY DATA
 FIGURE 22 GATHERED WITH LASER #68

	MARCH 82	BEST DATA FOR
---	10	1 SEC
---	10	10 SEC
—	9	100 SEC



STABILITY DATA
 FIGURE 23 GATHERED WITH LASER #68

the data sets containing the best data points for integration times of 1 sec, 10 sec, and 100 sec. Figure 24 shows a comparison of the frequency stability of a HP 10811 quartz oscillator, a HP 5065A rubidium atomic clock, and a HP 5062C cesium atomic clock. The best laser clock data falls between data for the cesium and rubidium standards from 1 msec to 0.3 sec.

ERROR ANALYSIS

This section covers the two main error sources in the best data as well as considering other potential error sources. The first covered is the quantum limited noise which has time dependence of $t^{-\frac{1}{2}}$. The second error source is the drift in the induced Faraday frequency which has a time dependence of τ . Potential error sources covered are drifting of the laser pathlength, stability of the discharge current, stability of the cavity geometry, and finally noise in the electronics.

The laser clock frequency stability data shown in Figure 24 for integration times from 1 to 100 msec is quantum limited. The Faraday drift starts affecting the data at 0.1 sec and the value of $\sigma_y(\tau)$ increases. The quantum limit was given in (14). The values used were $\nu_0 = 4.74 \times 10^{14}$ Hz, $\nu_{\text{clock}} = 582.203$ MHz, $Q = 4.47 \times 10^8$, and $P = 507.3 \mu\text{W}$. So the quantum limit is

$$\text{Quantum limit } (\tau) = 3.20 \times 10^{-11} \tau^{-\frac{1}{2}} \quad (26)$$

for $\tau_c < \tau < \infty$. Typical drift values of the temperature induced Faraday frequency shift were on the order of 110 Hz per hour or 30.5 mHz/sec.

- - - - CRYSTAL OSCILLATOR
 - - - CESIUM 5062C
 - - - RUBIDIUM 5065A
 ——— LASER CLOCK (BEST)

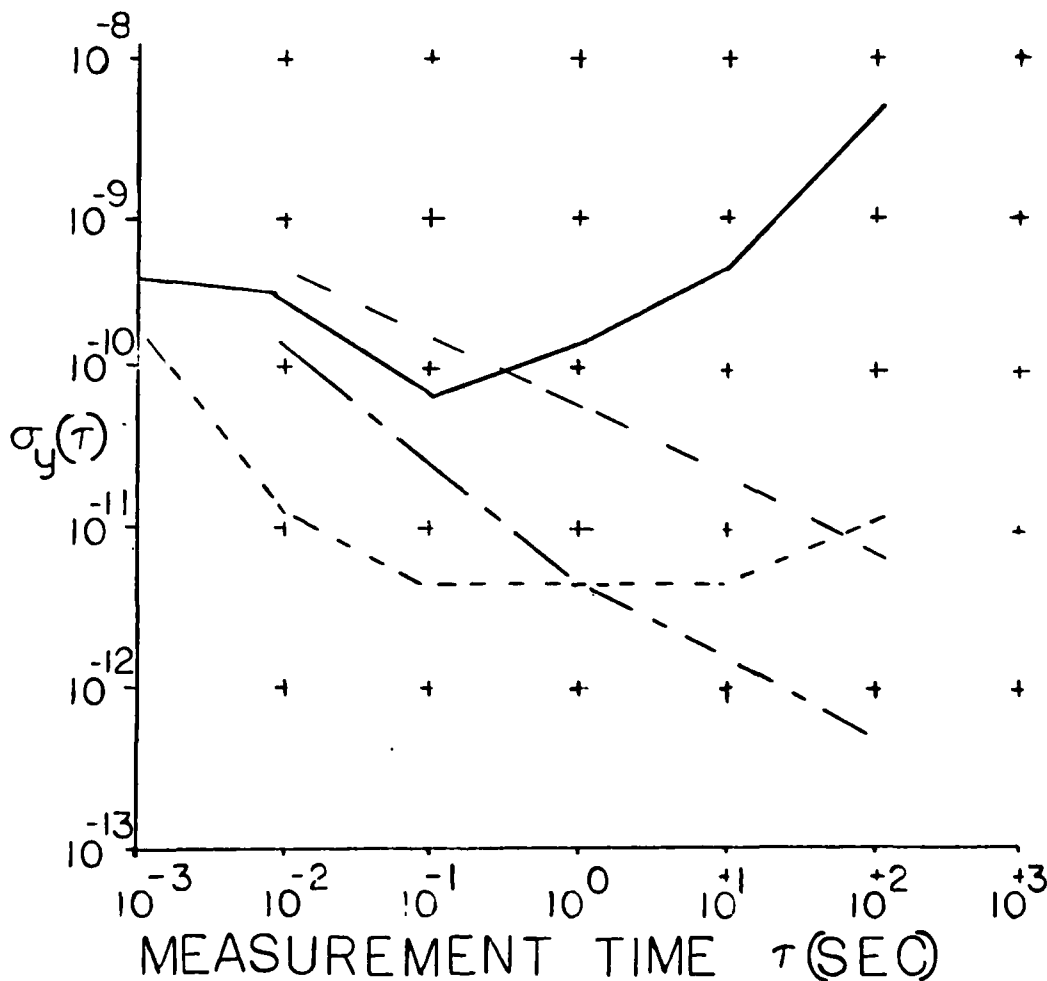


FIGURE 24 STABILITY COMPARISON

$$\text{Faraday limit} = \frac{30.5 \text{ MHz}}{582.203 \text{ MHz}} \frac{\tau}{\sqrt{2}} = 3.7 \times 10^{-11} \tau \quad (27)$$

for τ seconds and $\tau_c < \tau < \infty$. The two curves given by (26) and (27) cross over at about one second. The quantum limit is dominant for $\tau_c < \tau < 0.1$ seconds. Both must be considered in the range $0.1 < \tau < 10.0$ seconds. The Faraday limit is dominant for $\tau > 10.0$ seconds. Figure 25 shows the quantum limit given by (26), the Faraday limit given by (27), and the data. The data agrees very well with the above theory. There is also a higher frequency fluctuation in the temperature shown in Figure 26. If the temperature changed by 1 m°K in one second the effect is as follows

$$\Delta f = f \frac{\Delta T}{T} = .4 \text{ MHz} \frac{0.001 \text{ °K}}{300.0 \text{ °K}} = 1.33 \text{ Hz}$$

$$\frac{\Delta f}{\tau} = 1.33 \frac{\text{Hz}}{\text{sec}} = 4.8 \frac{\text{kHz}}{\text{Hr}}$$

Equation (27) looks like

$$\text{Faraday limit} = \frac{1.33 \text{ Hz}}{582.203 \text{ MHz}} \frac{\tau}{\sqrt{2}} = 1.6 \times 10^{-9} \tau$$

for τ in seconds and $\tau_c < \tau < \infty$. If the temperature changes by 1 m°K in 1 msec then the result is

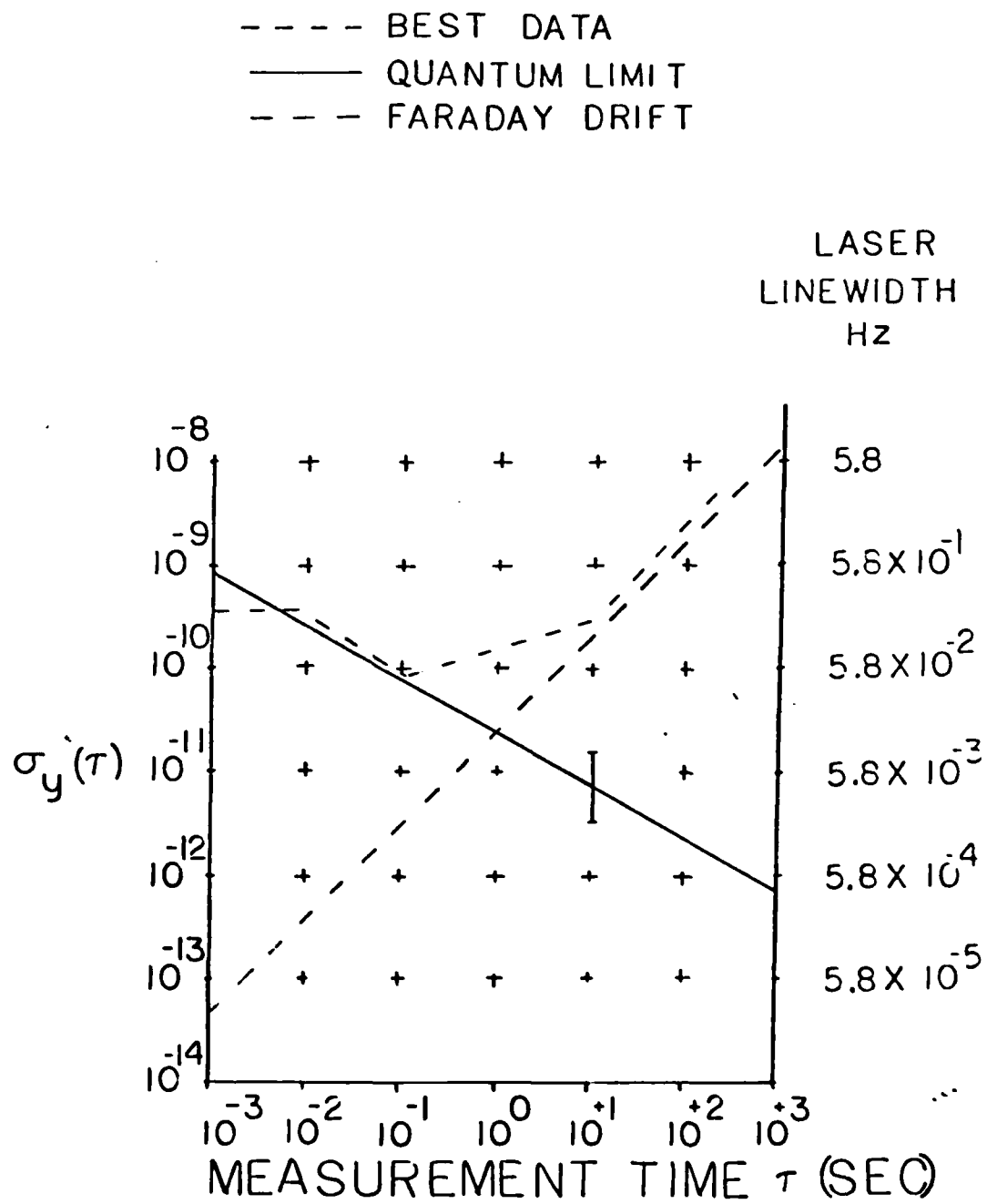


FIGURE 25 ERROR ANALYSIS

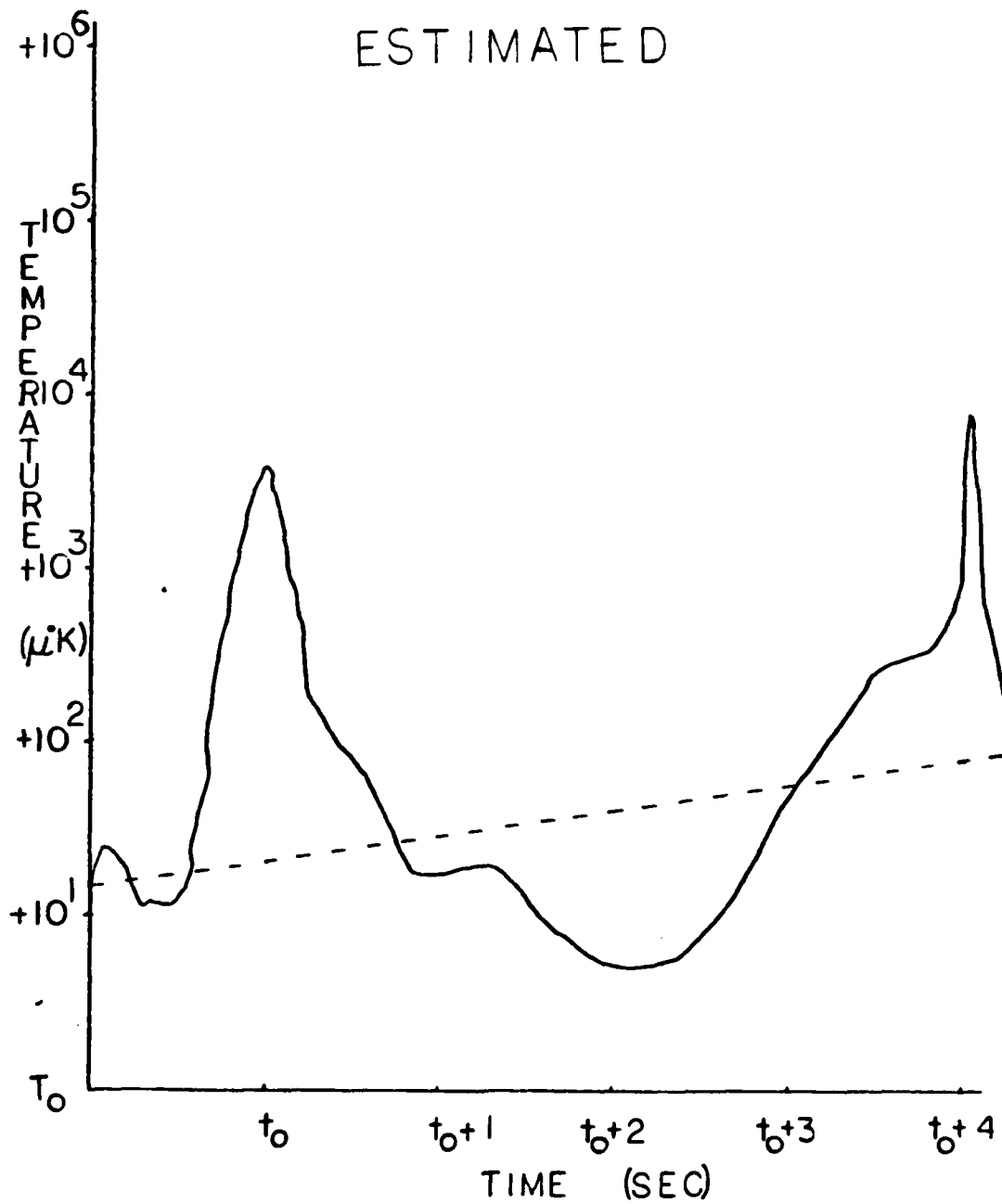


FIGURE 26 TEMPERATURE DRIFT

$$\begin{aligned} \text{Faraday limit} &= 1.6 \times 10^{-6} \tau && (\tau \text{ in seconds}) \\ &= 1.6 \times 10^{-9} \tau && (\tau \text{ in millisecond}) \end{aligned}$$

The short-term data was affected by the Faraday rotator. The best data is considered to be data taken when the Faraday induced noise was at a minimum. The best data was quantum limited for 1 - 100 milliseconds because the Faraday induced noise was less than the quantum limit. The long-term data, greater than one second, always has the Faraday induced drift present; that is to say, even the best long term data shows the Faraday induced drift.

POTENTIAL ERROR SOURCES

This section will discuss error sources of future concern. These might be observed as the present error sources are reduced and the device is made to operate over the temperature range -55°C to $+95^{\circ}\text{C}$. The error sources to be covered will be path length control, gain control, cavity stability and electronics noise.

If a state-of-the-art Raytheon path length control can hold the laser frequency to within 4,740 Hz or correspondingly the path length to 25 mÅ. The result of taking a delta of both sides of (9) is

$$\Delta f_p = q \Delta f_{\text{BEAT}} \quad (28a)$$

and using $\Delta f_p = 4,740 \text{ Hz}$ is

$$\Delta f_{\text{BEAT}} = \frac{\Delta f_p}{q} = \frac{4.74 \times 10^3 \text{ Hz}}{4.06 \times 10^5} = 11.67 \text{ mHz} \quad (28b)$$

where Δf_p is the limit on the PLC, q is the mode number of the cavity, and Δf_{beat} resulting deviation in clock frequency. However, the frequency is jittering between the limits with a natural frequency on the order of 10^3 Hz. This has the effect of reducing this error source. This error looks like

$$\Delta f_p(t) = \Delta f_{\text{BEAT}} \sin(\omega\tau) \quad (29)$$

where $\Delta f_{\text{BEAT}} = 11.67$ mHz and $\omega = 10^3$ Hz.

$$\text{MAX } \Delta f_p(t) = \text{MAX} \frac{\int_0^T \Delta f_{\text{BEAT}} \sin(\omega\tau) dt}{\int_0^T dt} \quad (30a)$$

$$= \Delta f_{\text{BEAT}} \int_0^{\pi/\omega} \sin(\omega\tau) dt \quad (30b)$$

$$= \frac{-\Delta f_{\text{BEAT}} \cos(\omega\tau)}{\omega T} \Big|_0^{\pi/\omega} \quad (30c)$$

$$= \frac{-\Delta f_{\text{BEAT}} (\cos \pi - \cos 0)}{\omega T} \quad (30d)$$

$$= \frac{2\Delta f_{\text{BEAT}}}{\omega T} \quad (30e)$$

Therefore, the error do to a state-of-the-art PLC is

$$\frac{\Delta f_p}{f} = \frac{2 \times 11.67 \text{ MHz}}{582.2 \text{ MHz} \times 1 \text{ kHz}} \frac{1}{\tau} \quad (31a)$$

$$= 2 \times 10^{-14} \tau^{-1} \quad (31b)$$

for $\tau_c < \tau < \infty$ and τ is in seconds. This error source is three orders of magnitude below the quantum limit at one second. This noise source also falls off much more rapidly. This error should never be a problem. However, over a wide range in temperature (-55°C to +95°C) the PLC electronics might be non-linear and cause a drift.

To minimize the effects of dispersion the gain must be controlled. This requires discharge current control. A typical value of the discharge current is 5 mA and a deviation from the mean of 50 nA for a stability, $\Delta i/i$, of 10^{-5} . This is done by the using of a split discharge that keeps the two currents balanced. This minimizes gas flow in the ring. If dispersion becomes a problem the current control will be a key problem or solution. It could be a solution if the current could be controlled to counter the effects of dispersion. See Appendix D for a discussion of dispersion.

The cavity stability has two issues. The first is cavity length that was covered in the PLC section. The second is effects due to thermal gradients on the laser body. If the mirror tilts, then the angle ϕ in (15) ceases to be 90° and there is a shift in the frequency. This could be a problem in harsh environments but the enclosed gyro has a thermal time constant on the order of three hours. If the outside environment changes rapidly the cavity is very slow

to follow and it is difficult to generate large temperature gradients. Also, the zerodur laser body has a very low expansion coefficient.

The final topic is noise in the electronics. If the electronics adds noise not present in the laser signal, then the stability will be degraded. As long as the components are military grade and care is taken during the design phase electrical noise should not be a problem.

VI SUMMARY AND CONCLUSIONS

The objective of this research was to establish the feasibility and initial technology base for the ring laser clock concept. Theoretical evaluation was done to determine if currently available ring laser technology could achieve performance levels comparable to the state-of-the-art high accuracy timing sources. Currently available ring laser gyro equipment was used with minimum modification to develop an operating laser clock. Tests were conducted and the results analyzed to evaluate performance and determine if the measured accuracy was compatible with current needs. Evaluations were conducted to determine if further effort in the laser clock area was warranted and to identify areas in which more detailed work should be performed.

State-of-the-art high accuracy timing sources were identified and available performance compared to current aircraft needs. The state-of-the-art in laser technology was identified, laser clock design approaches were developed, and error sources were identified which would limit the laser clock performance. Component level designs of the laser clock were developed for modification of existing ring laser equipment to provide a laser clock output. Test equipment was identified and configured to test the clock without masking the clock's true performance by measurement system error. The clock and test equipment approaches were presented to the Raytheon Company and due to their interest in the concept, they committed the necessary resources to support the development with only minor changes to the design. Raytheon built the clock electronics to be used with one of their research ring lasers and prepared the test equipment using their in-house resources. The experiment was conducted at the Raytheon plant

and the resulting test data was analyzed to determine the laser clock performance.

Short term stability for periods of 1-100 milliseconds was determined to be quantum limited by the laser linewidth under conditions of constant laser clock temperature and the short term performance was equal to that of existing precision time standards. The Faraday rotator induced frequency shift was the predominate error source for the integration times beyond 0.1 second. These were the only two error sources observed in the best data. Next generation laser clock electronic designs were developed to address improved long term stability and allow identification of additional performance limiting error sources which are not observable with currently available equipment.

In conclusion, good short-term stability has been obtained, but long-term stability needs to be improved. The laser clock is a transfer frequency standard which when used with Global Positioning System (GPS), Joint Tactical Information Distribution System (JTIDS), and radar techniques will meet high performance fighter application requirements without the need for a dedicated precision frequency standard. When implemented in conjunction with existing RLG systems, the additional cost of the clock function would be one thousand to three thousand dollars (depending upon the level of integration) with reduced life cycle cost compared to having a separate clock and gyro system. Careful packaging could yield a reduced volume when compared to separate clock and gyro devices. The multifunction ring laser gyro/clock could also be used for other applications on missiles, helicopters and other high performance vehicles. The ring laser clock

could be very useful for shipboard applications if the long-term Faraday drift problem is solved by the recommended approach. The precision frequency and time standard function could be performed at reduced life cycle cost with significantly simplified maintenance at sea since support would no longer be required for two independent clock and gyro systems using different technology, test equipment and spare parts.

VII RECOMMENDATIONS

RECOMMENDATION FOR CURRENT RLG

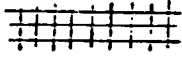
The temperature sensitivity of the Faraday rotator must be corrected. The method outlined in the section IV, RECOMMENDED CLOCK /GYRO OPERATION, of this thesis would eliminate the drift. The estimated quantum limited performance of the laser clock is shown in Figure 27. The recommended method for tuning as outlined in section IV, RECOMMENDED METHOD OF TUNING/SETTING, should be implemented. This would provide ease of setting and user defined reference frequencies.

RECOMMENDATIONS FOR FUTURE RLG'S

The clock frequency from a multioscillator with a magnetic mirror is derived the same way as the multioscillator with the Faraday rotator. The multioscillator with a quartz rotator instead of the non-planar cavity could be used as a laser clock. The quartz rotator approach might be limited by the temperature sensitivity of the quartz rotator. Another method that could be used is the $TEM_{q,0,0}$ and $TEM_{q,0,1}$ laser discussed in the theory section, see Figure 13, if the diode could detect the beat between the strong and weak modes. The same is true for the $TEM_{q,0,0}$ and $TEM_{q+1,0,0}$ also discussed in that section. There are various other types of possible ring laser clocks, but all have at least four frequencies.

RECOMMENDATIONS FOR OTHER TYPES OF LASERS

The use of a beat frequency between modes for producing a clock frequency could be used on the lasers shown in Figure 6, Figure 7, and Figure 8. However, since these are linear lasers they would only

Q- - - -Q CRYSTAL OSCILLATOR
 C - - - -C CESIUM 5062C
 R- - - -R RUBIDIUM 5065A
 ESTIMATED PERFORMANCE
 FOR LASER CLOCK

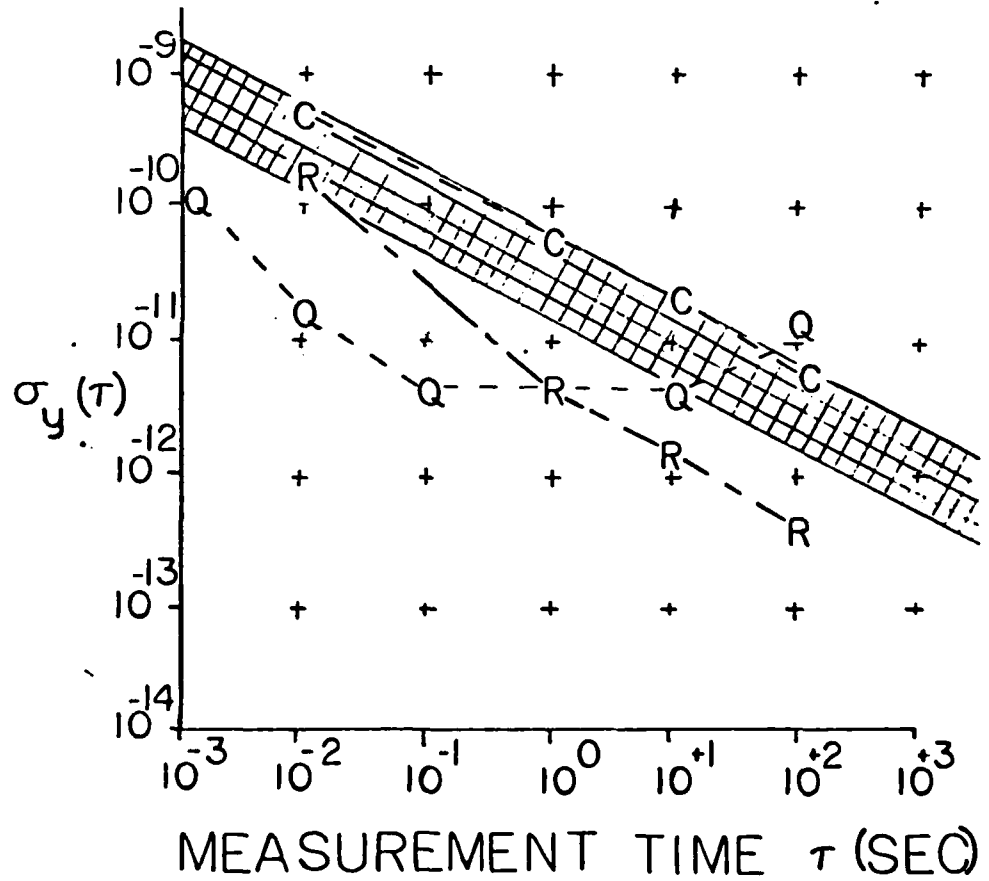


FIGURE 27 ESTIMATED PERFORMANCE

provide a clock function. There are several types of stabilized linear lasers that could potentially be used as laser clocks.

BIBLIOGRAPHY

1. BARNES, JAMES A. et al. "Characterization of Frequency Stability," IEEE TRANSACTION ON INSTRUMENTATION AND MEASUREMENT, IM20 (2): 105-120 (May 71).
2. CLEMENCE, GERALD M. "Quartz Clock," McGraw-Hill Encyclopedia of Science and Technology, Volume II New York: McGraw-Hill Book Company (1977).
3. GERBER, E. A. and R. A. SYRES "State of the Art - Quartz Crystal Units and Oscillators," Proceeding of the IEEE, 54 (2): 103-115 (Feb 66)
4. PRZYJEMSKI, JOSEPH M. "A Compensation Technique for Acceleration-Induced Frequency Changes in Crystal Oscillation" presented at NAECON 1978. Charles Stark Draper Laboratory, Inc. Paper p-606.
5. PETERS, HARVEY E. "Light-Weight Hydrogen Maser," RADC-TR-81-270 Rome Air Development Center, Air Force Systems Command, Griffiss Air Force Base, New York 13441.
6. HEWLETT-PACKARD, MEASUREMENT/COMPUTATION, ELECTRONICS INSTRUMENTS AND SYSTEMS 1981: 325-333, 557-558 (1981).
7. McCOUBREY A. D., KERN R. H. "Precision Frequency Sources," PROCEEDING OF THE FOURTH PRECISE TIME AND TIME INTERVAL PLANNING

CONFERENCE; GODDARD SPACE FLIGHT CENTER, 46-54 (Nov 14-16 1972)

8. MCCOUBREY A. D. "A Survey of Atomic Frequency Standards,"

PROCEEDINGS OF THE IEEE, 54 (2): 116-135 (Feb 1966).

9. WEIDNER, Richard T. and ROBERT L. SELLS. Elementary Modern Physics

Boston: Allyn and Bacon, Inc., 1973.

10. HELLWIG, HELMUT W. "Atomic Frequency Standards: A Survey,"

PROCEEDING OF THE IEEE, 63 (2): 212-229 (Feb 75).

11. ZAMPIELLO, ALLEN and DONALD PASIK. Multioscillator Ring Laser

Gyro:AFAL-TR-78-133 (May 76 - Jan 78).

12. SCULLY, M. O., V. SANDERS, and M. SARGENT III, "Novel multioscil-

lator approach to the problem of locking in two-mode ring laser gyros," OPTICS LETTERS, 3 (2): 43-45 (AUG 78).

13. ARONOWITZ, F. "The Laser Gyro-Tutorial Review" SPIE, 157 laser

inertial rotation sensors 1978: 2,20 (1978).

14. YARIV, Amnon, INTRODUCTION TO OPTICAL ELECTRONICS, Second Edit-

ion, New York, New York, Rinehart and Winston, 1976

15. DORSCHNER, T., H. A. HAUS, M. HOLTZ, I. SMITH, and H. STATZ

"Laser Gyro at Quantum Limit," IEEE Journal of Quantum Electronics, 16 (12): 1376-1379 (Dec 80).

16. SMITH, I. W. and T. A. DORSCHNER. "Electromagnetic Wave Ring Resonator," U.S. Patent #4,110,045, 29 Aug 78.

17. DIEKE, G. H. and W. WATSON. McGraw-Hill Encyclopedia of Science and Technology, Volume 8, New York: McGraw-Hill Book Company, 1977.

18. MEYER, J. R. Introduction to Classical and Modern Optics. Englewood Cliffs, N.J.: Prentice-Hill, Inc. 1972.

19. SMITH, I. W. and T. A. DORSCHNER. "Biasing the Raytheon Four-Frequency Ring Laser Gyroscope," SPIE, 157: 21-29 (1978).

20. SARGENT M. III, M. M. O. SCULLY and W. E. LAMB JR. Laser Physics, Addison-Wesley, Reading, MA. 1974.

21. WEICHEL, H., "The Uncertainty Principle and Spectral Width of a Laser Beam," American Journal of Physics, 44 (9): 839-840 (Sep 76).

22. LIPSCHUTZ, S., Schaum's Outline of Theory and Problems of Probability, New York: McGraw-Hill Book Company. 1973.

23. BURINGTON, R. S., Handbook Outline of Theory and Problems of Probability, New York: McGraw-Hill Book Company. 1973.

24. LONGHURST, R. S., Geometrical and Physical Optics (Third Edition) Hong Kong: The Continental Printing Company, Ltd., 1973.

25. JENKINS, F. A.; G. H. DIEKE and W. WATSON McGraw-Hill Encyclopedia of Science and Technology Volume 14 New York: McGraw-Hill Book Company, 1977.
26. DIEKE, G. G. and W. WATSON. McGraw-Hill Encyclopedia of Science and Technology Vol 5, McGraw-Hill Book Company, 1977.
27. WEST W., McGraw-Hill Encyclopedia of Science and Technology, Vol 1 New York: McGraw-Hill Book Company, 1977.
28. DORSCHNER T.A., and I. A. SMITH. Magnetic Bias Techniques for Laser Gyros AFWAL-TR-80-1133, September 1980.
29. Private conversations with Maj S. BALAMSO at AFIT. Figure 5 is a modification of an early design. Neither the early design nor Figure 5 have been built. Figure 6 shows that in a multimode ring the longitudinal modes alternate between S and P polarization.
30. Result of a conversation with S. EZEKIEL from MIT while at Rome Air Development Center, Hanscom AFB, MA., on 5 Mar 82.
31. SIEGMAN A. E., An Introduction to Lasers and Masers, New York: McGraw-Hill Book Company, 1971.
32. THOMAS M. A. "Laser Gyroscope Technology and Temperature Sensitivity of a Honeywell GG 1328AC Laser Gyro," Master of Science Thesis Naval Postgraduate School, Monterey, California, June 1978.

33. JACOBS S. F. "How Monochromatic is laser Light?," American Journal of Physics, 47 (7): 597-601 (July 79).

34. Private conversations with Irl Smith at Raytheon Research.

APPENDIX A: QUANTUM LIMIT

INTRODUCTION

The purpose of Appendix A is to determine the quantum limited clock accuracy. The first problem is to determine the uncertainty in frequency of a photon that was emitted by an excited atom in free space. The relationship between uncertainty in the photon's energy and the radiative lifetime of the atom is given by the Heisenberg uncertainty principle which is given by

$$\Delta E \Delta T \geq h/4\pi \quad (32)$$

where ΔE is the uncertainty in the photon energy, ΔT is the time in which the photon was emitted, and h is Planck's constant. In the single photon case the energy is given by $h\nu$. This gives

$$\Delta E = h\Delta\nu \quad (33)$$

where $\Delta\nu$ is the uncertainty in frequency. The uncertainty relation now becomes

$$\Delta\nu \Delta T \geq 1/4\pi \quad (34a)$$

$$\Delta\nu \geq 1/4\pi\Delta T \quad (34b)$$

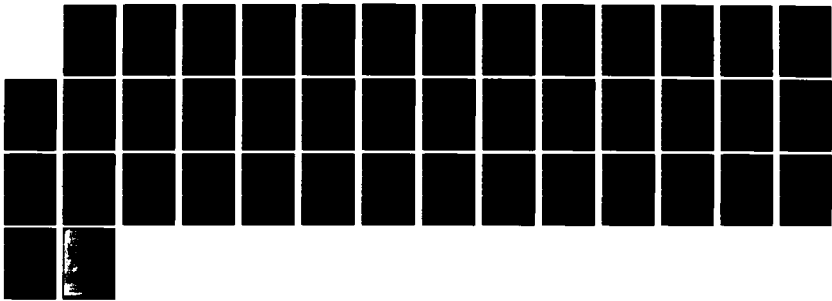
AD-A127 519

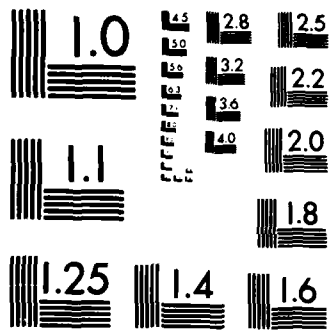
ULTRA-STABLE LASER CLOCK(U) AIR FORCE INST OF TECH
WRIGHT-PATTERSON AFB OH SCHOOL OF ENGINEERING
R L FACKLAM MAR 83 AFIT/GEP/PH/82D-28

2/2

UNCLASSIFIED

F/G 14/2 NL





MICROCOPY RESOLUTION TEST CHART
NATIONAL BUREAU OF STANDARDS-1963-A

taking $\Delta T = \tau_R$ (34c)

yields $\Delta \nu \geq 1/4\pi\tau_R$ (34d)

and τ_R is the radiative lifetime.

THE HEISENBERG UNCERTAINTY PRINCIPLE APPLIED TO COHERENT LASER STATES

This part the problem is to determine the uncertainty in frequency of a laser beam. The energy of the coherent state, a minimum uncertainty state, is given by

$$E = nh\nu \quad (35)$$

where n is the expectation value of the photon number, and ν is the photon frequency. The uncertainty in the energy is now given by

$$\Delta E = nh \Delta \nu + \Delta n h \nu \quad (36)$$

where Δn is the uncertainty in the number of photons (Ref 21: 839).

To determine if one term of the two terms in (36) dominates take one to be equal to zero and then the other. After this is done compare the two results to determine if either approximation is valid. Set the second term in (36) equal to zero and use this result in the uncertainty principle. This yields

$$nh\Delta\nu\Delta T \geq h/4\pi \quad (37a)$$

$$\Delta\nu\Delta T \geq \frac{1}{4\pi n} \quad (37b)$$

and using

$$\Delta T = \tau_c$$

$$\Delta\nu \geq \frac{1}{4\pi n\tau_c} \quad (37c)$$

where τ_c is the cavity lifetime.

Set the first term to zero and use this result in the uncertainty principle. This yields

$$\Delta nh\nu\Delta T \geq h/4\pi \quad (38a)$$

$$\Delta n\nu\Delta T \geq 1/4\pi \quad (38b)$$

and assume

$$\nu = \frac{\Delta\phi}{2\pi\Delta T}$$

yields

$$\frac{\Delta n\Delta\phi\Delta T}{2\pi\Delta T} \geq \frac{1}{4\pi} \quad (38c)$$

$$\Delta n\Delta\phi \geq 1/2 \quad (38d)$$

where $\Delta\phi$ is the uncertainty in phase. To solve (38d) we use the fact that for a coherent state, the photon statistics follow a Poisson distribution (Ref 20: 109). A Poisson distribution has the value of Δn given by

$$\Delta n \equiv \sqrt{n} \quad (39)$$

(Ref 22: 109). The Poisson distribution can be approximated by a binomial which can be approximated by a normal distribution for large n . In the case of a laser, n is so large that the Poisson distribution approximates a normal distribution. The area in the range $\mu \pm \sigma$ is 68.27% (Ref 23: 256-258). Then equation (38d) and (39) yields

$$\Delta\phi \geq \frac{1}{2\sqrt{n}} \quad (40)$$

From probability theory we know that the relationship between the standard deviation of the variable x and the variance of x is given by

$$\sigma_x = \sqrt{\text{VAR}(X)} \quad (41a)$$

Also,

$$\text{VAR}(X \pm Y) = \text{VAR}(X) + \text{VAR}(Y) \quad (41b)$$

where σ_x is the standard deviation of X , and $\text{VAR}(X)$ is the variance of X .

The purpose of equations (42) to (44) is to determine the uncertainty in the experimentally measured total phase. The following should be taken as definitions

$$\Delta n \equiv \sigma_n \quad (42a)$$

$$\Delta \phi \equiv \sigma_d \quad (42b)$$

$$\text{VAR}(\phi_{T=\tau_c}) = \sigma_{\phi_{T=\tau}}^2 \equiv (\Delta \phi_{T=\tau})^2 \quad (42c)$$

$$\text{VAR}(\phi_{T=0}) = \sigma_{\phi_{T=0}}^2 \equiv (\Delta \phi_{T=0})^2 \quad (42d)$$

The quantity to be measured is

$$\phi_{TOT} = \phi_{T=\tau_c} - \phi_{T=0} \quad (43)$$

where ϕ_{TOT} is the total phase in time τ_c . Using equation (43) and (41b) the result is

$$\text{VAR}(\phi_{TOT}) = \text{VAR}(\phi_{T=\tau_c} - \phi_{T=0}) \quad (44a)$$

$$\text{VAR}(\phi_{TOT}) = \text{VAR}(\phi_{T=\tau_c}) + \text{VAR}(\phi_{T=0}) \quad (44b)$$

$$\Delta \phi_{TOT}^2 = \Delta \phi_{T=\tau_c}^2 + \Delta \phi_{T=0}^2 \quad (44c)$$

$$\Delta \phi_{TOT} = \sqrt{\Delta \phi_{T=\tau_c}^2 + \Delta \phi_{T=0}^2} \quad (44d)$$

and assume that the uncertainty in measuring the phase at time equal zero is the same as uncertainty in measuring the phase at time equal τ_c

$$\Delta\phi_{T=\tau_c} = \Delta\phi_{T=0} = \Delta\phi \quad (44e)$$

this yields

$$\Delta\phi_{TOT} = \sqrt{2}\Delta\phi \quad (44f)$$

Using equation (44f) and (38d) yields

$$\Delta\phi_{TOT} \geq \frac{1}{\sqrt{2n}} \quad (45)$$

Equation (43) gives the value of the phase, equation (44d) gives the uncertainty in the phase and equation (45) relates the phase uncertainty to n . Equation (45) gives the uncertainty in the measurements of the phase in time τ_c . The frequency uncertainty is given by

$$\Delta\omega_{\tau_c} \geq \frac{\Delta\phi_{\tau_c}}{\tau_c} \geq \sqrt{\frac{1}{2\tau_c^2 n}} \quad (46)$$

If we sample for a time $T = N\tau_c$ the number of photons observed is given by

$$n_{OBS} = nN = nT/\tau_c \quad (47)$$

where N is the number of lifetimes. Using (46) and (47) the following is obtained

$$\Delta\omega_T \geq \sqrt{\frac{1}{2 \tau_c^2 n_{OBS}}} \quad (48a)$$

$$\Delta\omega_T \geq \sqrt{\frac{1}{2 \tau_c^2 n T/\tau_c}} \quad (48b)$$

$$\Delta\omega_T \geq \sqrt{\frac{1}{2 \tau_c n T}} \quad (48c)$$

Now use

$$P = nh\nu/\tau_c \quad (49a)$$

and

$$\frac{1}{\tau_c} = \frac{\omega_0}{Q} = \frac{c}{L} \times \text{LOSS PER PASS} \quad (49b)$$

where Q is the quality factor, c is the speed of light, and L is the cavity length (Ref 15: 1376-1377). This yields

$$\Delta\omega_T \geq \frac{\omega_0}{Q} \sqrt{\frac{h\nu}{2PT}} \quad (50a)$$

or

$$\Delta\nu_T \geq \frac{\nu_0}{Q} \sqrt{\frac{h\nu}{2PT}} \quad (50b)$$

Figure 28 shows plots of (34e), (37d), and (50b). Equation (50b) is larger than (37d) by \sqrt{n} , so for even low power (50b) is going to be the dominate term.

SPONTANEOUS PHOTON METHOD

Another way of computing the quantum limit is by means of the spontaneous photon method. In the laser cavity there is one

EXAMPLE WITH
 $P = 3.14 \text{ mW}$
 $\tau_c = 1 \text{ } \mu\text{S}$
 $h\nu = 3.14 \times 10^{-19} \text{ J}$
 $\langle n \rangle = 10^{10}$

EQUATION
 --- (34e)
 - - - (37d)
 - - - - (50b)

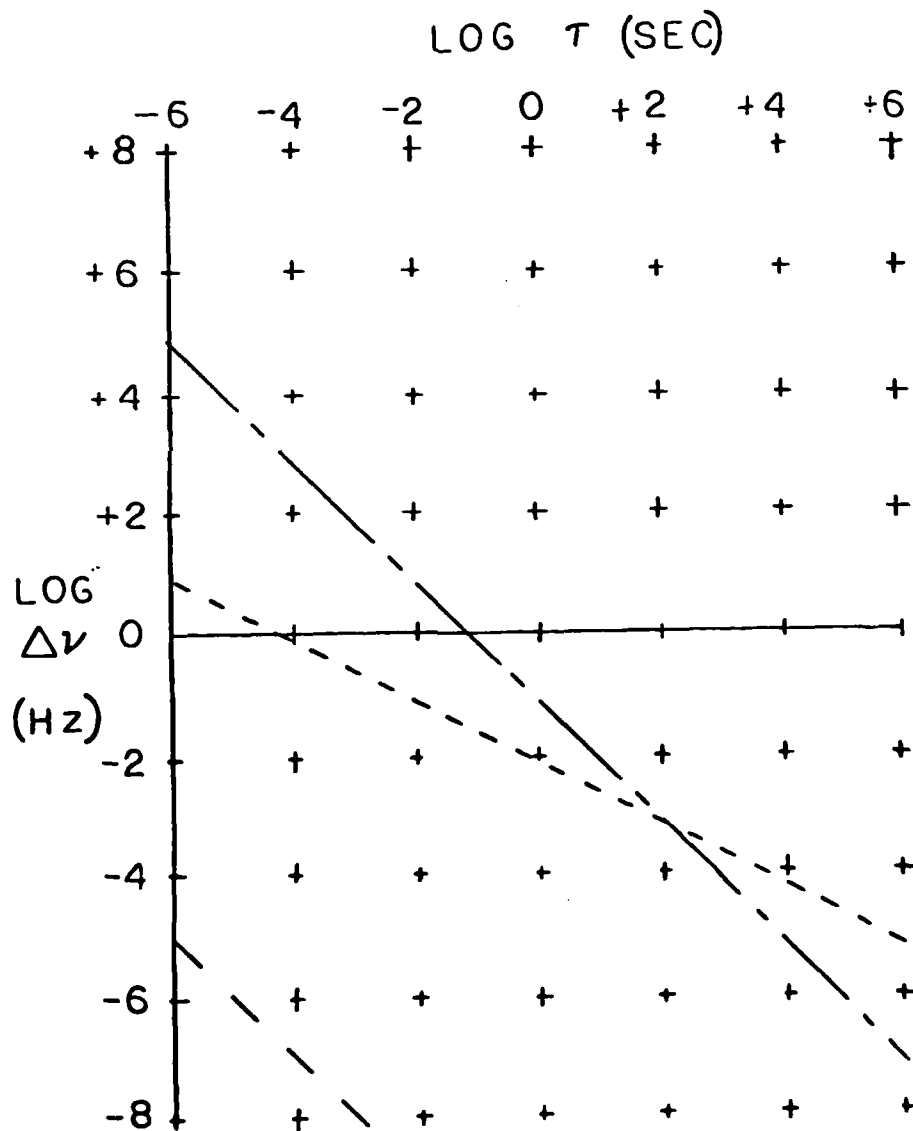


FIGURE 28 TIME DEPENDENCE OF LASER LINEWIDTH

spontaneous photon per mode and each mode contains n photons (see equation 4b). A spontaneous photon is emitted every cavity lifetime with a phase that is random when compared to the beam. The electric field phasor of a laser beam is shown in Figure 29. We see that the energy is given by

$$E = (\sqrt{n} E_0')^2 = n E_0'^2 = nh\nu \quad (51)$$

where E_0' is the electric field of one photon, E is the steady state energy in the cavity, and n is the number of photons. If a spontaneous photon is emitted with a relative phase angle θ then

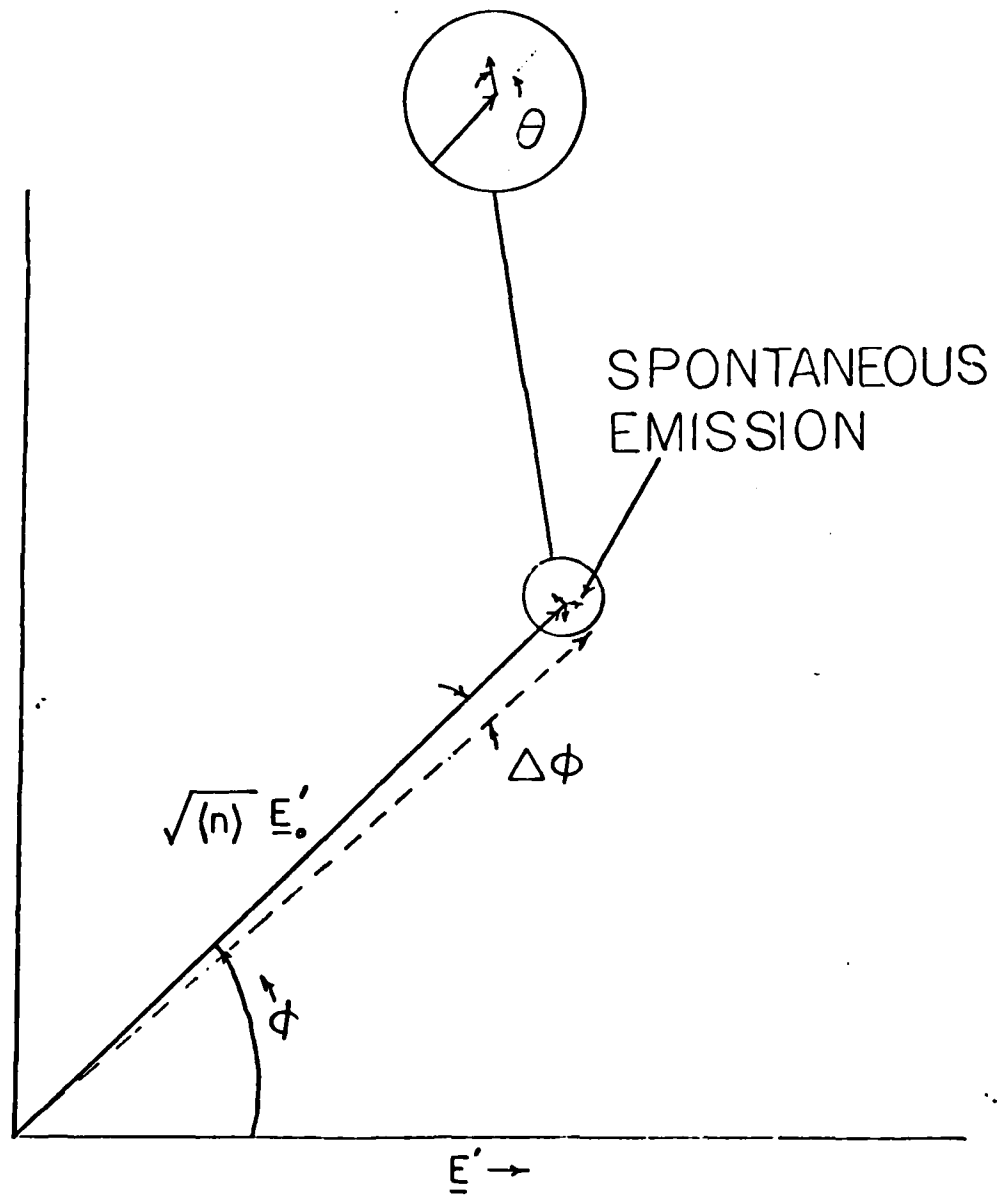
$$\Delta E_0(\text{rms}) = \frac{\int_0^\pi \sin^2\theta \, d\theta}{\int_0^\pi d\theta} E_0' = \frac{E_0'}{\sqrt{2}} \quad (52)$$

is the effective component that alters phase. The change in phase is given by

$$\Delta\phi_{\tau_C} = \frac{\Delta E_0(\text{rms})}{\sqrt{E}} = \frac{\frac{E_0'}{\sqrt{2}}}{\sqrt{n} E_0'} = \frac{1}{\sqrt{2n}} \quad (53)$$

The frequency uncertainty is given by

$$\Delta\omega_{\tau_C} = \sqrt{\frac{1}{2 \tau_C^2 n}} \quad (54)$$



(REF 20:336)
 FIGURE 29 ELECTRIC FIELD PHASOR

and again using (47) and (48a) gives

$$\Delta\omega_T = \sqrt{\frac{1}{2\tau_c n T}} \quad (55)$$

By using (49a) and (49b) the result is again (50a) or (50b).

INTENSITY FLUCTUATION

The purpose of this section is to prove that the distribution of photons in a coherent state is a Poisson distribution. This derivation requires considering both the wave properties and the particle properties of the photon. Take the initial value of E_i and E_i' as

$$E_i' = \sqrt{n} E_0' \quad (55a)$$

$$E_i = nh\nu \quad (55b)$$

where n is the number of photons, E_i is the initial energy of the coherent laser state, E_0' is the electric field of one photon with frequency ν , i is the initial value at time equal zero, f is the final value at time equal τ_c , and $E_{i,f}'$ is the initial/final total electric field. The effective number of photons in a coherent state can be defined as the number of photons that would be required to give the coherent state an electric field of E' . Assume the effective number of photons is a Poisson distribution with $\sigma = \sqrt{n}$. When the photon number increases by 2σ the following occurs

$$E_f = (n+2\sigma)h\nu \quad (56a)$$

$$E_f = (n+2\sqrt{n})h\nu \quad (56b)$$

$$E_f = E_i + (2\sqrt{n})h\nu \quad (56c)$$

and

$$E_f' = \sqrt{(n+2\sqrt{n})} E_0' \quad (57a)$$

$$E_f' = (\sqrt{n}+1) E_0' \quad \text{for } n \gg 1 \quad (57b)$$

$$E_f' = E_i' + E_0' \quad \text{for } n \gg 1 \quad (57c)$$

Without making any assumptions consider the case of one spontaneous photon being added in phase to a coherent state with the same initial values as given in (55) this yields the result

$$E_f' = (\sqrt{n}+1) E_0' \quad (58a)$$

$$E_f = (n+2\sqrt{n}) h\nu \quad (58b)$$

where (58a) is the same as (57b) and (58b) is the same as (56b). This means that the effect of adding one spontaneous photon in phase with the coherent state increases the energy of the coherent state by the $2\sqrt{n}$ during the lifetime of the spontaneous photon τ_c . In the quantum limited case the cavity lifetime is much shorter than the coherence time, so the phase difference between the spontaneous photon and the coherent state stays the same. The process of spontaneous emission is like a radioactive decay and so the statistics of spontaneous emission are Poisson. Poisson statistics allows of the occurrence of either several spontaneous photons in the cavity or none, but does yield a mean lifetime of τ_c . The quantities to be considered are then how many spontaneous photons are in the cavity at any one time as well as their phase relative to that of coherent state. The RMS effect of the spontaneous photon on the mode's phase depends on $\sin^2 \theta$ and so the RMS effect of the spontaneous photon on the mode's intensity depends on $\cos^2 \theta$. As shown in (52) the RMS value is the maximum

value divided by $\sqrt{2}$. The maximum change in energy that one photon can cause is $2\sqrt{n}$ so the RMS change is $\sqrt{2n}$. Finally, to determine the probability of a specific change in energy, one must consider both the value of θ and the number of spontaneous photons which is given by a Poisson distribution. The RMS value is further reduced by $\sqrt{2}$ to allow finite probability beyond the maximum points for one photon. The effective number of photons in the coherent state is a Poisson distribution, which is shown graphically in Figure 30. The distribution has a mean value of $n_t = n+1$ where n is the steady state number of photons in the coherent state and a width of $\sigma = \sqrt{n}$.

The effect of any spontaneous photon on the energy of the coherent state is only during the spontaneous photon's lifetime. Understandably, the effect is not cumulative. However, the effect of the spontaneous photon on the phase of the coherent state is cumulative. The phase of the coherent state is permanently altered by all the spontaneous photons that have existed during the observation time τ .

Since the above result is a quantum limited calculation it is assumed that

$$\frac{d}{dt} i_d = 0 \quad (59)$$

where i_d is the discharge current. The amount of fractional change in the discharge current required to increase the uncertainty in the effective number of photons in the coherent state by $\sqrt{2}$ is found as follows. Assuming that the two effects behave as independent random variables and the laser medium is not saturated then the following can be used

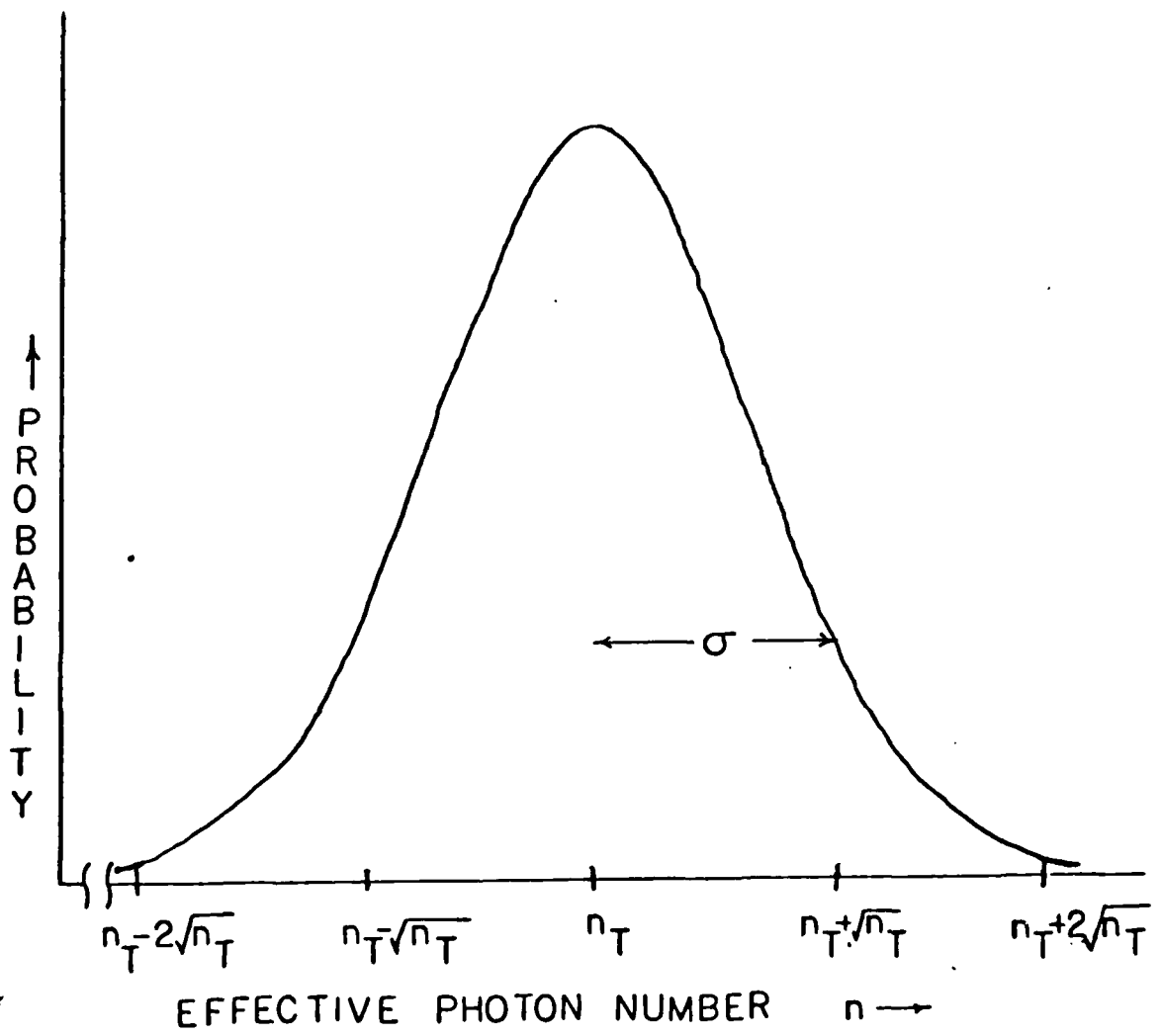


FIGURE 30 PHOTON DISTRIBUTION

$$\frac{\Delta i}{i} = \frac{\Delta n}{n} \quad (60)$$

now using $\Delta n = \sqrt{n}$ yields

$$\frac{\Delta i}{i} = \frac{\sqrt{n}}{n} = \frac{1}{\sqrt{n}} \quad (61)$$

where Δi is the drift in the current. For example if $n=10^8$, then (61) yields $\Delta i/i = 10^{-4}$. For comparison a good current control can hold $\Delta i/i = 10^{-5}$. The photons that result due to a drift in current are stimulated photon and do not increase the quantum limited linewidth. Fluctuations in the discharge current causes the beat frequency to drift via dispersion (see Appendix D).

CONCLUSIONS ON THE QUANTUM LIMIT

The results here agree with the results in Ref 15 but not with the results in Ref 21 or in Ref 33. The problem stems from the dual nature of the photon. In Ref 21 the photon was treated as a particle. It was assumed that the laser under consideration had a perfect current control. This assumption yields the result $\Delta n = 0$. The problem here is that the quantity desired is a wave property of the photon and not a particle property. The result presented here $\Delta n = \sqrt{n}$ is obtained by considering the photon as a wave that was added in phase to the electric field inside the cavity. Then from that, the effective number of photons was inferred. The approach presented here also yields the result that the number of photons when considered as a particle is a constant. As stated before, the phase of coherent state is permanently altered by every photon but the strength of the coherent field is only altered during the photons lifetime. Accordingly,

there is a random walk process occurring in the phase of the coherent state but not in intensity of the coherent state. At first glance it seems like a violation of the law of conservation of energy for a photon to add \sqrt{n} effective photons to the coherent state. However, the uncertainty principle says that there will be an uncertainty in the energy of the coherent state and to a very good approximation the uncertainty in energy is $\sqrt{n} h\nu$.

APPENDIX B: NON-PLANAR CAVITY

INTRODUCTION

The non-planar cavity is described in U.S. patent #4,110,045 (Ref 16). The cavity modes alternate polarization states such that every other mode is right circularly polarized with the in-between modes left hand circularly polarized (see Figure 31). The cavity allows only circularly polarized light to oscillate. Both modes undergo a -90° phase change upon one round trip. Figure 32 shows one form of non-planar cavity that is an optical equivalent to the laser used in the experiment.

EFFECTS OF THE CAVITY

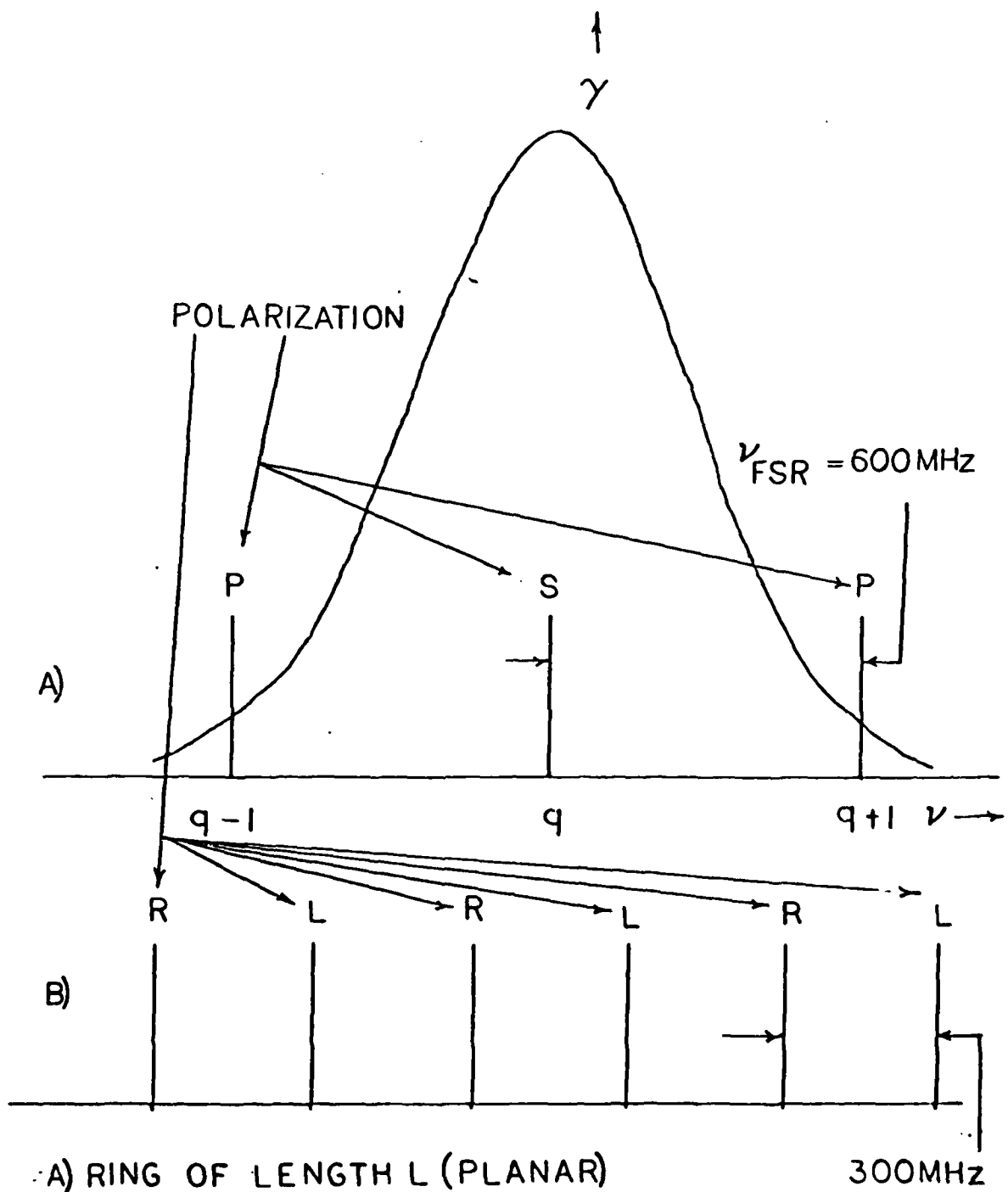
The effects of one roundtrip through the laser can be symbolized as follows

$$E_1 ! E_1' = -E_2 \quad (62a)$$

$$E_2 ! E_2' = E_1 \quad (62b)$$

where the symbol ! stands for one pass, E_1 is the initial electric field component in the +x direction, E_2 is the initial electric field component in the +y direction, and the prime stands for the value of E after one round trip. To interpret (62a) start with E_1 , then make one round trip and the result is E_1' which is equal to $-E_2$. A right hand circularly polarized mode is given by

$$E_r = (E_1 + E_2 e^{i\pi/2}) e^{-i\omega t} \quad (63)$$

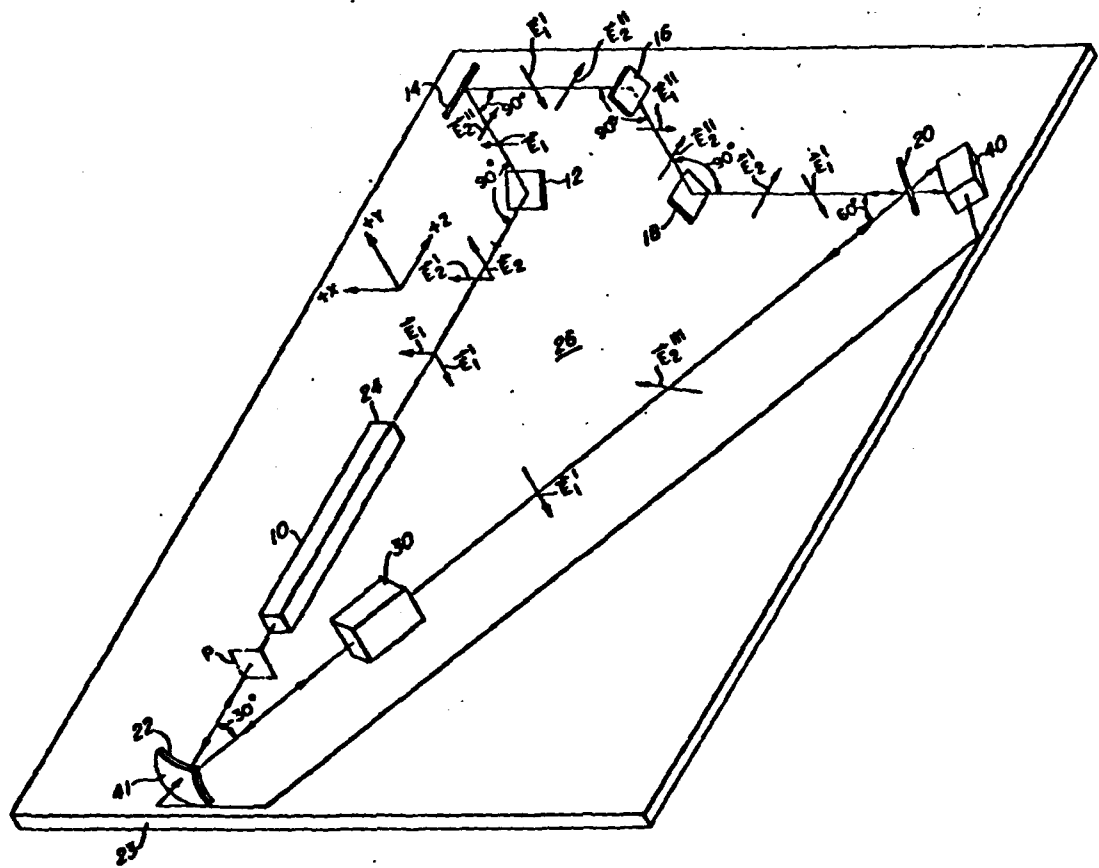


A) RING OF LENGTH L (PLANAR)

300MHz

B) RING OF LENGTH L (NON-PLANAR)

FIGURE 31 MODE STRUCTURE



U.S. Patent

Aug. 29, 1978

Sheet 1 of 3

4,110,045

FIGURE 32 NON-PLANAR CAVITY

where ω is the angular frequency of wave. The effect of one passage can be determined by using (62) and (63). The effect of one passage of a right hand circularly polarized mode is

$$E_r' = (E_1' + E_2' e^{-i\pi/2}) e^{i2\pi L/\lambda} e^{-i\omega t} \quad (64)$$

Using (62) to substitute for the prime values in (64) and simplifying the results in the following

$$E_r' = (-E_2 + E_1 e^{-i\pi/2}) e^{i2\pi L/\lambda} e^{-i\omega t} \quad (65a)$$

$$E_r' = e^{i\pi/2} (E_1 - E_2 e^{-i\pi/2}) e^{i2\pi L/\lambda} e^{-i\omega t} \quad (65b)$$

$$E_r' = e^{i\pi/2} e^{i2\pi L/\lambda} E_r \quad (65c)$$

where $-e^{-i\pi/2} = e^{i\pi/2}$. A left hand circularly polarized mode is given by

$$E_l = (E_1 + E_2 e^{-i\pi/2}) e^{-i\omega t} \quad (66)$$

The effect of one passage on a left hand circularly polarized mode is

$$E_l' = (E_1' + E_2' e^{-i\pi/2}) e^{i2\pi L/\lambda} e^{-i\omega t} \quad (67a)$$

$$E_l' = (-E_2 + E_1 e^{-i\pi/2}) e^{i2\pi L/\lambda} e^{-i\omega t} \quad (67b)$$

$$E_l' = e^{-i\pi/2} e^{i2\pi L/\lambda} E_l \quad (67c)$$

where $-e^{i\pi/2} = e^{-i\pi/2}$. The relative phase difference between the right and left hand components is

$$(2\pi L/\lambda + \pi/2) - (2\pi L/\lambda - \pi/2) = \pi \quad (68)$$

so the relative phase is 180° .

The resonant frequency can be computed as follows. First represent a RHCP wave as

$$E_R = R_e(\underline{e}_r) = \underline{e}_1 \cos(\beta s - \omega t) - \underline{e}_2 \sin(\beta s - \omega t) \quad (69a)$$

and

$$\beta_0 = 2\pi f/c \quad (69b)$$

$$\beta_0 = 2\pi/\lambda \quad (69c)$$

where S is along the direction of propagation, ω is the angular frequency, f is the circular frequency, c is the speed of light, and λ is the nominal wavelength. In a planar cavity the resonant condition is

$$\beta_0 = 2\pi q \quad (70)$$

and the resonant frequency is

$$f_0 = q \frac{c}{n_f L} \quad (71)$$

where q is the mode number. The effect of equation (62) is to give

$$E_R' = R_e(\underline{e}_r') \quad (72a)$$

$$= \underline{e}_1 \cos(-\omega t + \beta s + \pi/2) - \underline{e}_2 \sin(-\omega t + \beta s + \pi/2) \quad (72b)$$

Resonance imposes the following condition

$$\beta L + \pi/2 = 2\pi q \quad (73a)$$

$$\beta L = 2\pi q - \pi/2 \quad (73b)$$

and the resonance frequency of

$$f_r' = \frac{c}{2n_i L} (2\pi q - \pi/2) \quad (74a)$$

$$f_r' = q \frac{c}{n_i L} + \frac{c}{4n_i L} \quad (74b)$$

$$f_r' = f_0 + \frac{c}{4n_i L} \quad (74c)$$

The same argument holds for the LHCP mode and yields

$$f_l' = q \frac{c}{n_i L} + \frac{c}{4n_i L} \quad (75a)$$

$$f_l' = f_0 + \frac{c}{4n_i L} \quad (75b)$$

So the beat frequency between

$$\Delta f = f_l' - f_r' = \frac{c}{n_i L} \frac{2\phi}{2\pi} \quad (76)$$

and for $\phi = \pi/2$

$$\Delta f = \frac{c}{n_j L} \frac{2(\pi/2)}{2\pi} = \frac{c}{2n_j L} \quad (77)$$

Figure 31(A) shows the mode structure for a ring of length L , and Figure 31(B) shows a non-planar ring of length L . Note that the non-planar ring has twice as many modes.

APPENDIX C: FARADAY ROTATOR

INTRODUCTION

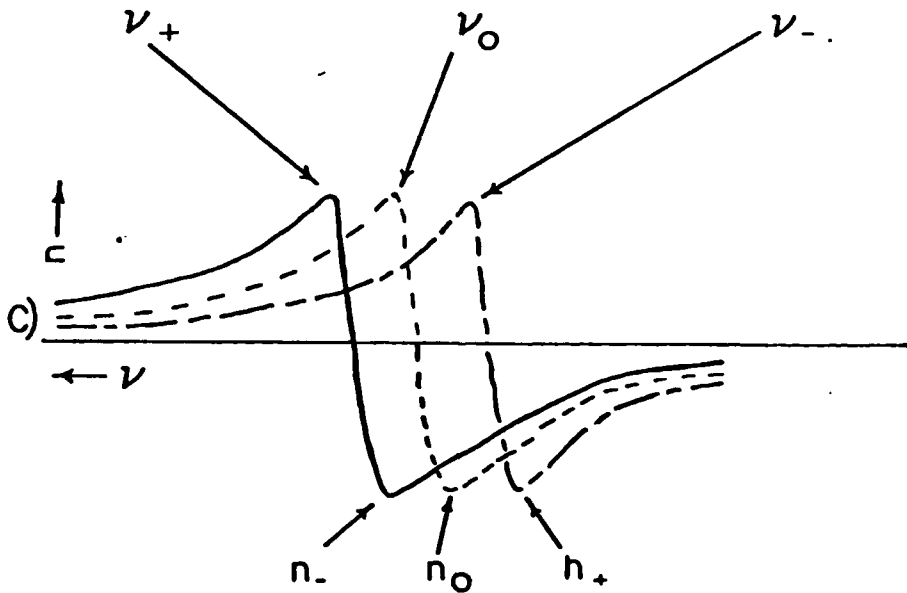
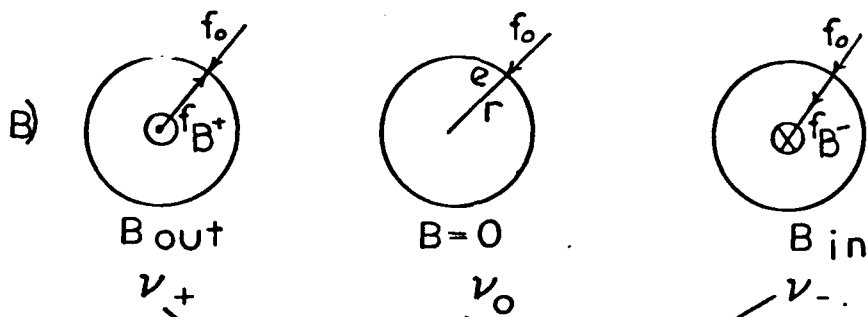
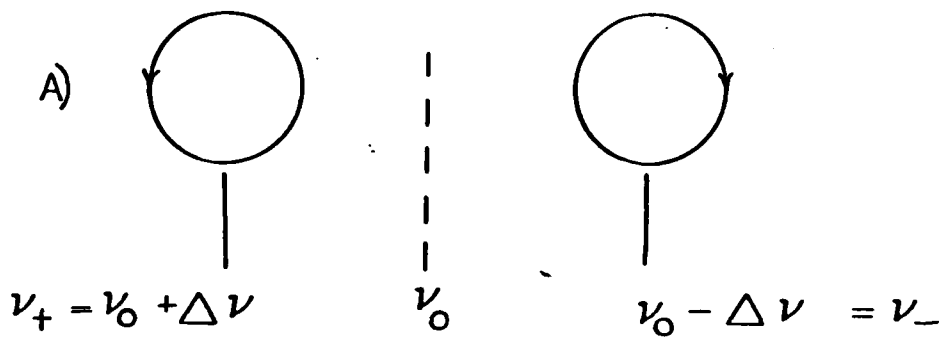
The Faraday rotator consists of an optically transparent medium which is under the influence of an external magnetic field. As polarized light passes through in the direction of the field, the plane of polarization is rotated. This effect was discovered by Michael Faraday in 1845 (Ref 24: 587). The amount of rotation $\Delta\rho_F$ is given by

$$\Delta\rho_F = VL_F |\underline{B}| \cos \theta_F \quad (78)$$

where V is the Verdet constant, L_F is the distance through the material, $|\underline{B}|$ is the magnitude of the magnetic field and θ_F is the angle between the direction of light propagation and the magnetic field (Ref 18: 299). The value of $\Delta\rho_F$ is positive when the rotation is in the clockwise direction when looking in the direction of the magnetic field. The Verdet constant is a function of wavelength, temperature and index of refraction of the material.

PHYSICS OF THE FARADAY ROTATOR

The Faraday effect is a magneto-optical effect which is a property of the material. The Zeeman effect is a splitting of atomic energy levels by means of external magnetic fields. The normal Zeeman effect has the properties shown in Figure 33. Figure 33a shows that looking parallel to the magnetic field the incident radiation is converted into a Right Hand Circularly Polarized mode (RHCP) and a Left Hand



A) SPLITTING OF PLANE POLARIZATION INTO (RHCP + LHCP)

B) MAGNETIC FORCE ON AN ELECTRON

C) INDEX OF REFRACTION AS A FUNCTION OF FREQUENCY

FIGURE 33 NORMAL ZEEMAN EFFECT

Circularly Polarized mode (LHCP) (Ref 25: 694). Figure 33B with (B=0) shows the centripetal force that holds the electron in orbit about the nucleus. Normally, this force on an electron is given by

$$F_0 = m_e \omega^2 / r \quad (79)$$

and the magnetic force, due to a magnetic flux through the electron's orbit, is given by

$$F_{B\pm} = eB (\omega \pm \Delta\omega) r \quad (80)$$

where m_e is the mass of the electron, ω is the circular frequency in rad per sec, e is the electron charge, and r is the orbital radius (Ref 24: 694).

The total force, F_T , on the electron for B^+ is given by

$$F_T = F_0 + F_{B+} = m_e \omega^2 r + eB(\omega + \Delta\omega)r \quad (81a)$$

$$= m_e (\omega + \Delta\omega)^2 (\Delta\omega \ll \omega) \quad (81b)$$

where F_{B-} yields the same results except for a minus sign in front of $\Delta\omega$ (Ref 25: 694).

The solution to (81) for ($\Delta\omega \ll \omega$) is

$$\Delta\omega = eB / 2m_e \quad (82a)$$

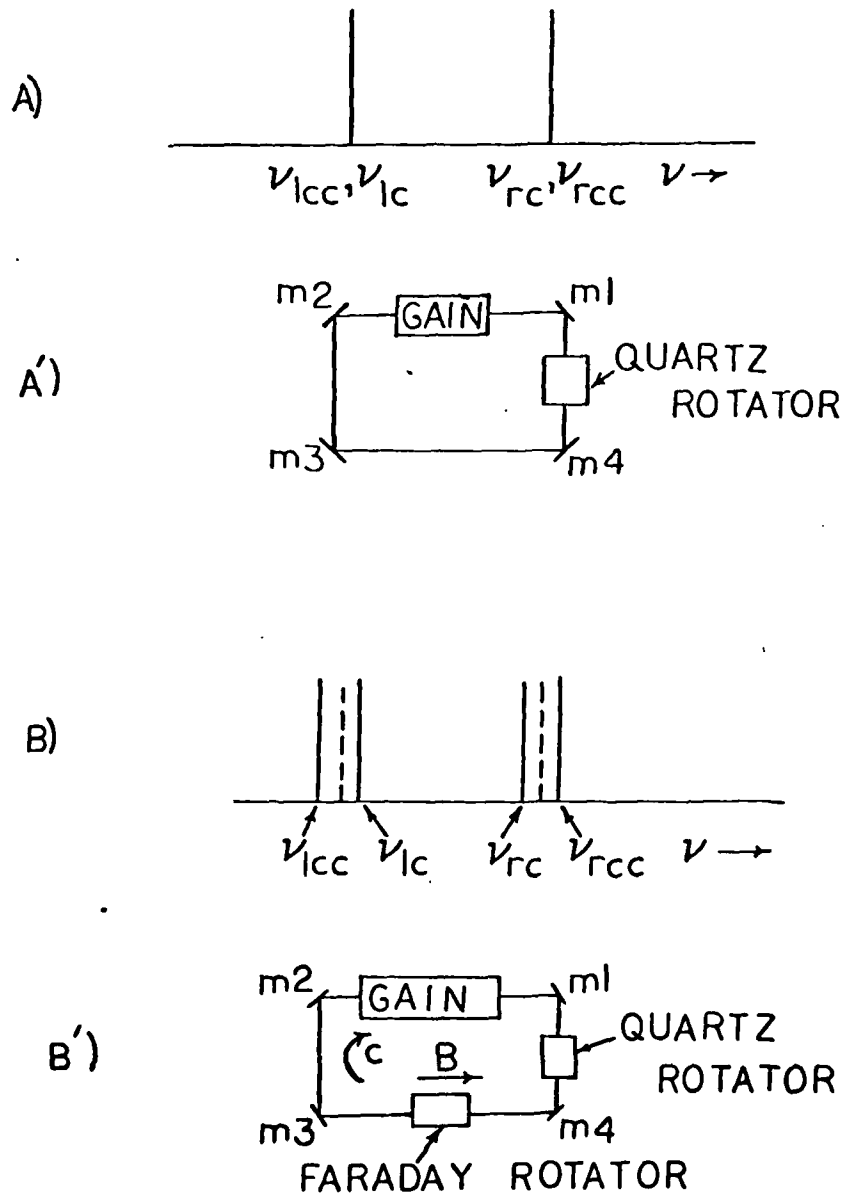
$$\Delta\nu = eB/4\pi m_e \quad (82b)$$

Equation (66b) yields

$$\Delta\nu = 1.3996 \times 10^6 |B| \quad \text{in Hz} \quad (83)$$

where $|B|$ is the magnitude of the magnetic field (Ref 25: 694). Figure 33c shows how the index of refraction changes in a dispersive medium near an absorption line (Ref 26: 196). A dispersive medium is a medium in which the index of refraction n varies greatly with wavelength. The dotted curve is for n_0 at zero magnetic field. The solid curve is n_- and identical to n_0 , but shifted higher in frequency. The dashed curve is n_+ and is identical to n_0 except shifted lower in frequency. Near n_0 , the right hand circular polarized wave has a higher index so it moves slower through the medium than the left hand circularly polarized wave. The result is a rotation of the incident plane of polarization through an angle of $+\Delta\phi$ given in equation 78.

The Faraday rotator is used to rotate the plane of polarization of linearly polarized light. The Faraday rotator can also be used as a nonreciprocal device in an optical cavity (RLG) because the index of refraction for the CW beam is not the same as the CCW beam. In a cavity without a Faraday rotator, the intensity as a function of frequency looks like Figure 34A (Ref 11: I-12). The clockwise and counterclockwise modes have the same frequency. When a Faraday rotator is inserted, the modes split apart as shown in Figure 34B. Figures (34A') and (34B') show a block diagram of the cavity optics without and with a Faraday rotator respectively, and with a quartz rotator to provide LHCP and RHCP (Ref 28: 5).



A) MODE STRUCTURE
 A') RING LASER WITH QUARTZ ROTATOR
 B) MODE STRUCTURE
 B') A') WITH FARADAY ROTATOR

FIGURE 34 FARADAY ROTATOR EFFECTS

The insertion of a Faraday rotator allows a reduction in cross energy transfer and increase RLG performance. The amount of the phase shift is the same for all modes but the sign is different. The phase is given by

$$\Delta\rho_{RCC} = VLB \cos 0 = VLB \quad (84a)$$

$$\Delta\rho_{RC} = VLB \cos \pi = -VLB \quad (84b)$$

$$\Delta\rho_{LC} = VLB \cos \pi = -VLB \quad (84c)$$

$$\Delta\rho_{LCC} = VLB \cos 0 = VLB \quad (84d)$$

The frequency in the laser cavity is given by

$$f_{RCC} = q \frac{c}{(n_{o,r} - \Delta n_F)l} = \frac{qc}{n_{o,r}l} + f_F \quad (85a)$$

$$f_{RC} = q \frac{c}{(n_{o,r} - \Delta n_F)l} = \frac{qc}{n_{o,r}l} - f_F \quad (85b)$$

$$f_{LC} = q \frac{c}{(n_{o,l} - \Delta n_F)l} = \frac{qc}{n_{o,l}l} + f_F \quad (85c)$$

$$f_{LCC} = q \frac{c}{(n_{o,l} - \Delta n_F)l} = \frac{qc}{n_{o,l}l} - f_F \quad (85d)$$

where q is the mode number, c is the speed of light in a vacuum, $n_{o,r}$ is the index of refraction for RHCP, $n_{o,l}$ is the change in the index of refraction caused by the Faraday rotator, l is the physical path length and f_F is given by

$$f_F = \frac{c}{n_i L} \frac{\Delta\phi_F}{2\pi} \quad (86)$$

in which symbols are the same as before (Ref 16). Note a positive $\Delta\rho$ for a RHCP mode increases the frequency and a positive $\Delta\rho$ for a LHCP mode decreases the frequency.

FARADAY ROTATOR

The rotator must have anti-reflection coatings to reduce losses. The surfaces must be normal to the optical axis and the $|\underline{B}|$ field parallel to the optical axis.

One problem with the Faraday rotator is its temperature sensitivity. The stability of the Faraday induced frequency shift is given by

$$\frac{\Delta f_F}{f_F} \propto \frac{\Delta T}{T} = (\alpha_i + \alpha_e(n-1))\Delta T \quad (87)$$

where f_F is the Faraday frequency, ΔT is the change in temperature of the Faraday rotator, T is the temperature, α_i is the temperature coefficient of the index of refraction, and α_e is the coefficient of expansion of the Faraday rotator (Ref 19). The error induced by a fluctuation in the magnetic field is given by

$$\frac{\Delta f_F}{f_F} \propto \frac{\Delta B}{B} \quad (88)$$

where ΔB is the fluctuation of the magnetic field. This error source was not directly observed during the experiment.

APPENDIX D: DISPERSION

INTRODUCTION

The effect of dispersion has been described in the theory section. The total dispersion is given in (21a) and (21b) gives the frequency pull-in of each mode. The effects of detuning on $\nu_{d,tot}$ are shown in Figure 16. This curve is generated by (21a) with $\Delta\nu_{\frac{1}{2}} = 500$ kHz, and $\Delta\nu_D = 2300$ MHz.

The stability of the total frequency pull-in is the key limiting factor for the long term stability. The temperature dependence of the total frequency pull-in comes from the temperature dependence of the Doppler broadened gain curve. The next area of concern is how a change in the total frequency pull-in effects the path length controller. The final part of Appendix D outlines an experiment that would determine if there was an ideal operating point at which the total frequency pull-in could be held constant.

TEMPERATURE EFFECTS

The effects of temperature on the total frequency pull-in are shown in Figure 35. For different temperatures T' , the value of $\Delta\nu_D(T')$ is given by

$$\Delta\nu_D(T') = \Delta\nu_D(T) \sqrt{T'/T} \quad (89)$$

Quantities also used to generate the curves are $\Delta\nu_D = 2300$ MHz, $\Delta\nu_{\frac{1}{2}} = 500$ kHz, and $T = 320^{\circ}\text{K}$. This yields the result, that for higher temperatures the dispersion is everywhere lower because the

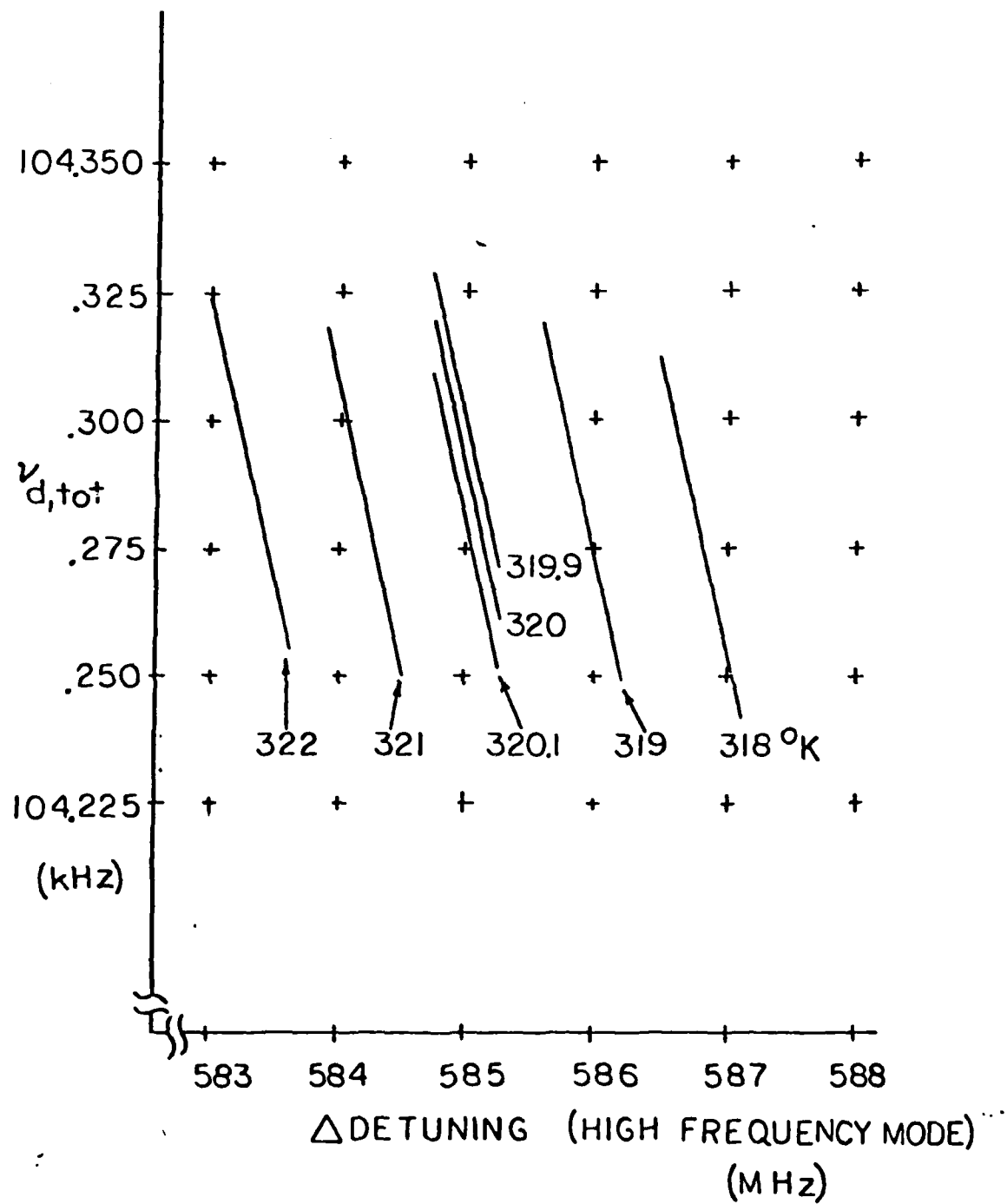


FIGURE 35 EFFECTS OF TEMPERATURE ON FREQUENCY PULL-IN

gain of the laser medium is lower and the inverse is true for lower temperatures. The effects of the temperature range 223⁰K to 373⁰K on total frequency pull-in is shown in Figure 36. This shows that the effect of temperature decreases as detuning increases. The dashed lines represent curves of constant total dispersion. If the detuning could be controlled, then a system could be designed to hold total dispersion constant.

The path length controller responds to the same effects that change the dispersion. When the temperature changes the intensity of the mode the path length controller responds. The path length controller holds the ratio of intensity of the strong mode to the weak mode constant. This is given by

$$\frac{I_{LOW}}{I_{HIGH}} = \frac{\gamma(\nu_L) - \gamma_{TH} \cdot K}{\gamma(\nu_H) - \gamma_{TH} \cdot K} \quad I_{LOW} > I_{HIGH} \quad (90a)$$

where $\gamma(\nu) = K e^{-\alpha(\nu - \nu_0 / \Delta \nu_D)^2}$ (90b)

$$\gamma_{TH} = \beta - \frac{1}{n_i} \ln(r_1 r_2 r_3 r_4) \quad (90c)$$

$$\gamma_{TH} = \gamma_{th} / K \quad (90d)$$

$$K = (N_2 - N_1) \frac{\lambda^2}{8\pi n_i^2 \tau_{spont}} \frac{2(\ln 2)^{\frac{1}{2}}}{\sqrt{\pi \Delta \nu_D}} \quad (90e)$$

$$\alpha = -4 \ln(2) \quad (90f)$$

$$\beta = \text{distributive losses (no mirrors)} \quad (90g)$$

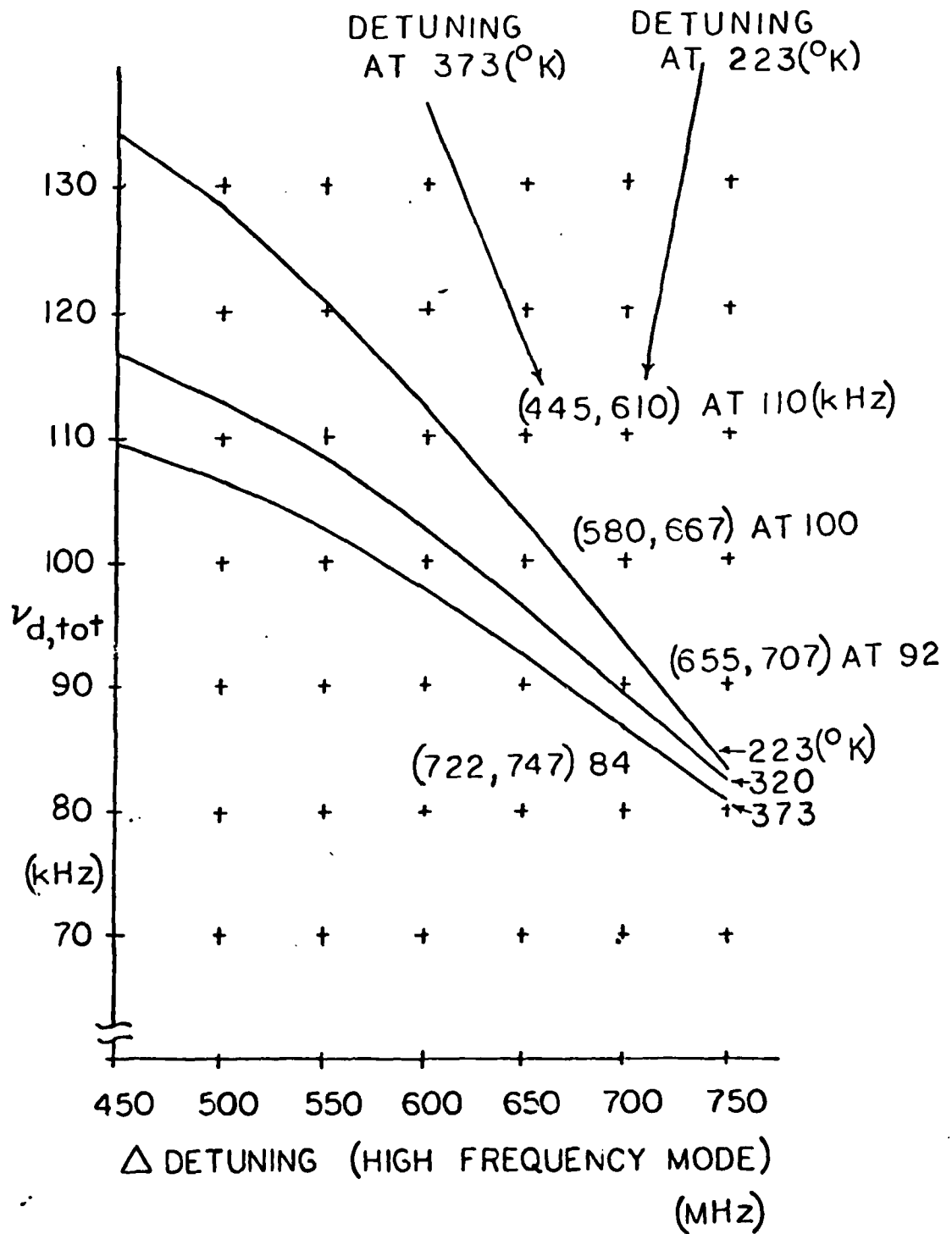


FIGURE 36 LARGE TEMPERATURE EFFECTS ON FREQUENCY PULL-IN

$$\Delta\nu_D = 2\nu_0 \sqrt{2 \ln 2 kT / mc^2} \quad (90h)$$

and ν is the frequency of the mode, ν_0 is the gain center, $n_i l$ is the average optical path length, r_i is the reflectance of the i^{th} mirror, $N_2 - N_1$ is the population inversion, λ is the wavelength, n_i is the average index of refraction, τ_{spont} is the time for a spontaneous decay, I_{LOW} is the intensity of the low frequency mode, and I_{HIGH} is the intensity of the high frequency mode. Equation (90a) becomes

$$\frac{I_{\text{LOW}}}{I_{\text{HIGH}}} = \frac{e^{-\alpha(\nu_L - \nu_0/\Delta\nu_D)^2} - \gamma_{\text{TH}}}{e^{-\alpha(\nu_H - \nu_0/\Delta\nu_D)^2} - \gamma_{\text{TH}}} \quad (91)$$

where ν_L is the frequency of the low mode and ν_H is the frequency of the high mode.

Figure 37 shows the effects of temperature on frequency pull-in for $\Delta = 600$ MHz. The result of (91) for $\gamma_{\text{TH}} = 0.3$, $\alpha = -4 \ln 2$, $\Delta\nu_D(320^\circ\text{K}) = 2300$ MHz, $\Delta\nu_D(T_i) = 2300 \text{ MHz } \sqrt{T_i/T}$, $T_1 = 320.1^\circ\text{K}$, $T_2 = 319.9^\circ\text{K}$ are shown for all ten points in Figure 38. The intensity ratios increase with increasing detuning or decreasing temperature. The vertical distance between 4 and 5 is 9.16 Hz. However, there are several approximations in equation (21b). Equation (21b) is an approximate equation for a Lorentzian lineshape. The He-Ne laser has primarily a Doppler broadened lineshape which is complicated by having two isotopes Ne^{20} and Ne^{22} whose linecenters are 875 MHz apart. The equation does not allow for laser power at

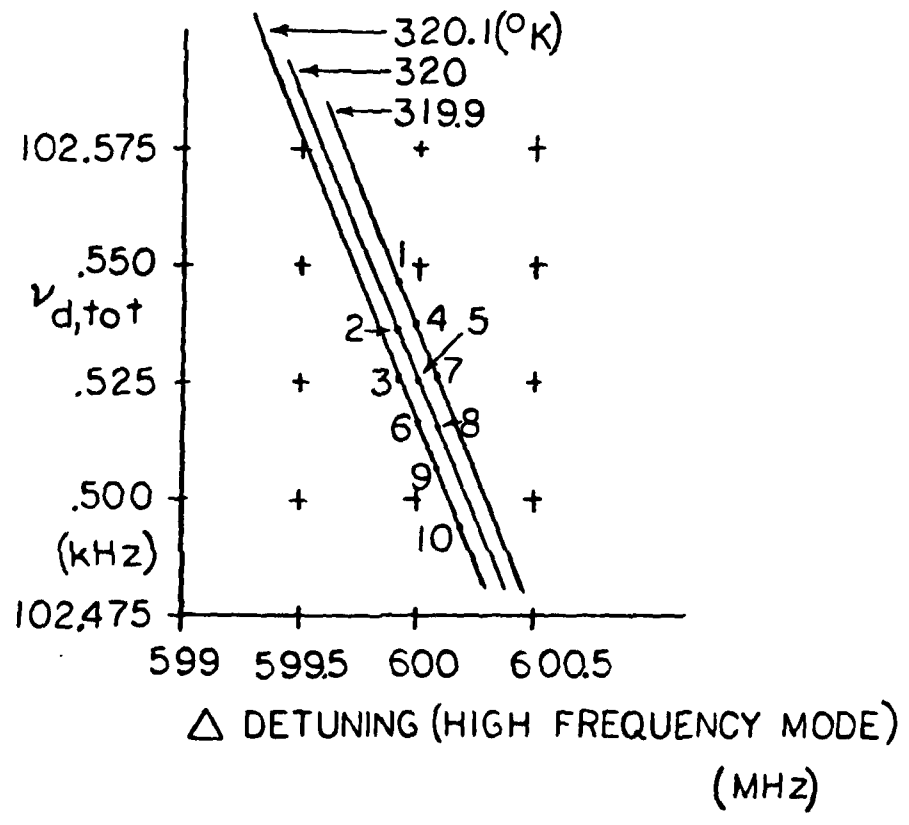


FIGURE 37 SMALL TEMPERATURE EFFECTS ON FREQUENCY PULL-IN

Equation (89) is only for a single isotope mixture. Also, (91) does not allow for fluctuations in discharge current.

Figures 37 and 38 show that if the path length controller tracks the intensity ratio 1.32564 and the temperature goes up 100m°K, then the controller will move to position 10 giving an error of 31.6 Hz instead of 9.16 Hz. Figure 39 does not reflect an actual calculation but looks at the reverse effect. If the controller tracks the intensity ratio 1.32500, the total dispersion remains constant. The above theory gives insight into the problem but is incapable of very accurate predictions due to the approximations.

EXPERIMENT

The following experiment was proposed but not carried out. This was due to the drift in the Laser # 18 pathlength control and the fact that there was not time to set up Laser # 68 for this experiment.

The first part of the experiment will generate an experimental curve for Figure 16 at a fixed temperature to within 15 m°K. Next, another curve will be generated for a temperature one degree higher. This is accomplished by inputting the clock signal into the frequency analyzer while the oven is stabilized at 320°K. A data point will be taken for many values of detuning Δ . Then, the oven stabilized at 321°K and this procedure is repeated. Consider the frequency difference between two temperatures at the same detuning

$$\delta v_{d,tot} = v_{d,tot}(T_L, \Delta') - v_{d,tot}(T_H - \Delta') \quad (92)$$

where $T_L = 302^\circ\text{K}$, $T_H = 321^\circ\text{K}$ and Δ' is the detuning.

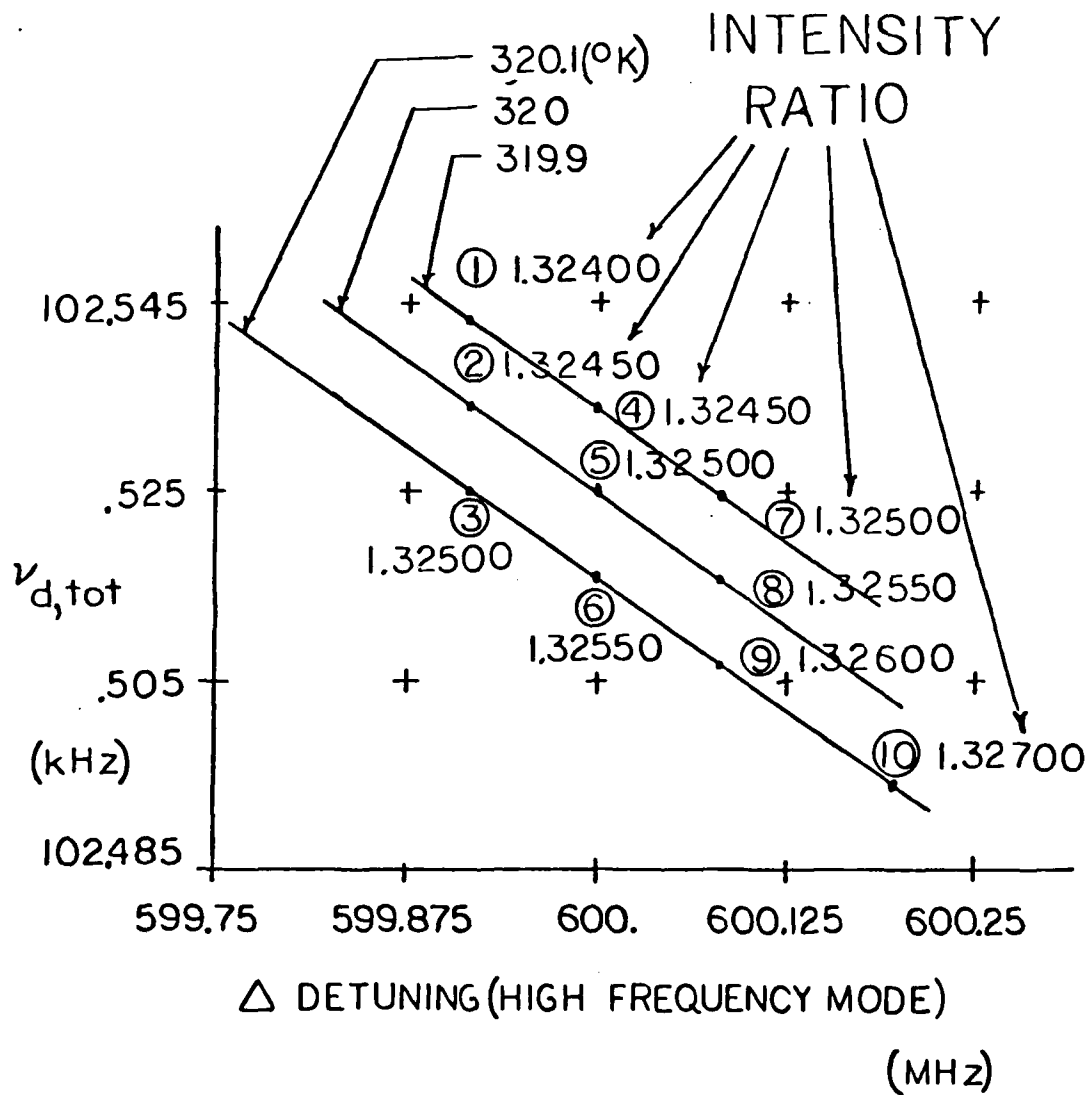


FIGURE 39 POSSIBLE INTENSITY RATIOS

This experiment will allow a comparison of (21) with actual data. Also, the key consideration is whether Figure 38 or 39 is correct. A path length controller running with balanced intensities has no detuning sensitivity, but as the intensity ratio increases the detuning sensitivity increases. For a value of detuning Δ' , if the measured quantity $\delta\nu_{d,tot}$ is larger than calculated, then the path length control is degrading performance and if the converse is true it is improving performance.

This experiment would have determined an optimum operating point. This was to be done to characterize the actual system because there may have been effects never before seen or effects not accurately accounted for.

If good and bad operating points were observed then the Allan variance should be measured at these points. This would be to show a bad point was indeed reducing clock stability and that the converse is true.

The above experiment was not run. Data taken at a controlled temperature ($\pm 20\text{m}^\circ\text{K}$), did not show the effects of dispersion. However, these effects might have been hidden by the large drift in the induced Faraday rotator frequency.

VITA

Roger Lee Facklam was born on 22 May 1955 in Abilene, Kansas. He graduated from Chapman High School; Chapman, Kansas in 1973. He attended Kansas State University from August 1973 to May 1976. He received the degree of Bachelor of Science, with Honors, in Physics in 20 May 1976. He attended the University of Missouri at Kansas City. He then worked at Kitt Peak National Observatory with the Voyager spacecraft team. He entered OTS in July 1979 and was commissioned in September 1979. He was assigned to the Reference Systems Branch at the Air Force Wright Aeronautical Labs, Wright-Patterson AFB, Ohio. He began taking classes part time in January 1980.

Permanent Address: RR#1 Enterprise

Kansas 67441

END

FILMED

6-83

DTIC